STRATEGIES FOR THE DEVELOPMENT OF MULTIPLEXED DIAGNOSTICS

By

Micaella Zuleika Jorge

Dissertation

Submitted to the Faculty of the

Graduate School of Vanderbilt University

in partial fulfillment of the requirements

for the degree of

DOCTOR OF PHILOSOPHY

in

Chemistry

December 17th, 2022

Nashville, Tennessee

Approved:

David W. Wright, Ph.D.

Renã A. S. Robinson, Ph.D.

Lars Plate, Ph.D.

John T. Wilson, Ph.D.

Dedicated to my supportive parents, Ana-Bela and Manny Jorge, who have been my biggest and most relentless allies from the beginning. This would not have been possible without you. We did it.

ACKNOWLEDGMENTS

As everyone who has walked this path before me knows, this Ph.D. journey is not completed without the support of many individuals over numerous years, all of whom I have so much gratitude for. I need to first start by thanking and acknowledging my biggest fans and the most important people in my life who have supported me from the moment I was born—my parents. Although I am a first-generation college graduate and soon-to-be Ph.D. graduate, my parents instilled the importance of education in me at an early age and have been there through countless tears, smiles, hurdles, celebrations, and everything in between. I simply would not have gotten this far without you both, and I am so lucky to have had you cheering me on throughout this wild ride.

I would be remiss to not also acknowledge the teachers and mentors who inspired me throughout my education, some igniting that passion for science as early as the 10th grade. To Ms. Susan Salb who is the reason I set forth on a chemistry path—thank you. If it were not for your A.P. Chemistry course, the Science Olympiad team, and Chemistry Club after school meetings, I would never have been here in the first place. Representation is critical and seeing you as the first female in science allowed me to envision myself in a similar position in the future. Thank you for being the first to teach me that chemistry is ubiquitous and most importantly—fun! I also must thank some professors at the University of San Diego who were instrumental in keeping that passion alive by introducing me to the world of research. First, Dr. Joan Schellinger: thank you for bringing me on as one of your earliest research students when you joined the

chemistry faculty at USD. Your belief in my abilities and consistent mentorship even throughout my graduate studies has been invaluable. I embarked on graduate research because I aspired to be the incredible professor you were to me and many others. I truly lucked out in having you as my research advisor. Another individual that expanded my mindset surrounding research, showing me new avenues of research that I could not have learned in a traditional classroom setting was Dr. Jim Bolender. Being part of your very first international chemistry course in Uganda showed me the real-world applicability that research can have and the potential impact it can have on communities, especially those in low-resource settings. I had never considered public health research before then, but that Uganda trip is not only one of my most favorite and cherished experiences, but also truly eye-opening and was the reason I pursued similar research. Lastly, if it were not for the McNair Scholars Program and Ramiro Frausto, I would not have been introduced to the idea of graduate school and would have been very lost in the application process. I am grateful for the extended research opportunities and comradery McNair gave me during my undergraduate education and for all the guidance and feedback throughout the graduate application process. Thank you, Ramiro.

As for the faculty at Vanderbilt who have lent their scientific knowledge and expertise: I would like to first acknowledge Dr. David Wright for opening his lab door to welcome me to his team of global health researchers. I have grown endlessly as an independent scientist and that would not have been possible without the space to think and operate freely within the Wright lab. Thank you. As for the rest of my committee—Dr. Renã

Robinson, Dr. Lars Plate, and Dr. John Wilson. I am grateful for your advice, knowledge, and support to better me as a researcher.

I would also like to thank some previous Wright lab members who either directly trained me during the early stages of my time in the lab or acted as a constant support system throughout my Ph.D. To Dr. Christine Markwalter who patiently got me up to speed on the world of diagnostics, of which I had zero previous experience—thank you. Even though you were juggling the last milestones of your own Ph.D., including writing your dissertation as I am now, you never failed to answer my questions, show me proper lab technique, and offer encouragement when I was feeling disheartened after a failed experiment. I often think of those early months of mentorship now and I consider myself lucky to have been trained by you.

I must also express my gratitude for Dr. Thomas Scherr who has been a continual mentor to me since I joined the Wright Lab. Thank you for always being available to talk through results and next steps, for reviewing materials for applications and exams, and always offering your help in any way. I am so appreciative of your guidance and for always lending an ear.

In terms of Wright lab members, I must acknowledge Dr. Jenna DeSousa, my co-author and #1 lab partner. Thank you for accompanying me during many late nights, early mornings, and weekend experiments. I would not have had as enjoyable of a time if it weren't for our music jam sessions, coffee and bagel runs between experiments and, of

course, schnack time that was full of fun stories and laughter. Thank you for your companionship.

Last, but certainly not least, I have been so fortunate to have family and friends near and far who have made this Ph.D. experience infinitely better simply by their presence and encouragement. Thank you, Dr. Jayme Verdi, my best friend, for your never-ending support. Even on opposite sides of the country, you listened to me recap my days in the lab and added much-needed sunshine on the difficult days. Thank you for your continued friendship. Kevin Do – I am so appreciative of your support and unwavering faith in my abilities. Thank you for encouraging me and always making me laugh, even 2,000 miles apart. To Josh, Katie, and Shelby – I am so glad we had each other, especially in the early days of lab rotations and teaching, to navigate graduate school. Our small group was a highlight in my graduate journey. Finally, I have had amazing support from my partner, Michael Weberman, during this last leg of my graduate school career. Thank you for sitting with me as I finish writing documents and preparing for presentations, listening to my worries, helping me to navigate an impending life change, and cheering me on during some of the most stressful moments to date in my graduate education. I am fortunate to have had you by my side during this time and I wouldn't have wanted to have anyone else there with me as I close out this chapter.

TABLE OF CONTENTS

APPENDIX

LIST OF TABLES

LIST OF FIGURES

ABBREVIATIONS

Word	**Acronym**
1. Anti-CRP	α-CRP
2. Anti-HRP2	α-HRP2
3. Anti-NGAL	α-NGAL
4. Anti-PCT	α-PCT
5. Antibody	Ab
6. Silver nanoparticle	AgNP
7. Analysis of variance	ANOVA
8. Affordable, sensitive, specific, user-friendly, rapid and robust, equipment-free, and deliverable to end users	ASSURED
9. Area under the curve	AUC
10. Gold nanoparticle	AuNP
11. Gold nanoparticle-antibody conjugate	AuNP-Ab conjugate
12. Bovine serum albumin	BSA
13. Centers for Disease Control and Prevention	CDC
14. Control line	CL
15. Conjugate pad	CP
16. C-reactive protein	CRP
17. Coefficient of variation	CV
18. Enzyme-linked immunosorbent assay	ELISA
19. Emergency use authorization	EUA
20. Food and Drug Administration	FDA

CHAPTER I

INTRODUCTION

The world has long relied on a range of diagnostic tools for efficient and prompt medical diagnosis, from x-ray technology to at-home pregnancy tests, to the recent widespread use of rapid COVID-19 tests. Diagnostic tools such as these are critical for public health surveillance and the implementation of appropriate treatment plans, ultimately improving patient outcomes. Further showcasing the utility of diagnostics and clinical laboratories, the Centers for Disease Control and Prevention (CDC) found that 70% of medical decisions were dependent on laboratory test results and that 14 billion laboratory tests were ordered in 2016, a number that greatly amplified in the years to follow. Recent epidemics and pandemics, namely coronavirus, monkeypox, and Ebola have only bolstered the globe's reliance and demand for accurate and versatile diagnostic tools. The last few decades have seen advances in diagnostic technology resulting in more accurate, sensitive, quicker, and equipment-free diagnostic strategies. With these advances has also come the development of diagnostic tools for a variety of health care settings, including hospitals, clinical laboratories, outpatient clinics, rural villages, and personal homes.[1] These tools largely focus on the detection of antigens and nucleic acids for the determination of the presence or absence of a particular illness.

Highly sensitive and specific diagnostic tests that are designed to be performed within the resources of a clinical laboratory are no doubt crucial to patient care, however, these

methods often require several hours to obtain a result. Ultimately, lengthy times-to-result of these laboratory tests can lead to a delay in patient treatment and, in some cases, inappropriate medication prescription when providers make decisions empirically. These disadvantages in current diagnostic methods have led to a push for more point-of-care (POC) diagnostics, or tests that can be performed rapidly without trained personnel and heavy laboratory equipment.

A notable example of a POC diagnostic that has improved access and quality of life for many globally is the handheld glucose monitor. This device is used by those who suffer from diabetes daily to self-monitor blood sugar levels and to administer insulin accordingly. The ability to continually monitor one's glucose has led to improved glycemic control, enhanced quality of life as well as peace of mind for those affected. The development and distribution of diagnostic tests similar to the glucose monitor not only allows for portable diagnosis, but also allows for low- and middle-income countries to have increased access to public health services and surveillance, ultimately improving patient outcomes.[2,3]

The utilization of POC tests worldwide has become instrumental in increasing access to health care in resource-limited settings. For example, the use of rapid diagnostic tests (RDTs) in countries where malaria is endemic has greatly expanded the capacity for malaria diagnosis. The clinical presentation of malaria is indistinguishable from other fever-causing pathogens. As such, rapid and appropriate malaria diagnosis is necessary to prevent mortality.[4] The development and dissemination of malaria RDTs in endemic

regions has enabled rapid and accurate diagnosis of malaria in situations where the gold standard diagnostic method, parasite microscopy, is unavailable.[5] The advent of malaria POC tools has been greatly beneficial to many as it is an effective tool that has adequate sensitivity to diagnose those infected with the malaria parasite, serving as a suitable alternative for the gold standard. Regardless, malaria RDTs and other similar POC diagnostics must meet certain criteria set forth by global health organizations in order to be implemented into standard clinical care.

Diagnostic Criteria for POC Diagnostic Tools

In 2003, the World Health Organization (WHO) released a list of criteria (ASSURED) that POC diagnostics should meet to be accessible, affordable, and accurate. ASSURED stands for **A**ffordability, **S**ensitivity, **S**pecificity, **U**ser-friendly, **R**apid and robust, **E**quipment-free, and **D**eliverable to those who need it. While this criterion was initially published as a set of guidelines for diagnostic development for the developing world, it is also relevant for POC tests intended to be used in primary care settings globally, where a diagnosis is needed quickly without the need for trained specialists or bulky laboratory equipment.
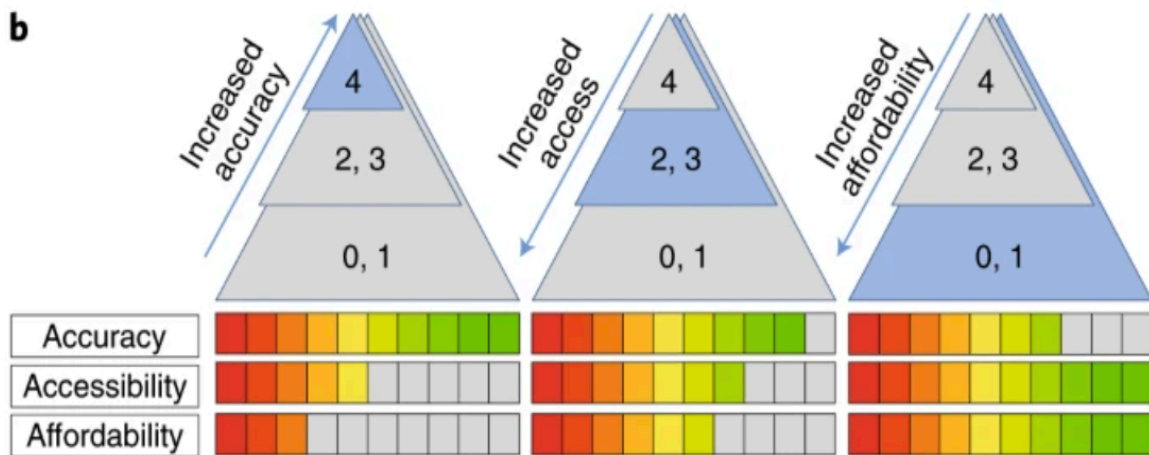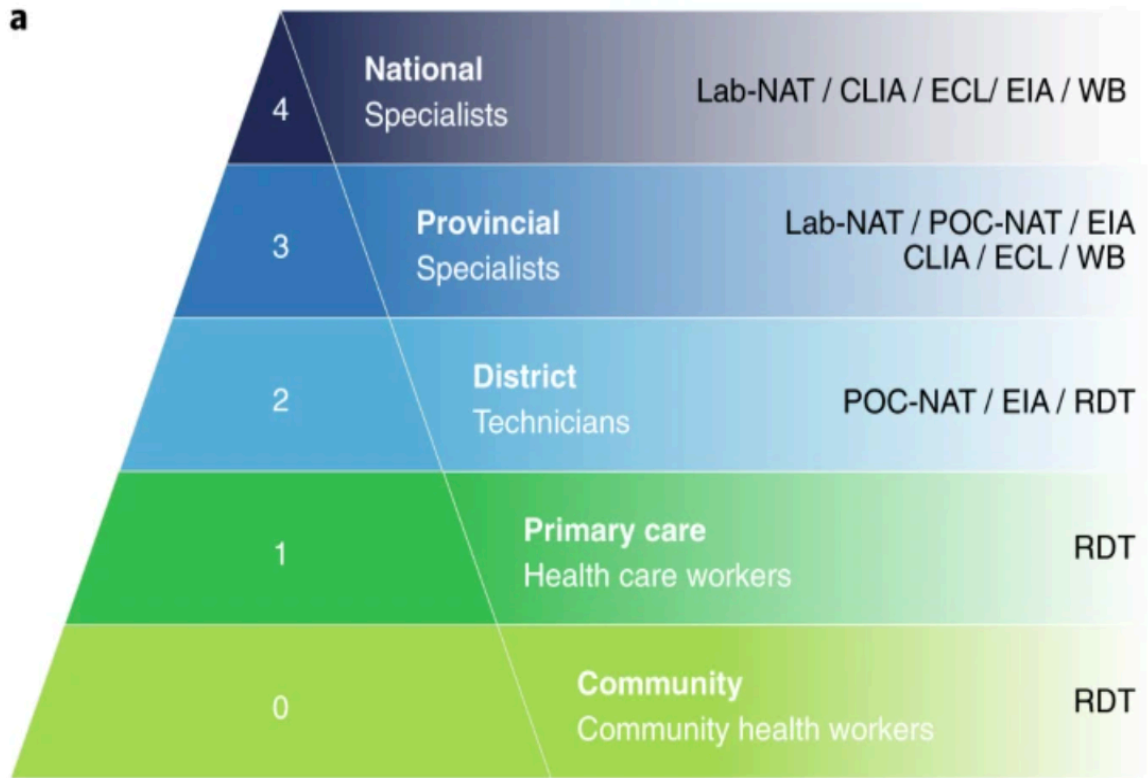
Figure 1. Trade-offs between diagnostic tests at varying levels of the healthcare system. **A)** Healthcare system levels from national to community care with diagnostic test types suitable for each level. Lab-NAT: laboratory-based nucleic acid tests; EIA, enzyme immunoassay; WB, western blot; CLIA; chemiluminescence immunoassay; ECL, electrochemiluminescence immunoassay. **B)** Diagnostic criteria reflecting trade-offs in accuracy, accessibility, and affordability at different healthcare levels.[9]

For diagnostics used in advanced clinical settings, such as hospitals or reference labs, analytical and clinical validation standards must be met. This includes prerequisites for sensitivity, specificity, accuracy, and precision. However, for diagnostics intended for use at the POC, these tests must not only be inexpensive to manufacture, but also designed to operate simply without complex laboratory equipment and personnel. These limitations in device manufacturing and operation must be implemented while remaining sufficiently sensitive and specific for the intended use case. These inherent differences between POC diagnostic device formats and clinical diagnostic tests result in trade-offs between accuracy, accessibility, and affordability (Figure 1).[6–8] For example, tests that are the simplest to perform, such as RDTs (levels 0, 1, 2), have increased access and affordability, but will be less accurate than diagnostics designed for clinical laboratories (levels 3 and 4) due to format constraints. Diagnostic benchmarks such as these are used by scientists and health care personnel to determine and rank the utility of different diagnostic tests.

Recently, the ASSURED criterion has been updated to reflect advances in technology, now becoming REASSURED with updated guidance. The new additions to the criterion are **R**eal-time connectivity and **E**ase of specimen collection.[6] Real-time connectivity refers to the ability of test results being transmitted to the user/patient and health care provider quickly, which come in the format of using mobile phones embedding connectivity into POC or near-POC instruments for signal readout. This integration with technology also allows for unambiguous test results, not relying on user interpretation that may be incorrect. Furthermore, by using a barcode or other identifiable marker on a diagnostic

test that can facilitate connectivity, important data points about the test can be shared with users. This technological advancement can include information such as lot numbers, expiration dates, and other manufacturing data. Regarding the second addition to the REASSURED criteria, ease of specimen collection, the sample collected for biomarker detection must be non-invasive, such as urine, blood from a fingerprick, or saliva, to meet POC requirements. This minimizes the need for a sample preparation step that lengthens time-to-result and generally requires more advanced laboratory equipment that would not be readily available at the POC. Although multiplexed POC diagnostics are highly desirable as noted in part by the uptick in publications addressing multiplexing (Figure 2), there are only a handful of clinically available multiplexed diagnostics.
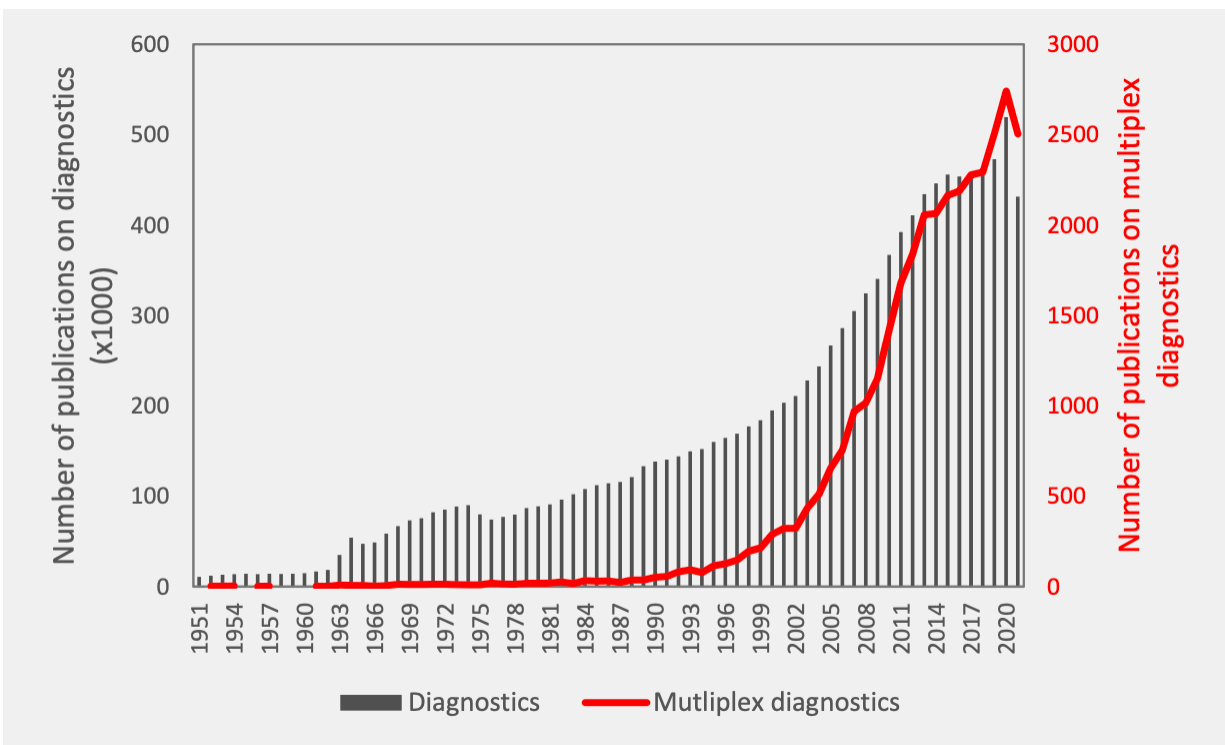
Figure 2. Diagnostic publications versus multiplexed diagnostics publications published from 1950 to 2021 from PubMed (National Center for Biotechnology Database).[7]

Multiplexed Point-of-Care Diagnostics in Academia

While singleplexed RDTs are now relatively common POC tools, they are limited in the quantity of biomarkers (antigens) they can detect and, as such, are limited in their diagnostic utility. Alternatively, multiplexed POC diagnostics allow for rapid detection of multiple biomarkers simultaneously. The specific biomarkers targeted for detection are chosen based on antigen(s) that are indicative of certain disease states. The detection of multiple disease markers allows for a more accurate diagnosis and, in some cases, identification of causative pathogens. This leads to a more targeted treatment plan and overall decreased morbidity and mortality rates. In cases where the question of whether an antibiotic should be prescribed, multiplexed diagnostics also promote antibiotic stewardship.

While the need for these tools is inarguably crucial for furthering public health efforts, multiplex paper-based assays largely exist in academic research settings, rarely making it to the clinical setting.[9] A number of these works from the last five years (2017-2022) with their test format, detection method, and use cases are shown in Table 1. These studies aim to develop a paper-based multiplexed assay capable of detecting at least two biomarkers simultaneously. The chosen works achieve multiplexing by a few methods: utilizing hydrophobic barriers for specific reaction zones, incorporating image processing, using 3D or vertical flow assays, and having multiple test lines or spots immobilized onto a paper membrane.[10–20]

Table 1. A summary of paper-based multiplexed diagnostics from the last five years.

Detection Method	Case Study	Ref.
Colorimetric	AMR resistance	10
Image processing/deep learning	Lyme disease	11
Colorimetric	Metal ions	12
Colorimetric	COVID variants	13
Barcode scanner	Drugs of abuse and blood-transmitted infections	14
Fluorescence	Small-molecule explosives	15
Chemiluminescence	Tumor biomarkers	16
Colorimetric/electrochemical	Protein and glucose	17
Colorimetric	Virus subtyping	18
Colorimetric	Malarial biomarkers	19
Colorimetric	Cardiac biomarkers	20

While there is consensus that multiplexed diagnostic tests are valuable to public health efforts, there are requirements these tests must meet to be U.S. Food and Drug Administration (FDA) approved and ultimately to be used routinely in clinical care settings. Developing multiplexed diagnostic tests is a challenge on its own but developing them with the intent of being used by inexperienced users and without heavy laboratory equipment is even more difficult. Furthermore, meeting these requirements while also remaining suitable for POC settings becomes exceedingly demanding when attempting

to simplify the test format. For this reason, the majority of clinical and FDA approved multiplexed diagnostics exist as complex laboratory tests.

FDA Approved Multiplexed Diagnostic Tests

One of the most common and sensitive diagnostic tests used in the clinical setting is the polymerase chain reaction, or PCR. PCR is a highly sensitive enzymatic assay that targets and subsequently amplifies a specific DNA or RNA sequence for detection. This technique detects the products of the reaction using gel electrophoresis for visualization. PCR utilizes Taq polymerase, primers, template DNA, and nucleotides, in conjunction with a thermal cycler, to carry out the reaction which generally takes a few hours to complete.[21,22] The usefulness of this diagnostic technique became apparent to the public during the COVID-19 pandemic, where testing for SARS-CoV-2 RNA in nasopharyngeal swab samples via reverse-transcription (RT) PCR was the gold standard for COVID testing and diagnosis.[23]

While traditional PCR is used to detect a single portion of a DNA or RNA sequence, multiplexed PCR was developed in the late 1980s for the detection of multiple nucleic acid sequences and since then has become an important tool for pathogen detection. To conduct a multiplexed PCR experiment, multiple distinct primer pairs, each designed to detect a specific target, are used to amplify several DNA sequences simultaneously. A number of multiplexed PCR assays have been FDA approved for public health surveillance, from respiratory pathogen panels to hepatitis C virus and human immunodeficiency virus (HIV) detection.[24–26] While these types of PCR assays have

become routine and crucial for clinical management and infection diagnosis, they are hindered by cost, time-to-result, and the need for trained technicians to run the equipment. These trade-offs come with the high accuracy and sensitivity of PCR-based diagnostics, with PCR falling into the third level of diagnostic tests shown in Figure 1. The decrease in affordability and access at this level makes PCR impractical for use at the POC. Because of this, there is a large push towards more accessible and affordable POC multiplexed diagnostic tests for public health surveillance.

A.)

B.)
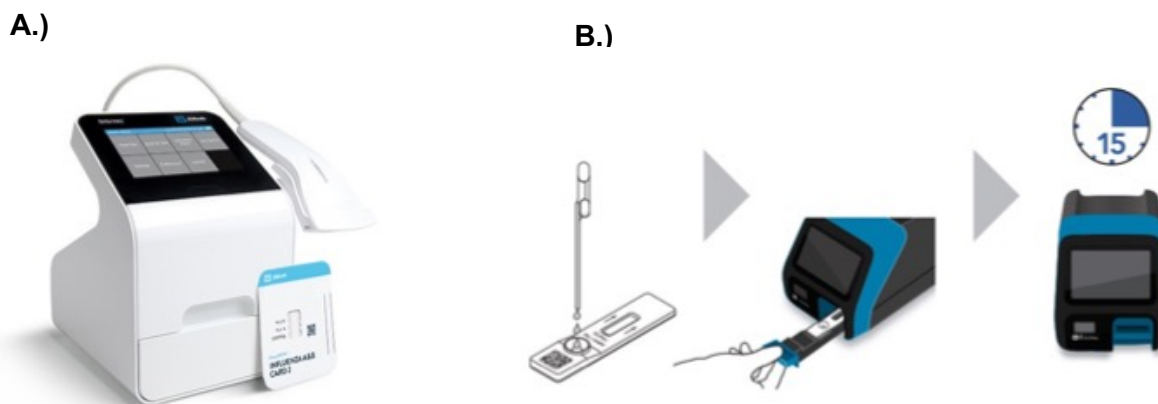
Figure 3. Images of the **A)** Abbott BinaxNOW Influenza A and B LFA with reader and the **B)** Quidel Sofia 2 Flu + SARS-CoV-2 immunofluorescent LFA with reader.

The move towards these diagnostic tools is further shown by FDA approved tests such as Abbott's BinaxNOW lateral flow assay (LFA) and Quidel's Sofia 2 Flu + SARS-CoV-2 LFA (Figure 3). The BinaxNOW paper-based diagnostic assay differentially detects the presence of two influenza antigens (A and B) simultaneously within fifteen minutes with 95.7% specificity and 87% sensitivity.[27] The Quidel Sofia 2 Flu + SARS-CoV-2 multiplexed immunofluorescent assay can differentially detect influenza A, influenza B,

and SARS-CoV-2, gaining FDA emergency use authorization (EUA) due to its relevance with the COVID-19 pandemic. This test has sensitivity and specificity ranging from 89% to 96% and 95% to 100%, respectively.[28] Both Abbott's and Quidel's assays require a reader to determine the outcome of the test. Though generally less sensitive than PCR, LFAs offer a few advantages to more complex diagnostic tools, including lower cost, decreased time-to-result, increased robustness, and the ability to be performed by non-trained users.

Lateral Flow Assays
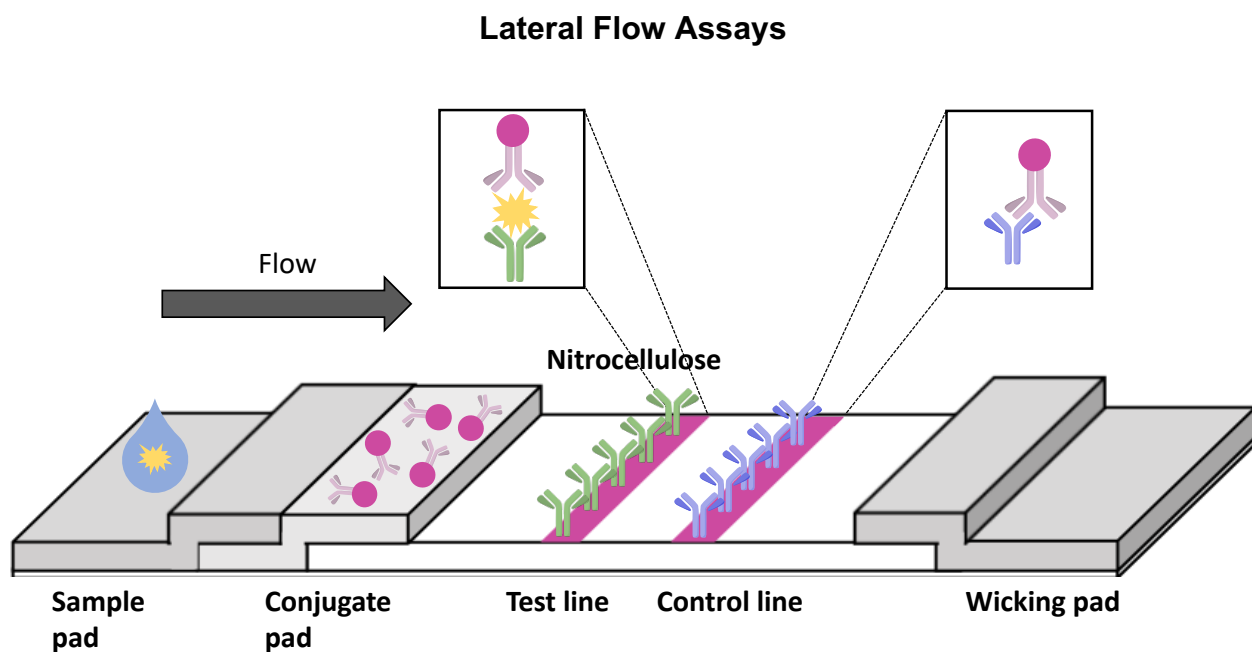
Figure 4. Traditional singleplex sandwich LFA format.

LFAs have become extremely useful tools for disease diagnosis at the POC, especially in resource limited settings. Namely, commercial singleplex LFAs have widely been used for the diagnosis of malaria, *Streptococcus*, influenza, HIV, tuberculosis, and COVID, to just name a few.[29–33] In a typical LFA format (Figure 4), a few drops of a sample are added

to the sample pad of the paper-based test. The sample then interacts with the conjugate pad which contains reporter elements (usually gold nanoparticles) that are conjugated to antibodies specific to the target protein (antigen). Any antigen present in the sample forms a complex (antigen-Ab complex) with the reporter elements and flow laterally down the length of the assay, next interacting with the test and control lines. Molecular recognition elements, commonly antibodies, are immobilized onto a nitrocellulose membrane to form the test and control lines. The test and control lines become visible to the naked eye when the antigen-Ab complex and unbound reporter elements bind to these sections of the test, respectively. The resulting colorimetric signals appear due to the aggregation of the gold nanoparticles (AuNPs) at these locations.

The complex described above is referred to as a sandwich assay and it is the most common format for LFAs, although other formats, such as a competitive assay, can also be used in LFA design. These assays are generally developed iteratively, through trial-and-error, to choose the optimized reagent and concentrations for each component.[34,35]

Cross-reactivity and Other Challenges in Multiplexed Diagnostic Development

While singleplex LFAs are commonplace in the diagnostics and healthcare world, multiplex LFAs largely exist in academic research settings, rarely making it to the clinical setting.[9] This is largely due to the difficulty associated with meeting ASSURED or REASSURED diagnostic criteria while maintaining a simply manufactured test that could be administered without the need for heavy laboratory equipment and trained personnel. Additionally, transitioning from a singleplex to a multiplex diagnostic test has inherent

challenges, especially when using antibodies as molecular recognition elements. This is in part due to the potential of the chosen antibodies to bind to similar epitopes (non-homologous amino acid sequences) of non-target antigens.[36] To illustrate this point, Schwenk *et al*. found that approximately 95% of 11,000 affinity-purified monoclonal antibodies bound to non-target proteins.[37]

Immunoassay interference such as this leads to false positive or false negative results, impacting the sensitivity and specificity of the assay. As the number of varying components of an assay increase, so does the potential for interference, especially in a paper format. Cross-reactivity and assay interference remain one of the main barriers to widespread multiplex diagnostic development and commercialization.[38–40] These issues are further compounded when using commercial antibodies for assay development, in contrast to producing antibodies in-house. This is due to the proprietary nature of commercial sources and their antibody screening processes being conducted solely by the manufacturer. With manufacturing details remaining proprietary from the scientist who is utilizing the antibodies downstream during assay development, any potential cross reactivity can only be caught by the scientist late in development, potentially hindering the successful development of a multiplexed assay. Still, there is a lack of scientific research surrounding cross-reactivity in multiplexed diagnostics, even with its prevalence being detrimental to advances in multiplexed assays.[40]

Since a multiplexed diagnostic assay requires the mixing of reagents, the likelihood of encountering non-specific cross-reactivity increases as more protein targets are included

in the assay. This cross-reactivity can lead to higher background noise, lack of reproducibility, or false positive and false negative results in the worst-case scenario. In the case of sandwich immunoassays where a capture and detection antibody are used to make a "sandwich" with the biomarker of interest, there are at least five potential cross-reactivity scenarios (when detecting two biomarkers simultaneously), as shown in Figure 5.[40] These scenarios occur with antibody-antibody (Ab-Ab), Ab-protein, and protein-protein interactions. A 2012 study analyzing cross-reactivity in multiplex sandwich assays introduced these interaction possibilities as "liability pairs", with the number of these interactions increasing proportionally to the square of the number of targets in a multiplexed assay as shown by the following:

$$4N(N-1) \qquad (1)$$
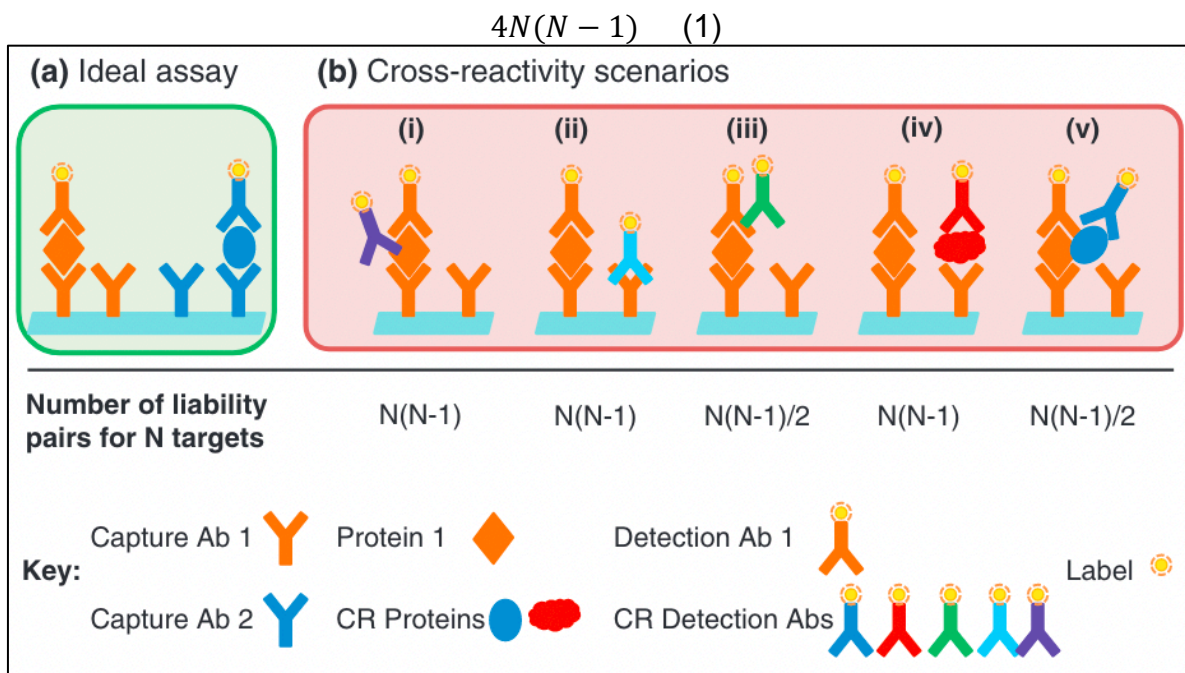
Figure 5. Possible cross-reactivity scenarios resulting from reagent mixing in multiplexed sandwich assays. **A)** An ideal sandwich assay for two targets. **B)** Potential liability pairs for a multiplexed assay with *N* targets showing binding of **(i)** detection Ab to target protein, **(ii)** detection Ab to capture Ab, **(iii)** detection Ab to detection Ab, **(iv)** another protein in sample to target protein capture Ab, and **(v)** protein-protein interactions of two target proteins.[40]

where N is the number of targets in the assay.[41] Due to the frequency of cross-reactivity found in multiplex assays, they are often not recommended for clinical studies when the assay involves reagent mixing, lacking separation of reagents meant to detect individual targets.[42,43]

Strategies to Overcome Cross-reactivity in Paper-based Multiplexed Diagnostics

The demand for more multiplexed diagnostics and the well-known barriers to their widespread use has led to modifications to combat cross-reactivity. These adjustments are largely implemented in well-based immunoassays, where there are greater opportunities for optimization. Due to the small size of a typical LFA and limited chemistries to modify nitrocellulose (the most frequently used membrane for LFAs), there are limited methods to overcome cross-reactivity challenges. The main strategy employed to prevent these unwanted interactions from occurring is spatial separation of reagents so that each capture Ab is exposed to a single detection Ab during the execution of the assay, reducing the possibility of liability pairs. Different research groups have accomplished this in various ways, including creating an array of individual LFAs, designing a protein microarray, using laser ablation technology for the generation of distinct channels for each target protein, and utilizing paraffin wax to develop individual wells within a paper assay.[41,42,44–46]

Scope of this Work
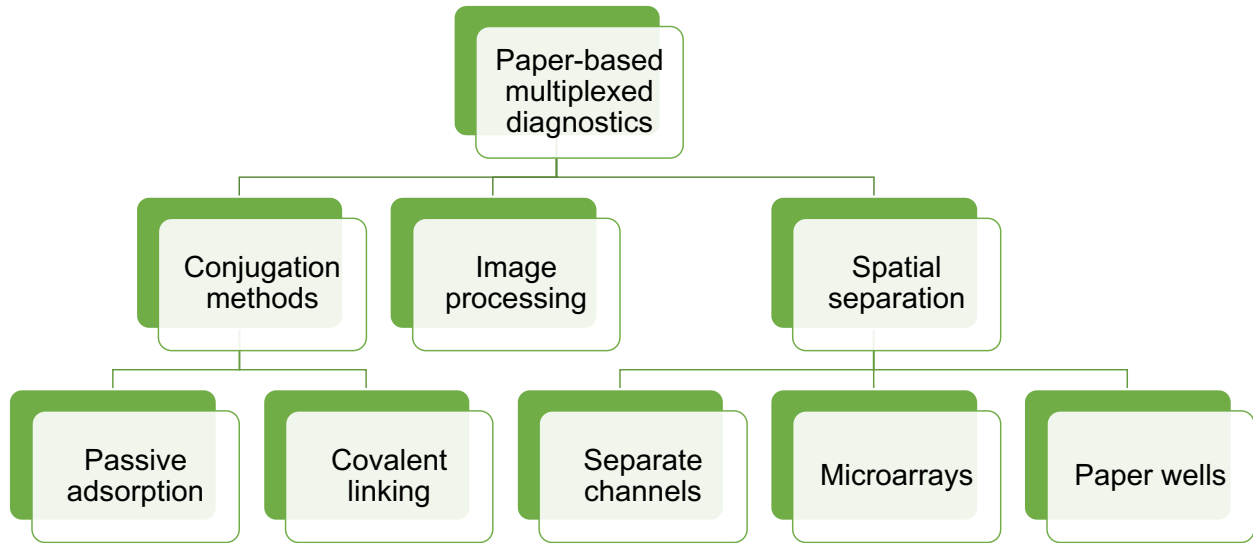
Figure 6. Potential alterations to paper-based multiplex diagnostic devices to reduce cross-reactivity.

In this work, methods to develop a multiplexed paper-based diagnostic assay with off-the-shelf commercially available reagents are explored as well as several different strategies to bypass cross-reactivity. The approaches discussed herein encompass alterations to conventional LFA design, including spatial separation methods and the use of image processing (Figure 6). Specifically, spatial separation of reagents by wax printed hydrophobic barriers on a traditional dipstick assay format, the study of different Ab-gold nanoparticle conjugation strategies, the design of a 3D printed and modified LFA cassette to house individual LFAs in parallel, and the use of competitive assays were probed to reduce or eliminate cross-reactivity.

Chapter II focuses on the study of colloidal gold distribution using inductively coupled optical emission spectroscopy (ICP-OES) within different brands of commercially available malaria LFAs. This research analyzes and compares how colloidal gold from AuNP conjugates travels and settles within different regions of an LFA and how this might impact test performance.

In **Chapter III**, individual in-house enzyme-linked immunosorbent assays (ELISAs) are developed for biomarkers indicative of bacterial infection. These ELISAs are used to screen commercial antibodies against each of these biomarkers as well as to serve as a gold standard assay to compare downstream results to. Chapter III also describes the development of individual dipstick assays for the same bacterial biomarkers along with challenges associated with designing a multiplexed paper-based diagnostic test. Lastly, this chapter explores modifications to the standard LFA format for the purposes of developing a multiplexed LFA and curbing cross-reactivity due to reagent mixing.

In **Chapter IV**, modifications to the standard dipstick assay format are explored for the purposes of developing a multiplexed dipstick assay and curbing cross-reactivity due to reagent mixing. This includes both chemical and physical changes to the test including AuNP conjugation methods, physical reagent separation, and alterations to test format. This chapter also describes strategies towards the development and analysis of a multiplexed diagnostic test for malaria fever differentiation.

Lastly, **Chapter V** summarizes the work discussed in Chapters II-IV and looks into the future of multiplexed POC diagnostics, including the benefits and drawbacks of current diagnostic development approaches. This chapter will include a discussion of diagnostic assay integration with mobile phones and other digital readers (one of the recent additions to ASSURED criteria) that are becoming more commonplace and increasingly necessary for sensitive and specific diagnostics in low-resource settings.

CHAPTER II

EVALUATION OF GOLD DISTRIBUTION ON LATERAL FLOW ASSAYS USING

INDUCTIVELY COUPLED OPTICAL EMISSION SPECTROSCOPY

Introduction[1]

As was discussed previously, when rigorously developed, LFAs meet the World Health

Organization's ASSURED guidelines,[47] making these immunoassays an ideal choice for

POC devices, particularly in resource-constrained settings. LFAs can utilize a range of

binding chemistries, however most implementations share similar components: a sample

pad (SP), conjugate pad (CP), nitrocellulose membrane (NC), and a wicking pad (WP)

(Figure 1A). The sample pad and conjugate pad are commonly composed of glass fiber

materials while the wicking pad is typically made of cellulose fibers.[48,49] In the classic

sandwich assay format,[50,51] capture reagents are immobilized onto the nitrocellulose

membranes in two locations: 1) a test line with capture agents against a specific antigen

or analyte (often monoclonal antibodies), and 2) a control line downstream from the test

line (often a species-specific secondary antibody, i.e., goat anti-mouse IgG antibody). A

detection reagent, typically a reporter element conjugated to a monoclonal antibody that

is specific to the target analyte, is deposited onto the conjugate pad. A variety of reporter

elements can be used to detect binding at the test and control lines,[48,52] including fluorophores, cellulose nanoparticles, dyed polystyrene microbeads, and, colloidal gold nanoparticles (AuNPs).[53,54] Colloidal gold is inexpensive, exhibits high stability, and generates signal that is detectable by visual inspection, rendering it one of the most widely used reporter elements.[48]
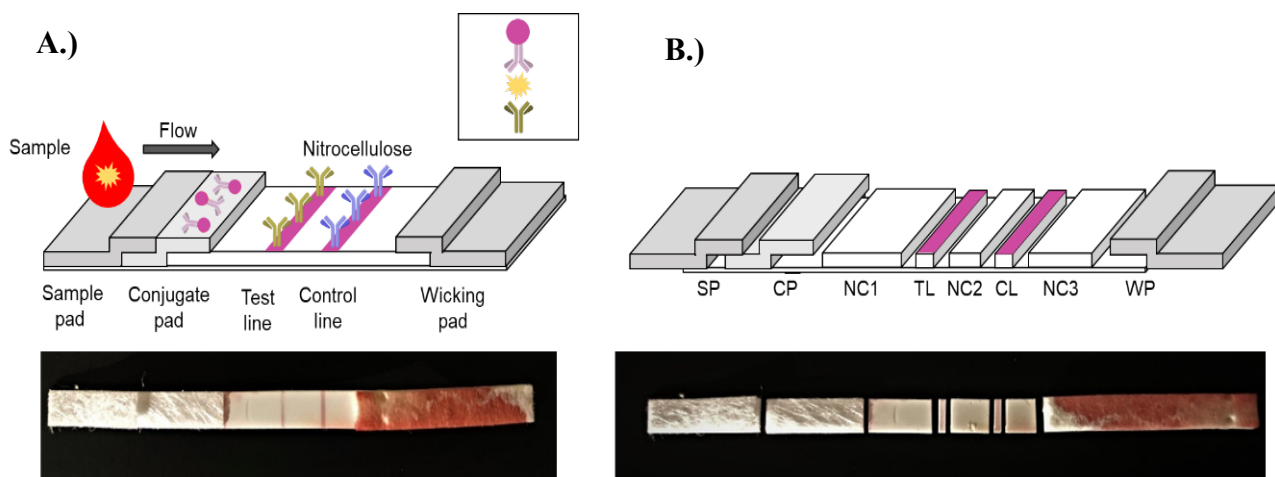
Figure 7. Sandwich LFA before and after segmentation: **A.**) Whole LFA before division; **B.**) LFA divided into sections before aqua regia digestion for ICP-OES measurement. (SP = sample pad, CP = conjugate pad, NC1 = first nitrocellulose pieces, TL = test line nitrocellulose, NC2 = second nitrocellulose piece, CL = control line nitrocellulose, NC 3 = third nitrocellulose piece, WP = wicking pad)

To perform a test, a sample is added to the sample pad where it flows down the test strip by capillary action, first interacting with the reporter elements on the conjugate pad, and then with the capture agents at the test and control line. When antigen is present in the sample, it binds to the antibody-AuNP conjugate (often referred to simply as "conjugate") and flows until the analyte-conjugate complex forms a sandwich with immobilized antibodies at the test line. Conjugate that is unbound at the test line continues to flow downstream and a fraction of it binds to the secondary antibody at the control line. In the absence of antigen, only the control line is detectable which serves as an operational

control for each test by validating that the sample and conjugate have moved past the test line. Residual sample and unbound conjugate continue to flow until absorbed by the wicking pad.[55]

While sufficient in many use-cases, LFAs have several drawbacks, including: test-to-test variability,[53,56] limited sensitivity[51,57], and varying specificity.[58] Recently, extensive experimental and modeling efforts have been undertaken to understand how to manipulate the signal of LFAs to maximize diagnostic performance.[59–62] Despite its apparent maturity, there is still much left to be discovered about the optimal LFA design, and most variables are empirically chosen on a per assay basis, including: material and reagent selection, buffer compositions, blocking conditions, and assay formats.

The ideal lateral flow design would be expected to have several key characteristics. First, the visual indicator at the test line should be proportional to the concentration of the analyte in the sample. Second, sufficient conjugate should bind to the control line to indicate that the test has performed as expected. Third, all the visual indicator initially at the conjugate pad should be entrained by the flow and none should be captured non-specifically at locations other than the test and control lines of the lateral flow strip. A test that exhibits each of these features would encompass the ideal redistribution of colloidal gold on the LFA after use and achieve the best limit of detection (LOD) with the selected reagents.

In this work, we used inductively coupled plasma optical emission spectroscopy (ICP-OES) to quantify the distribution of gold before LFA use and its redistribution after LFA use of three commercially available *Plasmodium falciparum* (*Pf*) malaria LFAs. ICP-OES is a highly sensitive analytical technique that determines the elemental composition of a sample by measuring the emission spectra when a solution is introduced to plasma. This technique demonstrates a wide linear dynamic range, experiences little chemical interference and background emission, is highly robust to matrix effects, and shows exceptional sensitivity in the parts-per-billion concentration range for most elements.[63] The use of ICP-OES in this work enables spatial analysis of gold content before and after lateral flow use. In this study, ICP-OES was utilized in conjunction with a lateral flow reader (LFR) for the quantitative evaluation of the LFAs with the goal of measuring platform fundamentals of three existing commercial products and identifying features where improvement might lead to enhancements in the limit of detection of LFAs.

Materials and Methods

LFA Selection

Three brands of LFAs for the diagnosis of malaria were selected from the list of WHO-evaluated diagnostic tests for *Plasmodium falciparum (Pf)*.[29] These LFAs were operated according to corresponding manufacturer protocols, and the completed tests were analyzed using an LFR to obtain quantitative signals for the test and control lines prior to analysis with ICP-OES. The LFA brands are denoted as: Brand A, Brand B, and Brand C. The purpose of this work is to illustrate the use of analytical techniques to understand

and improve LFAs. Therefore, each manufacturer is kept blinded so as to keep the primary focus on the methods and resulting data analysis.

Materials and Reagents

Gold standard for ICP (999 mg/L ± 2 mg/L) was purchased from MilliporeSigma (Burlington, MA, USA). Trace metal grade hydrochloric acid (HCl) and nitric acid (HNO$_3$) were purchased from Fisher Scientific (Hampton, NH, USA). Polyvinylidene fluoride syringe filters, 13 mm, 0.22 μm, were purchased from Tisch Scientific (North Bend, OH, USA). Deionized water used in this study was purified with a resistivity greater than or equal to 18.2 MΩ•cm. Pooled human whole blood with anticoagulant citrate phosphate dextrose was purchased from BioIVT (Westbury, NY, USA). An in-house malaria *Pf* D6 strain culture was used to evaluate the LFAs.

LFA Protocol

LFAs were performed according to each manufacturer's instructions to detect *Pf* Histidine-rich protein 2 (HRP2) antigen. Briefly, 5 μL of sample was added to the test, followed by 5 drops of running buffer. The sample and buffer took 20 minutes to completely flow the length of the membrane. The *Pf* culture aliquots used were at a parasitemia of 43,600 parasites/μL (p/μL) which, for this parasite culture, corresponds to 97.2 nM HRP2. Parasite concentrations were prepared by spiking varying amounts of *P. falciparum* into pooled human whole blood. This method was utilized to closely mimic positive and negative patient samples in the evaluation of commercial LFAs. While individual field-collected patient specimens will have variability that is homogenized with

pooled human whole blood, the inherent biochemical and rheological complexity of the sample matrix is retained. Previous work has used malaria parasite culture spiked into human whole blood to create mock patient samples, with comparable results to field-collected samples.[64,65] Parasite concentrations of 0, 25, 50, 100, 200, 400 and 800 p/µL were studied for Brand A. Test Brands B and C were evaluated on a subset of these parasite concentrations: 0, 25, 100 and 800 p/µL.

LFA Flow

LFAs from Brands A-C were run in triplicate following manufacturer's instructions and a video was taken using an Apple iPhone 11 Pro. 150 µL of running buffer from the corresponding manufacturer was added to the sample pad of the test and allowed to flow. Digital frame-by-frame analysis was performed in ImageJ to identify the leading edge of the fluid front on the LFAs.[66] The distance from the sample pad to that of the fluid front was measured in pixels and converted to millimeters using the in-frame ruler as a reference. The time for the fluid front to reach the test line was measured in ImageJ, starting from the time that the sample was added to the well.

LFR Operating Conditions

Upon completion, the LFAs were analyzed by a Qiagen ESEQuant LFR (Stockach, Germany) operating in reflective mode on the E1/D2 channel. In addition to the previously mentioned concentrations, unused LFAs were also evaluated. For the test and control line, signal intensity was measured in mm*mV. Each test was measured from 0 to 60 mm in the LFR, starting from the wicking pad and ending at the sample pad. The signal

generated by the conjugate at the test and control lines were quantified by integrating the area under the signal curve, using a fixed baseline and including 1 mm upstream and downstream of the peak in the line scan.

Preparation of LFA Strips for Gold Digestion

Each section of the LFA was cut by hand with stainless steel razor blades (Figure 7), resulting in eight sections: sample pad (SP), conjugate pad (CP), the first section of nitrocellulose (NC1), test line (TL), the second section of nitrocellulose (NC2), control line (CL), the third section of nitrocellulose (NC3), and wicking pad (WP). Each section was placed into an individual microcentrifuge tube. Unused LFAs were also analyzed in this study, and in the absence of liquid sample, there was no test or control line on the test, resulting in the digestion and ICP-OES analysis of only four sections: SP, CP, NC, and WP.

Digestion of LFA Components for ICP-OES

Solutions of aqua regia were prepared using 3-parts HCl to 1-part HNO_3 (v/v) and 0.667 mL of the mixture was added to each tube for the dissolution of gold. Fresh solutions of aqua regia were made as necessary and remaining aqua regia was disposed of appropriately.[67] Each tube was vortexed and left to digest for 3 hours. Preliminary results suggested that a longer digestion time (up to 24 hours) had no effect on gold extraction from the LFA sections (data not shown). Any material that appeared pink from the gold content turned white after digestion, suggesting that gold was effectively extracted from the nitrocellulose. The digestion of some test sections resulted in a fibrous solution and

required filtration through 0.22 μm PVDF filters. The samples were then diluted with 4.333 mL DI water and filtered through PVDF syringe filters. The samples were immediately analyzed by ICP-OES after acid digestion and filtration.

ICP-OES Operating Conditions

The amount of gold extracted from each section of the LFA was quantified with a Perkin Elmer Optima 7000 DV ICP-OES (Perkin Elmer, Waltham, MA, USA). Table A1 lists the instrument's operating conditions. A sample matrix blank was comprised of 13.3% aqua regia in DI water. In order to analyze the colloidal gold on the LFAs, five ICP-OES standards of 1.0, 0.1, 0.01, 0.001 and 0.0001 ppm Au at a wavelength of 267.595 nm were utilized to generate standard curves (n=3) (Figure A1) for each individual experiment.

Calculation of Minimal Amount of Gold for Visual Detection

The minimum amount of gold necessary for visual detection was calculated using (Eq. 2), where r is the radius of the gold nanoparticle, ρ is the true density of the colloidal gold solution, V is the sample injection volume, and TL_{Au} is the gold concentration found on the test line at the lowest parasite concentration (Figure 13). For this calculation, the following assumptions were made: spherical gold nanoparticles were 40 nm in diameter, 19.32 g/cm^3 density, and a sample injection volume of 0.5 mL.

$$\text{Minimum amount of gold} = \frac{TL_{Au}V}{\left(\frac{4}{3}\pi r^3\right)\rho} \qquad (2)$$

Statistical Analysis for Limit of Detection and Coefficient of Variation

The LOD for both the LFR and ICP-OES were calculated using $3\sigma/\kappa$, where σ is the standard deviation of the blank and κ is the slope of the calibration curve. Each sample was performed in triplicate. The average and standard deviation for each section of the LFA for each concentration were calculated. A coefficient of variation (CV) was calculated using $(\sigma/m)*100$, where σ is the standard deviation and m is the average of the data set. The total gold content was calculated by adding the amount of gold found on each of the constituent sections together. The average and standard deviation were calculated for the total gold content.

Statistical Analysis for Distribution of Gold Content

Statistical analyses were performed in the GraphPad Prism software v. 9.0. Statistical significance was determined using two-way analysis of variance (ANOVA) with *post hoc* Tukey's multiple comparisons test comparing total gold concentration at varying parasite concentrations within and between brands. One-way ANOVA with *post hoc* Tukey's multiple comparisons test was used to compare gold concentration on conjugate pads of different brands.

Results and Discussion

LFA Flow Results

Anticipating that the rate of fluid flow can impact binding efficiencies, a study was performed to examine how fast gold conjugate travels each test strip for all three brands (Figure 8). Initially, visibility of the fluid front was obscured by the opaque cartridge that

houses the LFA. In this region, the buffer wicks from the sample pad to the conjugate pad, where it resuspends dried gold conjugate. From there, the gold conjugate is wicked onto the nitrocellulose membrane, where it is eventually visible in the LFA's test window. The fluid fronts on LFAs from Brand B were the first to emerge from the viewing window, followed by Brand C, and finally, Brand A. The time to reach the test line location (denoted as a dashed line in Figure 8) was analyzed and found that gold conjugate from Brand B tests reaches the test line in approximately 9 seconds, which is faster than both Brand A (14 seconds) and Brand C (17 seconds). `
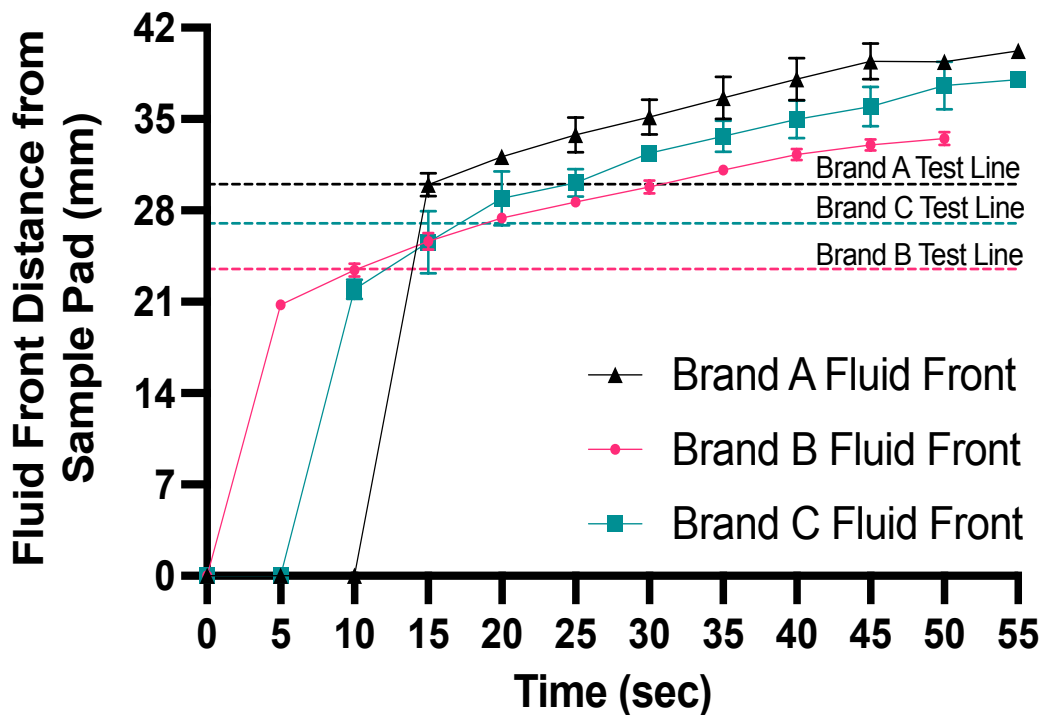
Figure 8. Time study to analyze how fast (in seconds) gold conjugate flows down the membrane (in mm) to the control line and wicking pad for each brand. The test line location for each brand is denoted on the graph as a dashed line. Some error bars are smaller than width of marker.

LFR Results

In these experiments, a dilution series of *Plasmodium falciparum* was added to commercially available Brand A LFAs. Representative photos of these tests can be found in Figure A2. A faint test line begins to visually appear at a concentration of 25 p/µL. The test line becomes visibly darker with increased parasite density. The intensity of the test and control lines were then analyzed using an LFR (Figure 9). As expected, only a control line was observed for the blank sample. The area under the intensity linescans from the LFR for the test line signal increases as parasite concentration in the sample is increased (Figure 10). Over the range of concentrations evaluated (0 p/µL – 800 p/µL), the area for the test line signal is approximately linearly proportional to analyte concentration.

Figure 9. Representative LFR signal profiles for individual Brand A LFAs at 0, 25, 100, and 800 p/µL. The LFR obtains signal by scanning from the wicking pad to the sample pad.

A standard curve was generated in order to determine the lowest detectable signal. A LOD for this method was calculated t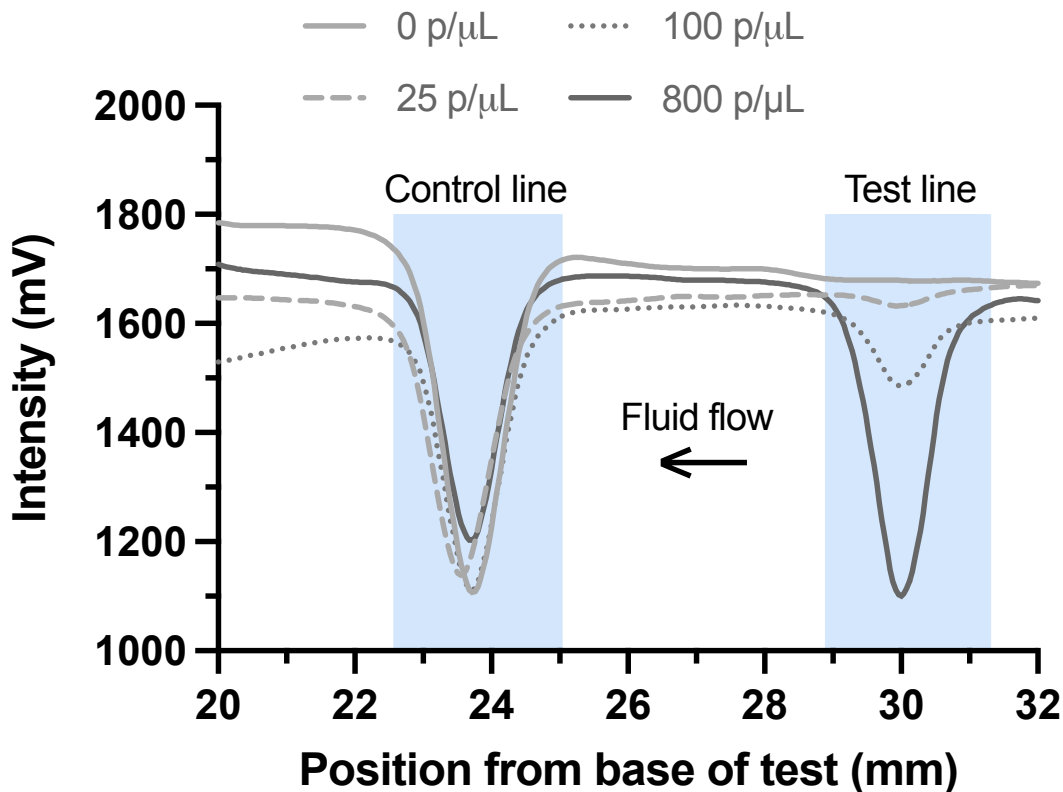o be 130 p/μL (denoted as a horizontal dashed line on Figure 10), which is similar to other literature reports.[29,68–70] The data demonstrates a directly proportional relationship between parasite concentration and test line intensity. Brand B and Brand C were also analyzed via LFR. As expected, parasite concentration and test line area intensity were shown to be directly proportional for these brands as well. The only observable difference was clearance of blood on the nitrocellulose membrane in Brand B that led to a decreased test line area in comparison to Brands A and C (Figure A2).

ICP-OES Results

After test completion and LFR analysis, LFAs were cut into their constituent sections (Figure 7B) and digested in aqua regia prior to conducting ICP-OES. The amount of gold present on the conjugate pad of an unused LFA was first analyzed for each brand. As this is the only place conjugate is deposited, this value represents the total amount of gold found on each LFA. The conjugate pad contained the most amount of gold for all brands (Figure A4), as expected. Brand B contained 72% more gold than Brand A, and 44% more gold than Brand C, highlighting the variation in proprietary formulations of the LFAs. Only 2% of gold was detected on the sample pad of Brands B and C. Finding gold dispersed throughout an LFA before use may indicate improper storage as moisture can cause migration of the gold. The relatively small amount found just outside the conjugate pad is likely a result of the physical overlap between the conjugate and sample pads, more so than a suggestion that the tests were improperly stored.
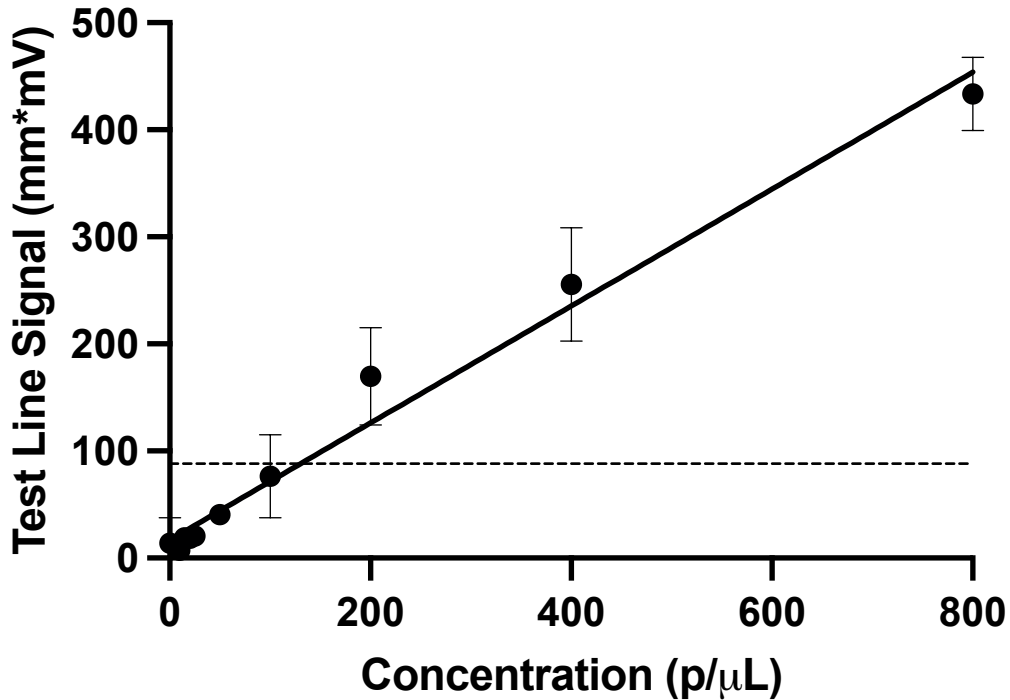
Figure 10. LFR standard curve measuring test line signal at varying parasite concentrations for Brand A.

To evaluate intra- and inter-brand manufacturing variability, 15 additional conjugate pads were cut from unused tests and gold content was analyzed by ICP-OES. This data was combined with the conjugate pads from the previous unused tests to obtain a total of 18 samples for all three brands (Figure 11). For Brand A tests, the gold content on conjugate pads ranged from 0.092 ppm to 0.157 ppm Au, with an average of 0.129 ppm ± 0.017 ppm Au. There is some fluctuation in gold content among the 18 samples, with a CV of 13.5%, illustrating variability between tests. The total gold found on Brand B was almost three times higher than Brand A at an average of 0.381 ppm ± 0.053 ppm Au, where the CV was 14.0%. Brand C had a slightly lower average at 0.233 ppm ± 0.040 ppm Au with a CV of 17.2%. Comparison of CV values between brands demonstrates that Brand C has higher test-to-test variability compared to Brands A and B. There is also

clear variability between manufacturers as demonstrated by the higher amount of total gold found on Brands B and C LFAs (Figure 11).
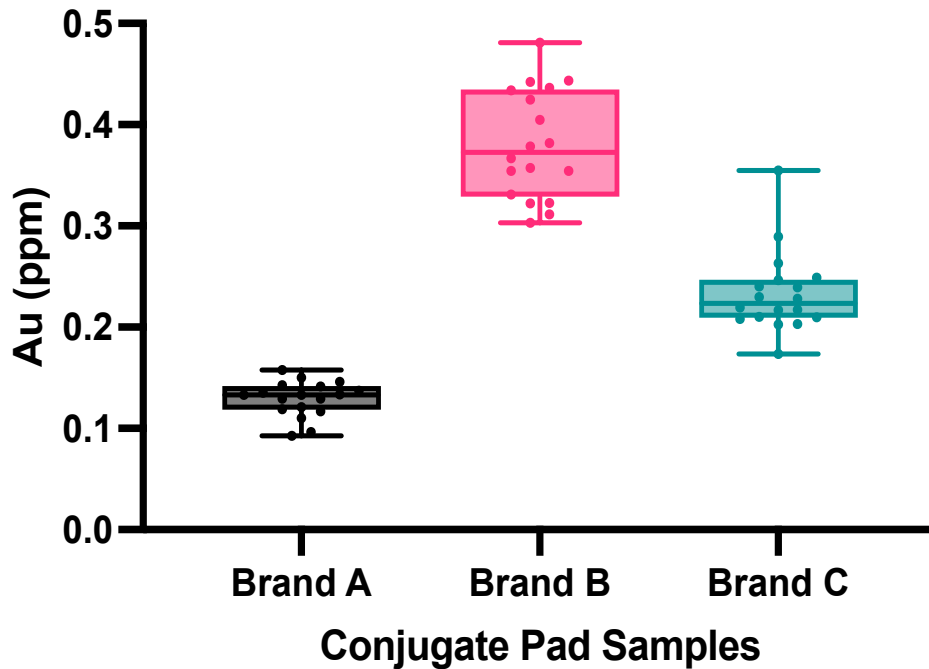
Figure 11. Comparison of gold content on 18 same-manufacturer conjugate pads for Brand A, Brand B and Brand C. Significant differences were found between all three brands ($p < 0.0001$).

The data shown demonstrates a discrepancy in the manufacturing process during gold deposition, leading to possible differences in test outcome. With initial gold content on an LFA being directly linked to the potential signal at a test line, and hence a major determinant for test sensitivity and limit of detection, along with an increased demand from test users for quantitative results,[54] there is an opportunity for improved manufacturing procedures to more uniformly deposit conjugate.
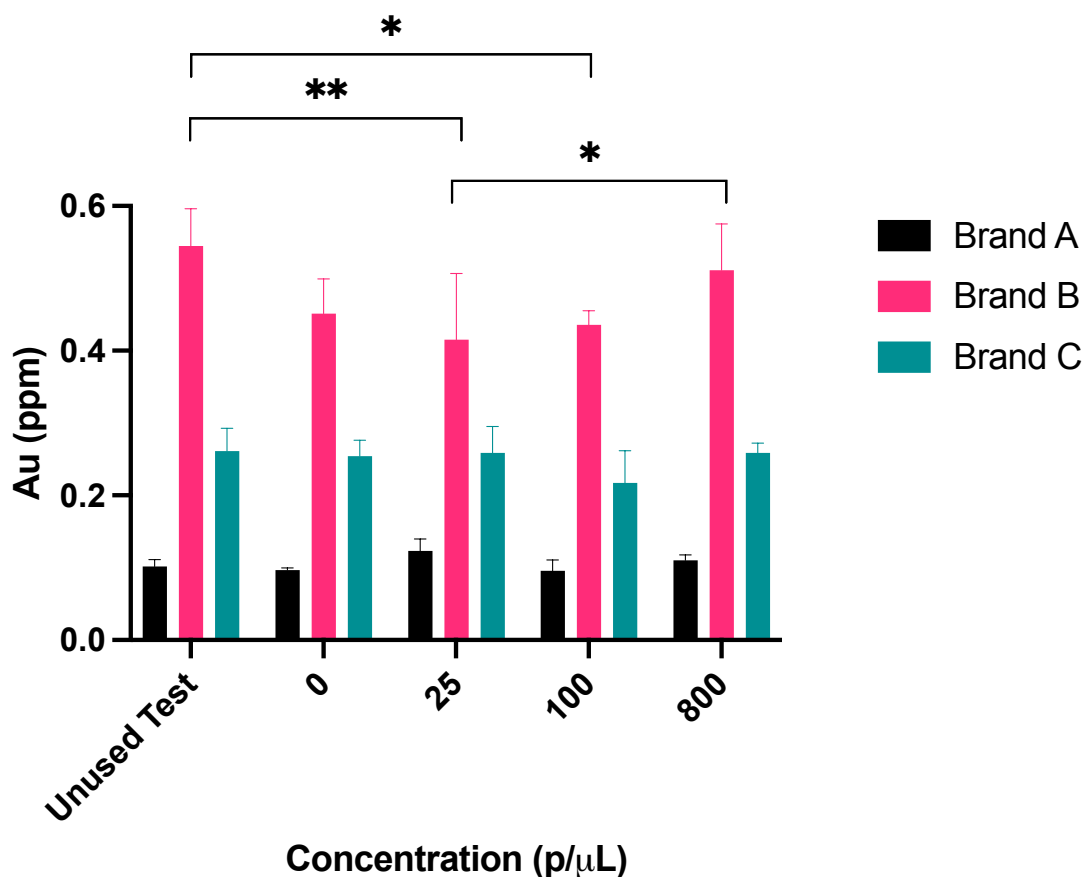
Figure 12. Total gold content as a function of parasite concentration and brand of test (n=3). In the above figure, * represents $p < 0.0427$, ** represents $p = 0.0032$. All other interactions within a single brand were found to be nonsignificant. Total gold concentration between brands was deemed statistically significant ($p < 0.0001$)

A mass balance of gold on the LFAs was calculated for each LFA that was run (Figure 12) by adding together the gold found on each section of the LFA. It was expected that the mass balance (total gold redistribution) would remain approximately constant, regardless of target analyte concentration, within the variations seen on the dry conjugate pads analyzed in Figure 11. This hypothesis was true for all brands of LFAs tested. Gold content for Brand A ranged from 0.090 ppm to 0.123 ppm with an average of 0.106 ±

0.011 ppm, with CVs varying from 3.13% (0 p/µL) to 15.2% (100 p/µL). It is observed that any Brand A test should have roughly 0.105 ppm total gold content, regardless of the analyte concentration. As noted before, Brands B and C contained more gold than Brand A (Figure 12). The tests from Brand B had between 0.386 ppm to 0.545 ppm total Au when comparing both used and unused tests, demonstrating a large amount of test-to-test variability within the manufacturer. On average, Brand B resulted in 0.466 ± 0.038 ppm gold per test. Moreover, an average of 0.250 ± 0.019 ppm of gold was reported for tests from Brand C, with gold content values ranging from 0.217 ppm to 0.261 ppm gold. As expected, overall gold remained constant, within the amount deposited on the conjugate pads of unused LFAs, for all brands – i.e., the total mass of gold does not change with LFA use.

To identify the amount of gold that could be detected on each of the LFA components, ICP-OES standard curves were generated for each separate experiment performed, which resulted in a LOD of 0.0039 ppm Au for Brand A and LODs of 0.0023 ppm Au for Brands B-C (depicted as horizontal dotted lines in Figure 13A-C). These LODs fall just below the amount of gold found on the test line of a test run with a 25 p/µL sample. This indicates that parasitic concentrations less than 25 p/µL would likely be undetectable by this method. The use of ICP-OES to analyze LFA's afforded almost a 5-fold improvement in sensitivity compared to the LFR. While this analysis approach is more sensitive, we are not suggesting the use of ICP-OES for point-of-care analysis, as this technique is cost-intensive and requires laboratory infrastructure and trained personnel. Rather, we have identified that even with an instrument that can measure on the order of parts-per-billion,

there is a limit for how much of a performance improvement can be extracted. This five-fold increase, while substantial, suggests that the major limitation, where improvements can generate larger returns, remains the signal generated from the POC device. As a result, ICP-OES can be used to aid the manufacturing process of LFA's to focus on increasing the sensitivity of the device, rather than improving detection instrumentation.

Additionally, our studies indicate that a minimum of 2.49 ng Au (3.85×10^6 Au nanoparticles) is required (from Eq. (2)) on the test line to achieve a visible signal (at 25 p/µL) for Brand A. This calculation provides an estimate for the amount of gold nanoparticles necessary to obtain visual signal at a test line that is 5 mm wide and 1 mm thick, the area of the segment that was cut for test line digestion in these experiments. We hypothesize this calculation to be similar for every brand at the resulting limit of detection. This analysis derives from straightforward calculations, and is subject to many theoretical parameters (i.e., antibody coverage on gold nanoparticles, multiple epitopes on target biomarkers). However, it provides an approximation approach for quick feasibility calculations to determine if a target analyte is in sufficient concentration for detection.

As expected, the amount of gold conjugate bound at the test line increases with concentration regardless of brand, while the amount of gold on the control line remains relatively constant. For Brand A samples containing a visible test line (25-800 p/µL), the nitrocellulose sections closest to the wicking pad, the second section of nitrocellulose (NC 2) and the third section of nitrocellulose (NC 3), contained an amount of gold below the

A.)

B.)

C.)
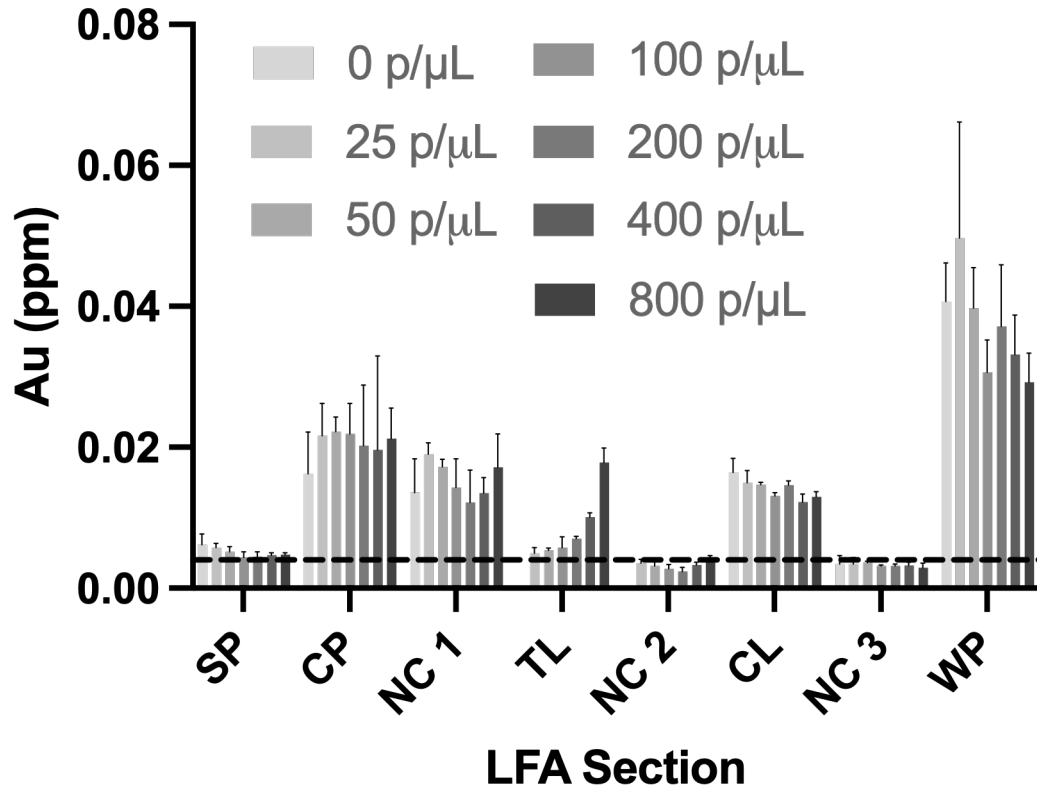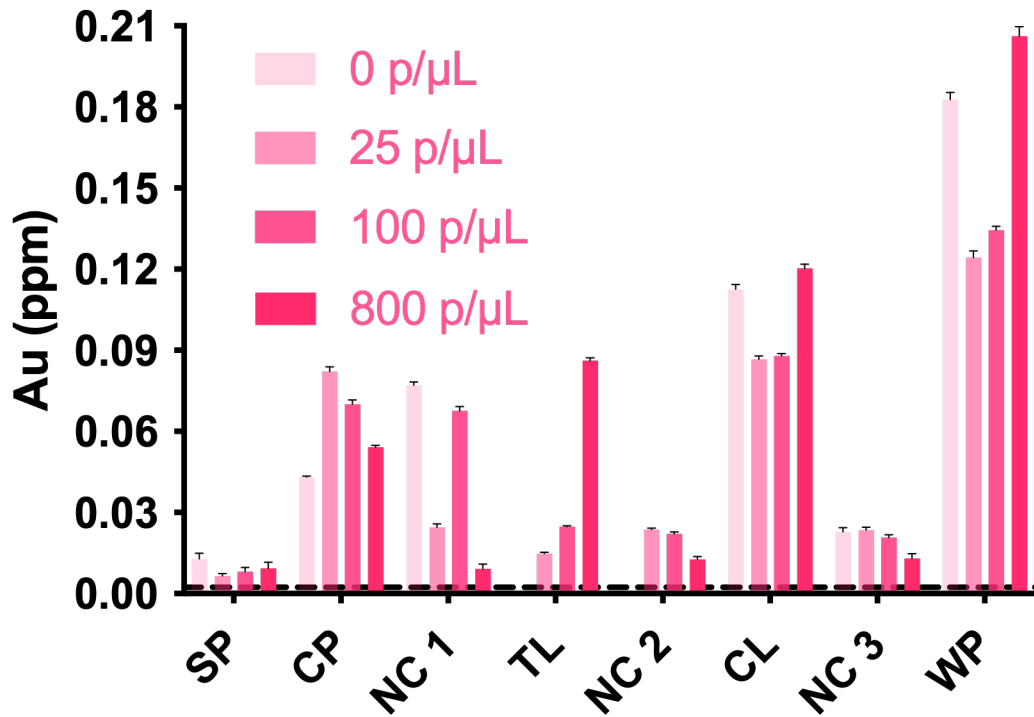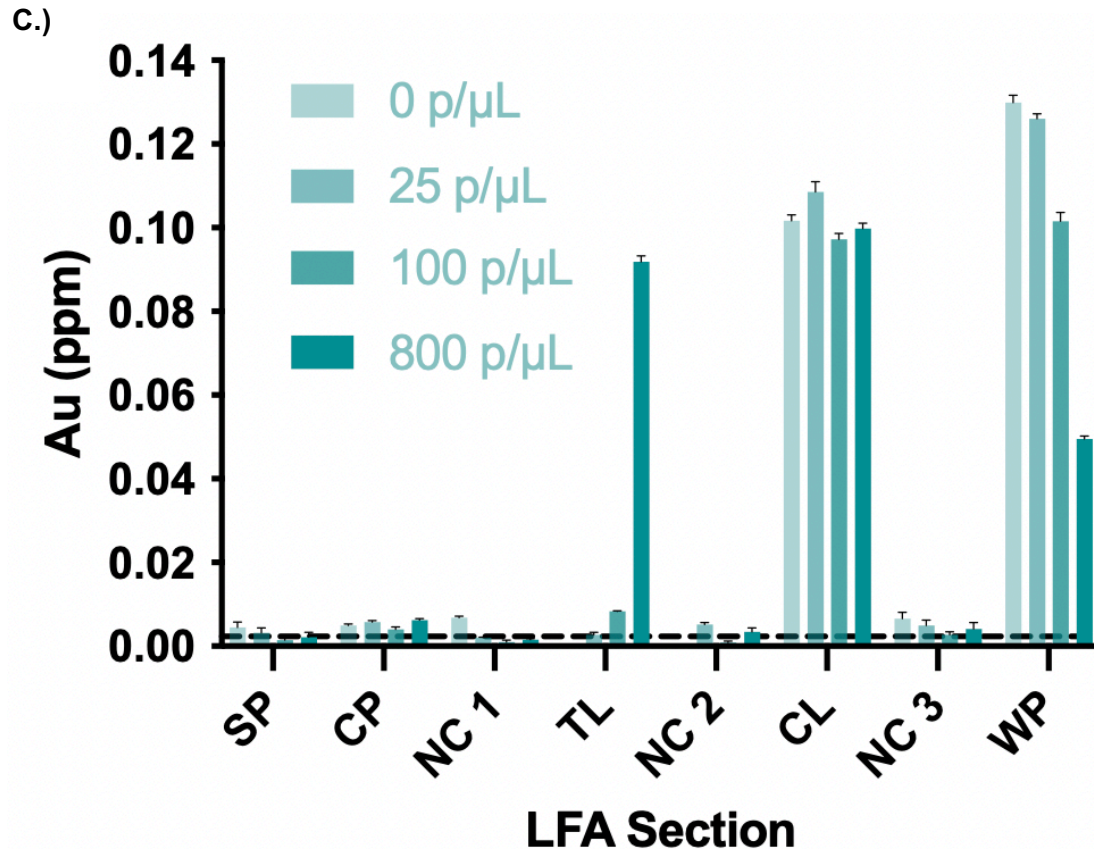
Figure 13. The gold concentration within each section of the LFAs as a function of brand and parasite load. **A.)** Brand A; **B.)** Brand B; and **C.)** Brand C.

In contrast to Brands A and B, the amount of gold on numerous sections for Brand C was below the LOD (0.0023 pm Au). Roughly 2% of the gold conjugate remained on the CP for Brand C, which is one tenth of the amount of gold found on the CP for Brands A-B, demonstrating some variability in design. In contrast to Brands A-B, Brand C had a more drastic change in gold content on the TL when moving from low to high concentration (Figure 13C). This resulted in barely visible test line for the low concentration and amount of gold very close to the LOD of the ICP-OES (0.0023 pm Au). For this brand, 48% of the total gold conjugate was contained to the WP for 0-100 p/μL, except at 800 p/μL, where only 2% was identified. This discrepancy likely correlates with the higher gold content

found on the test lines for those samples. Although there was minimal non-specific binding for Brand C, a higher concentration of analyte was necessary to identify a true positive result, exemplifying a need for LFA design optimization to maximize binding potential on the test and control lines at low concentrations. The test line signal intensity would be expected to plateau as parasite concentration increases further, but the point of saturation would be different for each LFA analysis instrument. Further increasing the parasite concentration would eventually lead to a decrease in signal due to the Hook effect. It appears that the concentrations evaluated in this study are well within the linear dynamic range of the instrumentation.

In this work, we demonstrated experimental approaches to determine two key parameters of this relationship: the initial concentration of detection gold nanoparticles, and the speed at which reagents wick down the nitrocellulose membrane. Other analytical techniques, like biolayer interferometry and surface plasmon resonance, could be used to measure binding kinetics.

Still, commercial development of LFAs must consider other metrics beyond optimal test sensitivity and specificity, including time-to-result and cost. For instance, it is reasonable to assert that manufacturers may elect to use more gold conjugate on a faster membrane to reduce the time-to-result. In contrast, reduction of the amount of colloidal gold may not have a large effect on test signal when the target biomarkers are in abundance, which would be a reasonable approach to lower costs. While these other factors must be

considered when constructing an LFA, underlying knowledge of the design selections made can improve both device performance and speed to market.

Conclusion

LFAs have been globally used as point-of-care diagnostic tools for decades, but the empirical optimization of new tests remains slow and expensive. Analytical techniques can improve the development process by providing a more fundamental understanding of current LFA design that can lead to more strategic test development. Inefficiencies were found in the design of three different commercial devices, all of which counter ideal LFA characteristics that would lead to optimal performance. In this report, we highlight the use of ICP-OES to measure the redistribution dynamics of colloidal gold within LFAs. We are not suggesting this instrument be used to analyze tests at the POC (due to size, instrument and maintenance costs, weight, and power requirement). Rather, we envision ICP-OES be used to inform manufacturing decisions in the future, prior to test deployment. As a demonstration, we use ICP-OES to measure the widely understood, but poorly quantified manufacturing variations. Comparisons of gold binding and flow speed across different test brands shows that test developers have flexibility in selection of parameters to meet their technical requirements. The use of ICP-OES allowed for a precise, comprehensive examination of the binding efficiencies of gold conjugate, and can be used in conjunction with modeling efforts to improve test development. Ultimately, this may lead to POC devices with improved LOD, less variability among tests and manufacturers, and ultimately, reduced cost and faster time to market.

Future Directions

The analysis of colloidal gold distribution within different brands of malaria LFAs that was described in this work is just one step towards systematically understanding how empiric LFA development might impact LFA performance. Since LFA manufacturing and optimization processes are largely not described in the literature, LFAs that are designed to detect other illnesses other than malaria could be analyzed in a similar way as what was done here to determine the amount of discrepancy in gold distribution across different manufacturers and LFAs for varying disease states. Depending on the results of that study, LFA brands that have increased gold retention at the test and control lines could be further analyzed to determine if there is a technique or specific material(s) being used by that manufacturer to eliminate nonspecific binding on other parts of the test. Furthermore, colloidal gold is just a single component in a dynamic system of multiple reagents and moving parts. To further determine the cause of AuNP-Ab retention on different parts of an LFA, in-house LFAs could be developed for malaria with varying conjugate pad materials, nitrocellulose membranes, and wicking pads. ICP-OES could then be used to analyze and compare the gold distribution among LFAs made with different components. These results could be compared against those obtained for the commercial LFAs. This study could also give further insight as to how the material of each of the components might affect both gold retention and overall test sensitivity.

Acknowledgements

CHAPTER III

PROCESS AND CHALLENGES OF THE DEVELOPMENT OF A MULTIPLEXED

DIPSTICK ASSAY

Introduction

Antibiotic resistance remains one of the largest threats to global health, attributing to more

than 35,000 deaths yearly in the United States.[71] Leading reasons for this resistance

include antibiotic overuse and misuse, extensive agricultural use, and a stalled antibiotic

pipeline. The Centers for Disease Control and Prevention (CDC) estimates that at least

30% of antibiotics prescribed in outpatient settings in the United States are unnecessary;
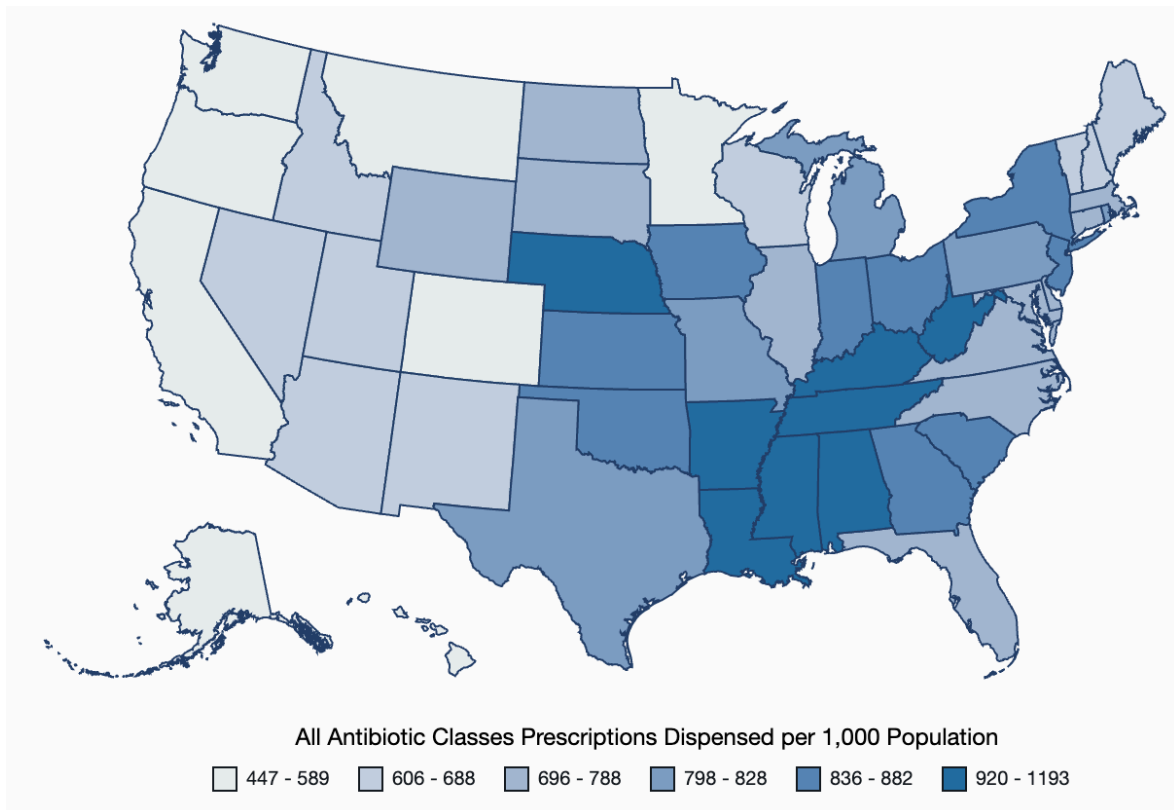
Figure 64. Outpatient prescription rate of all antibiotic classes dispensed in United States pharmacies (CDC, 2019).

in 2019, there were approximately 250 million outpatient antibiotic prescriptions dispensed.[72] Furthermore, it is estimated that 80-90% of human antibiotic use occurs in this setting and that the southern United States has the highest outpatient antibiotic prescription rate (Figure 14).[73] Additionally, regional antibiotic prescription rates in the United States correlate with regional antibiotic resistance percentages (Figure 15). This antibiotic overuse can largely be attributed to physicians prescribing medications prior to receiving notice of a confirmatory bacterial infection via laboratory results. Due to increased antibiotic resistance, there is a global focus on antibiotic stewardship—the effort to measure and improve physician prescription practices as well as patient antibiotic use.[73] The last decade has seen a shift towards using host biomarkers as a tool for guided antibiotic therapy, since clinical presentations can look very similar for infections caused by varying agents. By investigating the roles of host proteins involved in the human immune response, clinicians may use these markers to make more informed antibiotic prescription decisions.
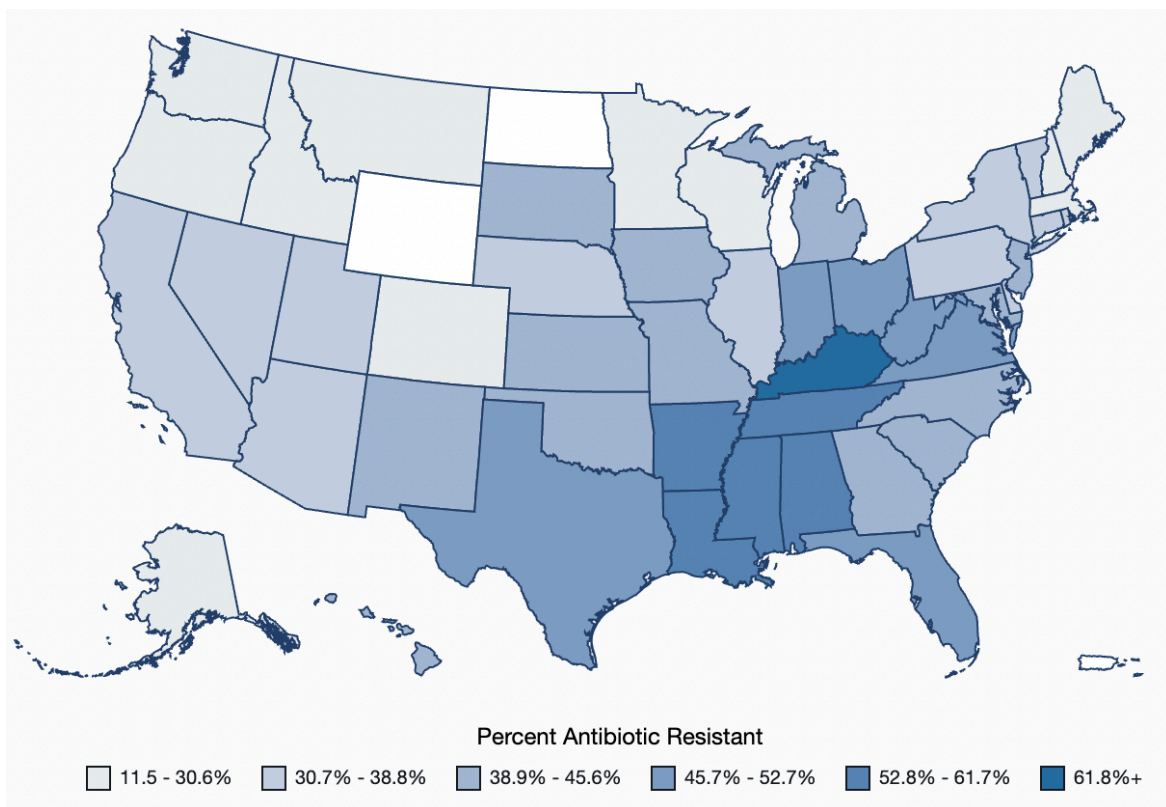
Figure 15. Variation in percent methicillin resistance among *Staphylococcus aureus* causing all event types (CDC, 2019).

Procalcitonin (PCT), C-reactive protein (CRP), and neutrophil gelatinase-associated lipocalin (NGAL) were chosen as biomarkers of interest in this work due to these proteins being host biomarkers that have been shown to be indicative of bacterial infection etiology and severity, depending on each biomarker's specific role in the host immune response. The most popular and widely studied bacterial biomarker is CRP, an acute-phase reactant produced primarily by the liver.[74] This marker has been shown to be more elevated in cases of bacterial infection when compared to viral infection. Increased CRP levels show a correlation with the severity of infection and quickly fall with the removal of the inflammatory stimulus.[75,76] Two other acute-phase reactants are PCT and NGAL. PCT is

a peptide precursor of calcitonin that is at low or undetectable concentrations in the serum of healthy individuals. In cases of bacterial infection however, PCT can be detected as early as 4 hours after pathogen invasion and can increase up to 5,000-fold in severe infections.[77–79] Several studies have investigated the diagnostic accuracy of PCT and have found it to be a more specific and sensitive marker than CRP with great potential as a tool for guiding antibiotic stewardship.[80,81] Another bacterial biomarker, NGAL, also referred to as human neutrophil lipocalin or lipocalin-2, is a glycoprotein released from activated neutrophils in response to bacterial infections that has also been shown to have serum levels correlating to that of CRP.[82–86]

It should be noted that these biomarkers are not as valuable in differentiating bacterial infection from viral infection when detected alone compared to when they are analyzed within a "signature" assay in combination with other appropriate markers. This is due to CRP, PCT, and NGAL levels rising in the event of any inflammatory stimulus or in the case of NGAL, acute kidney injury. Multiple studies analyzing several host biomarkers simultaneously for infection etiology differentiation have revealed signature assays to be more specific and sensitive compared to single immunoassays.[87–90] For example, Oved *et al.* showed a host-proteome signature consisting of three host biomarkers significantly outperformed any single protein evaluated for the differentiation of acute bacterial and viral infections, with an area under the curve (AUC) of close to one (an indication of high diagnostic sensitivity and specificity) (Figure 16).[89]
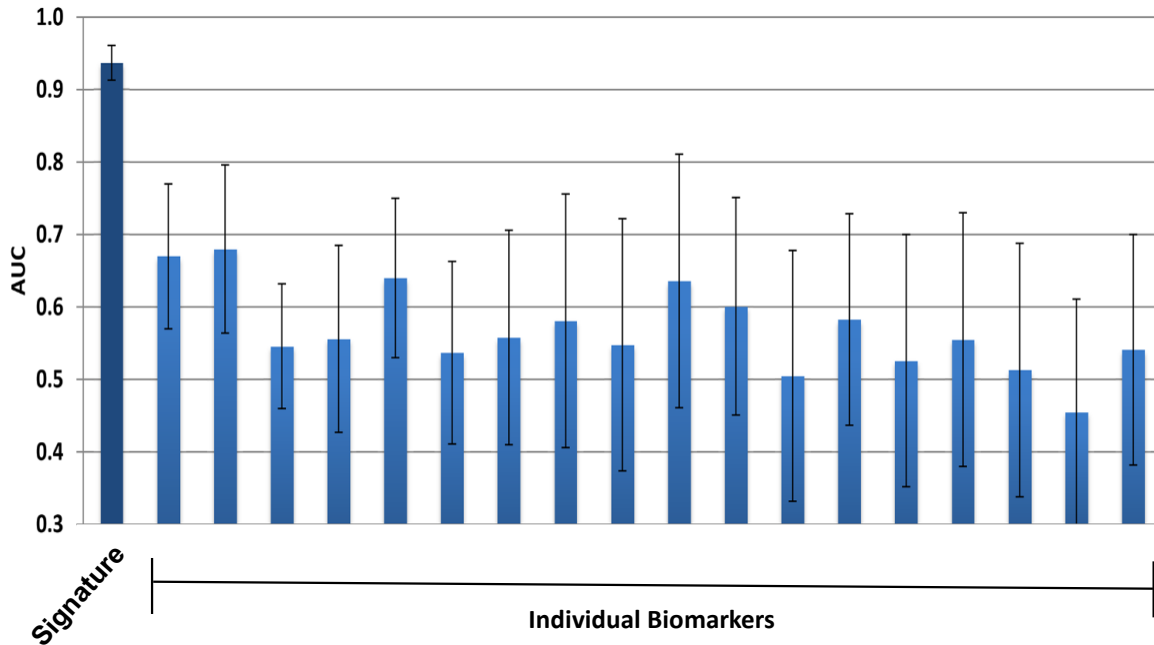
Figure 16. Analysis of AUC for a signature of three host biomarkers compared to the AUC for individual biomarkers. Adapted from Ref. 88.

Current ELISAs are available to physicians for the measurement of relevant host biomarkers that can be used to inform prescription decisions. ELISAs have long been considered the gold standard for biomarker (antigen) detection and quantification in clinical laboratory settings. These plate-based immunoassays are sensitive, reliable, and versatile.[91–93] There are four major ELISA formats: indirect, sandwich, direct, and competitive. All these formats rely on specific antibodies to detect the target antigen via antibody-antigen interactions. The format used for an application depends on the size of the target antigen, available antibodies, and the degree of assay flexibility required.[94] ELISAs may also be used for antibody detection, such as in the case of antibody development and titer measurement.

The general procedure of an ELISA (Figure 17) includes first coating the bottom of a microwell plate with antigen or antibody, depending on the format, followed by a blocking step to ensure any remaining free sites on the bottom of the plate are blocked. Standards containing a known amount of antigen are used along with the samples being tested to quantitatively detect the target antigen in a sample. The last step is the detection step which involves a colorimetric readout resulting from the reaction between secondary antibodies labelled with enzymes, most often horseradish peroxidase (HRPx) or alkaline phosphatase, and their corresponding substrates. Optimizations in ELISA development and the need for more sensitive detection has also resulted in fluorescent and luminescent readouts. There are also necessary washing steps in between the major steps described above to remove any unbound reagents. While ELISAs remain a mainstay in clinical laboratories, they take several hours to obtain a result due to lengthy incubation times and recurring washing steps. This has led to increased efforts for the expansion of POC diagnostic tools, such as LFAs described previously.

Due to differences in the reaction substrates of ELISAs and LFAs (wells versus paper), assay conditions of one may not necessarily translate to the other seamlessly. However, it is helpful to use ELISAs for initial antibody screening as well as a control measure to compare results in downstream LFA development and validation. This chapter will first focus on the development and optimization of individual sandwich ELISAs and individual dipstick assays (precursor for full LFAs) for CRP, PCT, and NGAL. The in-house ELISAs are used to screen commercial antibodies against each of these biomarkers and to test for cross-reactivity. The development of individual LFAs for each of these biomarkers will

47

then be discussed followed by alterations to traditional LFA test design to mitigate cross-reactivity issues.
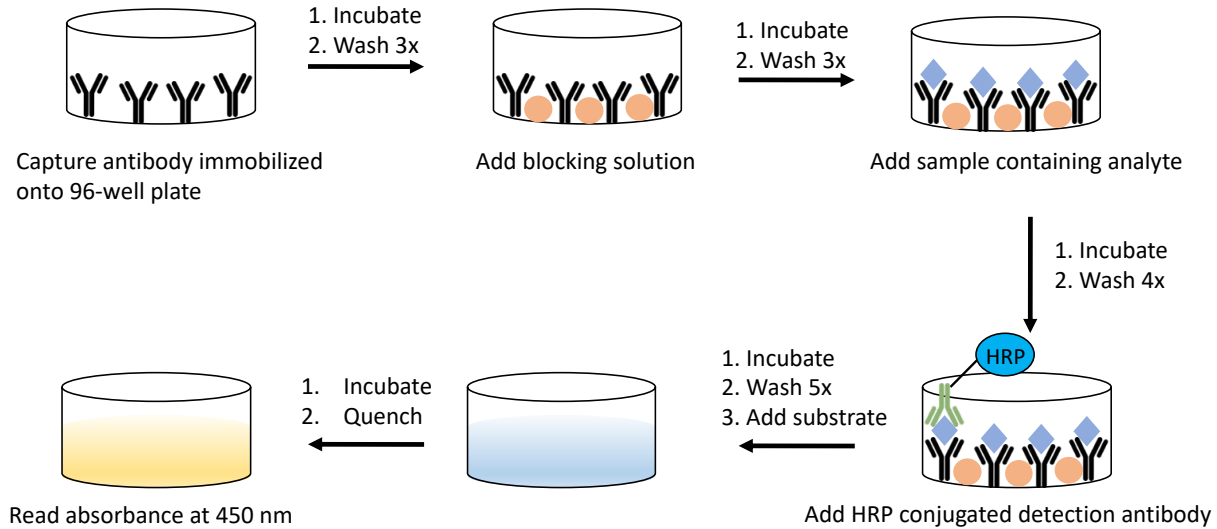
Figure 17. Standard sandwich ELISA protocol.

A roadmap to develop multiplexed POC diagnostics is largely missing from the literature. Since LFA development typically occurs empirically, rather than through defined steps, new researchers in this space have a difficult time troubleshooting any problems that should arise. Any hurdles encountered during LFA development is only magnified when added in the complexity of multiplexing. This chapter serves as a guide for the design and optimization of a multiplexed LFA.

Methods

Reagents and materials

Anti-CRP (α-CRP) antibodies (HM121, HM122), α-PCT antibodies (HM563, HM564, HM365, HM364, HM699, HM698), α-NGAL antibodies (HM306, HM307, HM308,

HM309), and all recombinant (rc) antigens were purchased from EastCoast Bio (Maryland Heights, MO). An additional α-CRP antibody (C5) was purchased from ThermoFisher Scientific (Waltham, MA). Goat α-mouse antibodies were purchased from Fitzgerald (Acton, MA). HRPx was conjugated to antibodies using EZ-Link™ Plus Activated Peroxidase Kit from ThermoFisher Scientific (31489). Pooled whole blood was purchased from BioIVT (Westbury, NY). TMB One was purchased from Promega (G7431). Absorbance was measured using a Biotek Synergy H4 microplate reader and LFA signal was analyzed using a Quiagen ESEQuant LFR (Stockach, Germany). Custom printed cassettes were printed using a Prusa i3 MK3 3D printer (Prague, Czech Republic) with polyethylene terephthalate with added glycol (PETG) filament. Dynabeads MyOne™ Streptavidin T1 beads were purchased from Life Technologies (#65601). Colloidal gold nanoparticles (40 nm) (#15707) were purchased from BBI Solutions (Redding, CA). Antibodies were biotinylated using EZ-Link NHS-PEG4-Biotin from ThermoFisher Scientific (#21329). Unreacted biotin was removed using Zeba Spin Desalting Columns with a 7 kDa molecular weight cut-off from ThermoFisher Scientific (#89882). Whatman FF120HP nitrocellulose membranes and Whatman CF7 wicking pads were purchased from Cytiva Life Sciences (Marlborough, MA). 1X phosphate buffered saline (PBS) was purchased from Corning (Corning, NY). Pierce™ Protein-Free (PPF) blocking buffer and bovine serum albumin (BSA) was purchased from ThermoFisher Scientific.

ELISA Protocol

Briefly, a 96-well plate was coated with 100 µL of capture antibody solution in PBS. The plate was incubated on a shaker for 1 hour and subsequently washed three times with

250 µL/well PBS with 0.1% Tween-20 (PBST). The plate was then blocked for 2 hours with 250 µL of PBST with 5% bovine serum albumin (BSA). The blocking solution was discarded, and the plate was washed three times with PBST before samples were added (buffer or lysed blood spiked with various concentrations of analyte). Sample matrix without analyte was also added as a control. Next, the plate was washed four times with PBST before 100 µL/well of detection antibodies (conjugated to horseradish peroxidase) in PBST with 0.5% BSA solution was added. The plate was then incubated on a shaker for one hour and washed five times with PBST. Finally, the enzymatic reaction was visualized with 100 µL/well of TMB substrate in hydrogen peroxide. The reaction was then quenched with 100 µL/well 2 M H_2SO_4 and spectrophotometric analysis was performed at 450 nm. The following optimized concentrations for capture and detection antibody were used for CRP, PCT, and NGAL: 3.0 µg/mL capture antibody and 0.25 µg/mL detection antibody, 2.0 µg/mL capture antibody and 0.5 µg/mL detection antibody, 1 µg/mL capture antibody and 0.1 µg/mL detection antibody, respectively.

AuNP Conjugate Methods

For passive adsorption, detection antibodies were incubated with AuNPs for 30 minutes on a plate shaker at 0.01 mg/mL. After this, 10% (w/v) BSA in 50 mM borate buffer solution was added (10% based on total volume) and incubated for 1 hr on a plate shaker. The solution was then centrifuged for 30 min at 4 °C and 2500 g before the supernatant was removed and the remaining pellet was resuspended in 50 mM borate diluent buffer with 1% (w/v) BSA. The solution was centrifuged again for 30 min at 4 °C and 2500 g. The supernatant was removed, and the pellet was resuspended in the diluent buffer and

adjusted to an optical density (OD) of 10. This was measured by analyzing the absorbance at 535 nm with an Agilent 6453 G1103A spectrophotometer (Santa Clara, CA). The final AuNP-Ab conjugates were stored in 0.1% (w/v) Tween-20 at 4 °C.

Dipstick Assay Development and Test Conditions

A dipstick assay for each biomarker was created by first using a BioDot AD 1520 Aspirate and Dispense Platform (Irvine, CA) to immobilize 1 mg/mL goat anti-mouse IgG antibody in 50 mM borate solution onto the control line and 1 mg/mL of appropriate capture antibody in 50 mM borate buffer with 0.1% isopropanol (chosen during checkerboard ELISA screenings) onto the test line of a pre-backed nitrocellulose membrane card. The antibody solutions for the test and control lines were dispensed 5 mm apart. The card was then dried in an oven at 37 °C for 2 hours and subsequently blocked using PPF blocking solution. The card was dried again in an oven at 37 °C overnight, a wicking pad was added to the top of the card with approximately a 3 mm overlap with the nitrocellulose membrane, and the card was cut into 4 mm wide test strips using a BioDot CM4000 Guillotine Cutter (Irvine, CA). To test the dipstick assays, 100 µL of buffer was added to a single well with 5 µL of AuNP-Ab conjugate. The test strips were run for 20 minutes and analyzed by an LFR immediately after. Several components of these assays were optimized including nitrocellulose card type, running buffer, AuNP conjugate concentrations, and buffer pH.

Results and Discussion

Checkerboard sandwich ELISAs were used to screen commercial antibodies for each biomarker (Figure 18). The checkerboard ELISAs for CRP and NGAL were performed using 2 µg/mL capture antibody solutions and 1 µg/mL detection antibody solutions. For the PCT checkerboard ELISA, a 1 µg/mL capture antibody solution and 0.5 µg/mL detection antibody solution were used. The signal-to-noise (S/N) ratio was calculated for each antibody pair by dividing the average A_{450} at a specific concentration for each analyte (1.5 ng/mL CRP, 1.5 ng/mL rcPCT, 4.0 ng/mL rcNGAL) by the average absorbance of each corresponding blank.
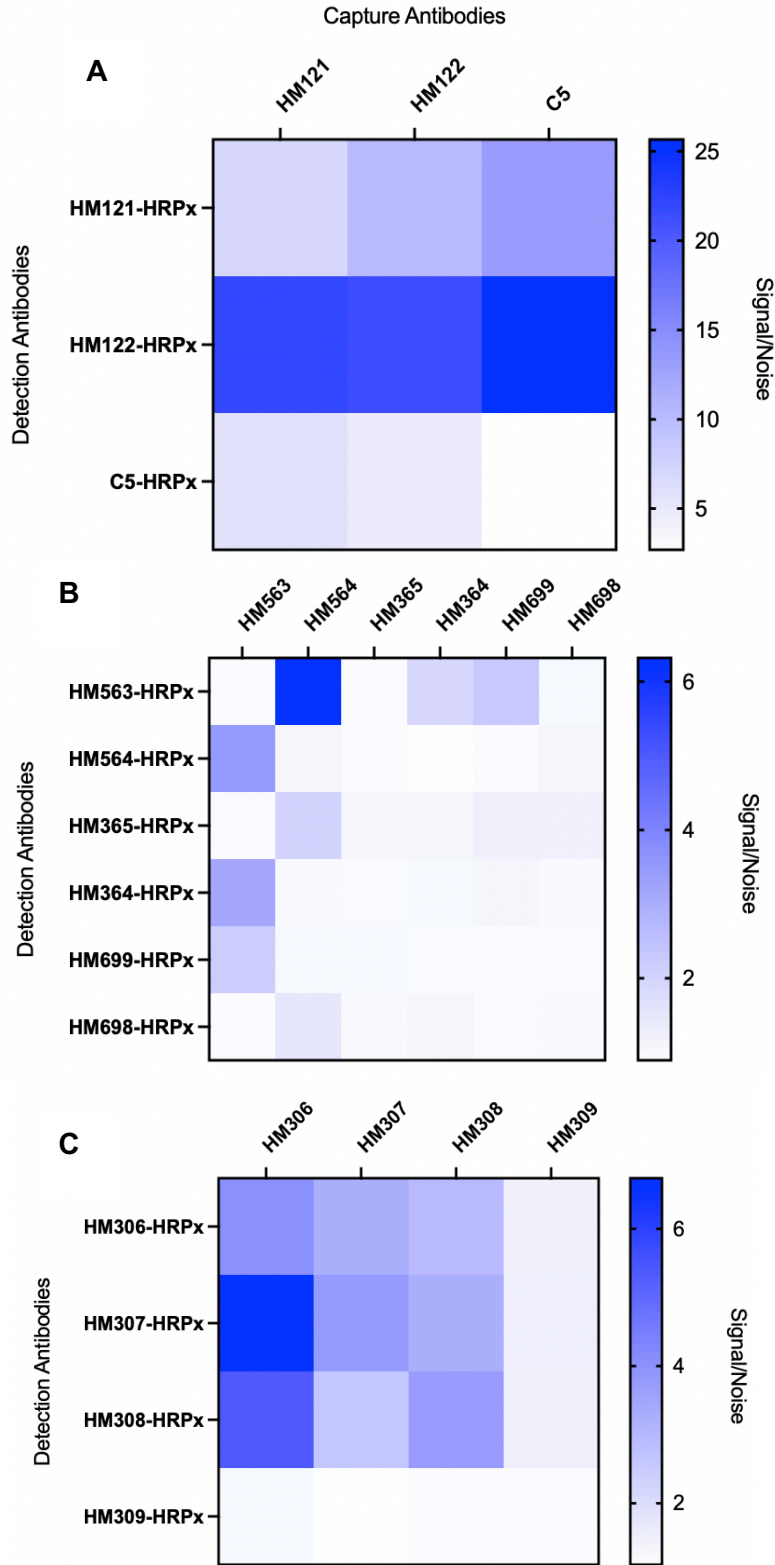
Figure 18. Signal-to-noise results for checkerboard ELISAs comparing antibody pairs for **A.)** CRP; **B.)** PCT; and **C.)** NGAL.

The antibody pairs with the highest S/N were chosen for PCT and NGAL. For CRP, the second highest S/N was chosen due to cost-effectiveness of the chosen pair over C5. Based on these results, the following antibody pairs (capture antibody, detection antibody) were chosen for CRP, PCT, and NGAL to move forward, respectively: HM121, HM122; HM564, HM563; and HM306, HM307. Standard curves using these chosen antibody pairs were obtained to determine LOD for each (Figure 19). The following concentrations for capture and detection antibody solution were used for CRP, PCT, and NGAL: 3.0 µg/mL capture antibody and 0.25 µg/mL, 2.0 µg/mL capture antibody and 0.5 µg/mL detection antibody, 1 µg/mL capture antibody and 0.1 µg/mL detection antibody, respectively. LODs were calculated as 0.13 ng/mL CRP, 13.3 pg/mL PCT, and 1.12 ng/mL NGAL. These LODs were calculated using $3\sigma/\kappa$, where σ is the standard deviation of the blank and κ is the slope of the calibration curve. For reference, the clinical ranges for CRP, PCT, and NGAL that generally indicate a bacterial infection are listed in Table 2.[74,82,83,95]

A.)
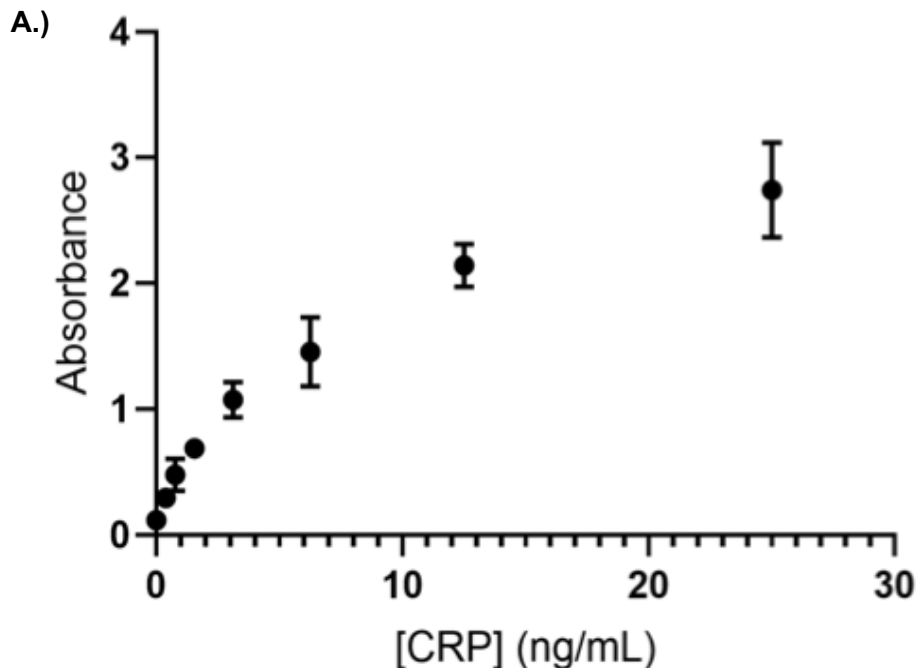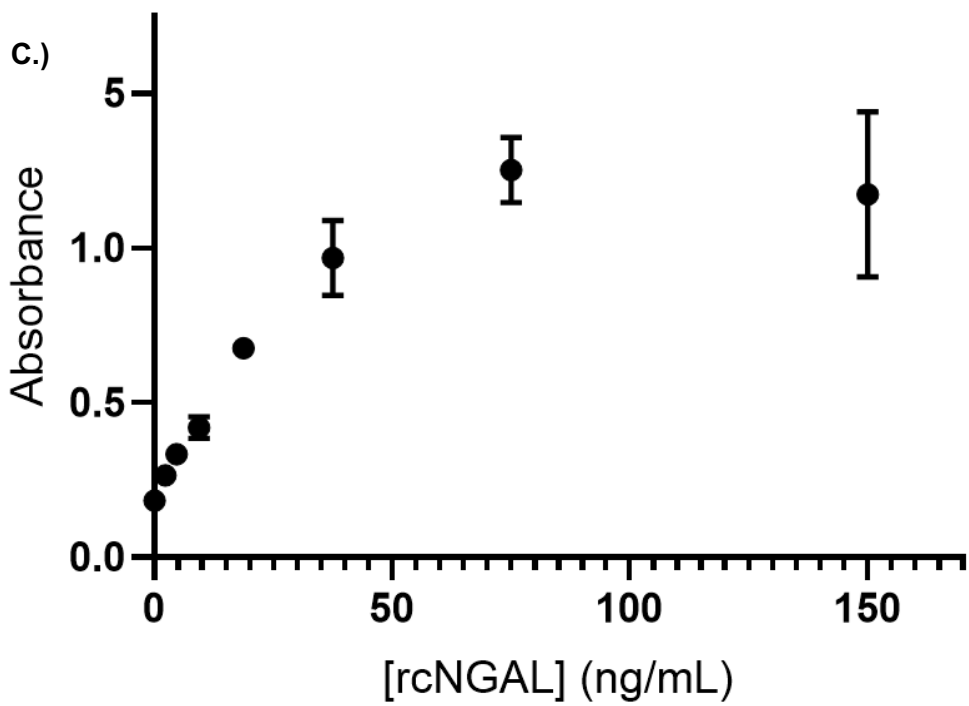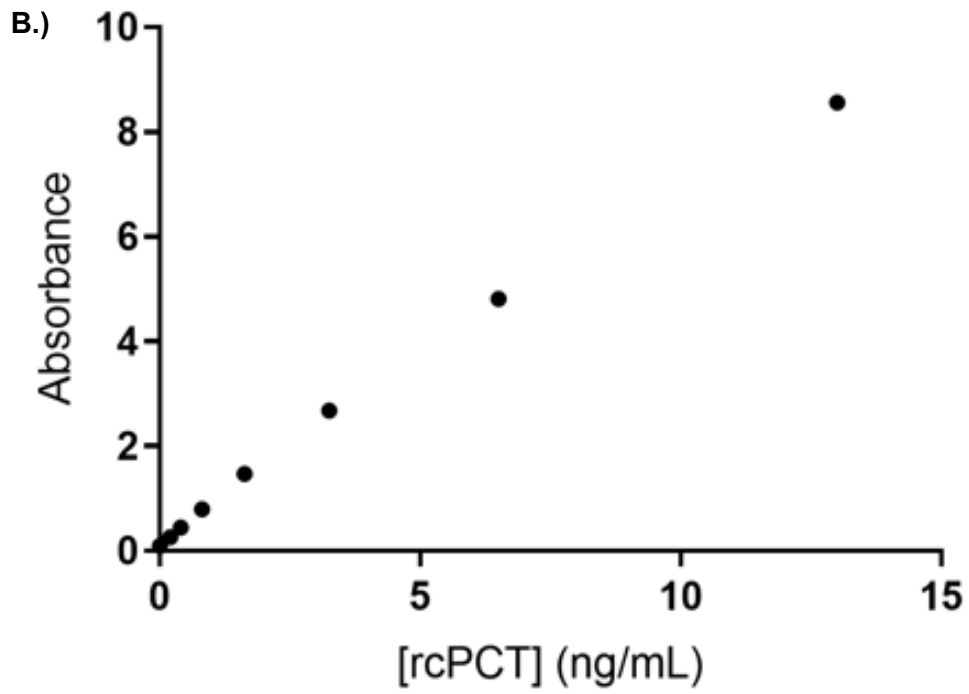
Figure 19. ELISA standard curves for **A)** CRP; **B)** PCT; and **C)** NGAL. Note: some error bars are shorter than height of symbol.

Table 2. Target analyte detection ranges for clinical utility.

__Analyte__	__Required Range__
C-Reactive Protein (CRP)	50-175 µg/mL
Procalcitonin (PCT)	0.25-10 ng/mL
Neutrophil gelatinase associated lipocalin (NGAL)	150-500 ng/mL

Individual dipstick assays were then developed for CRP, PCT, and NGAL using the same antibody pairs selected previously. Dipstick assays have the same format as an LFA, except they are missing the sample and conjugate pads. The reagents that are normally added or immobilized on the sample and conjugate pads (sample with analytes and AuNP-Ab conjugates) are instead added to a well or liquid reservoir prior to addition of the dipstick assay (Figure 20). Developing and analyzing dipstick assays before assembling a full LFA allows for troubleshooting early, especially when the desired final format is a multiplexed LFA.

A.)

B.)

57
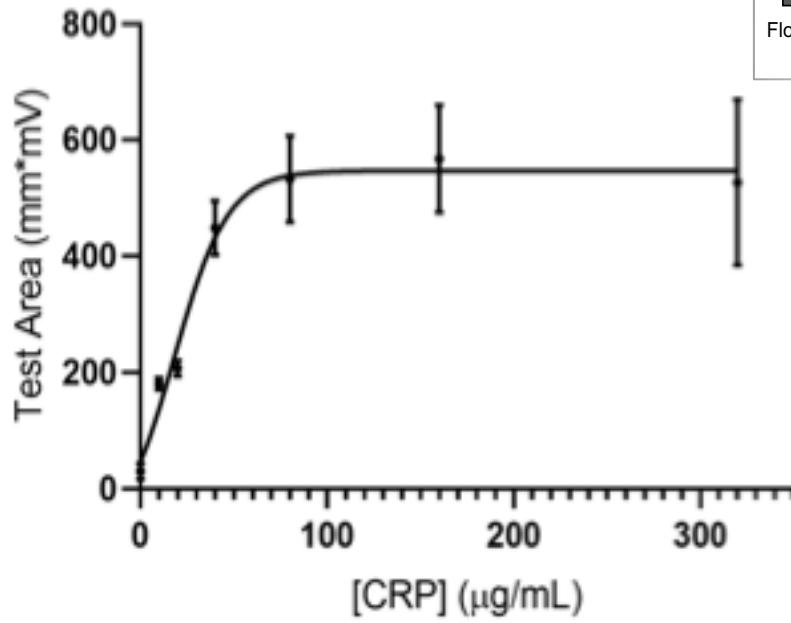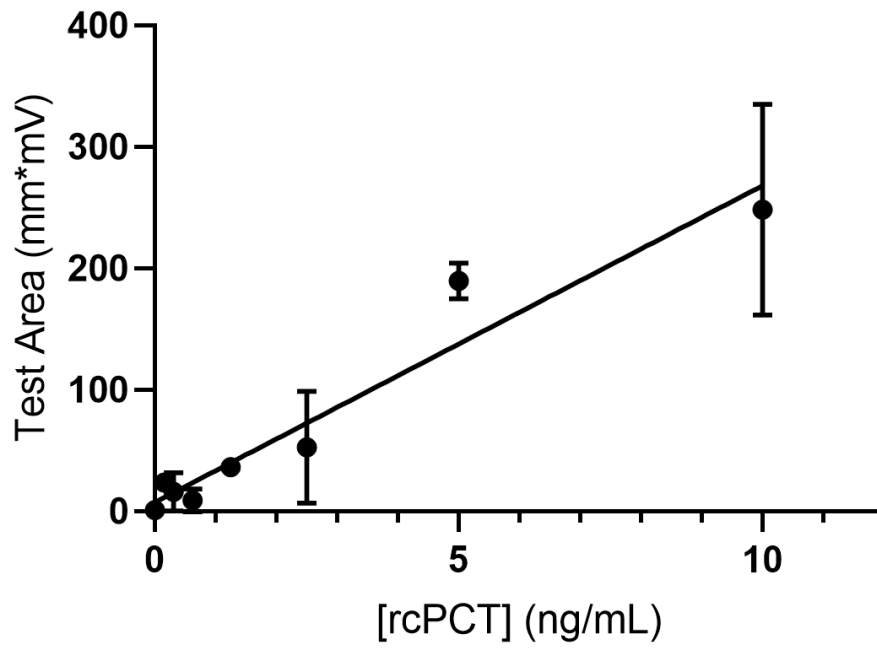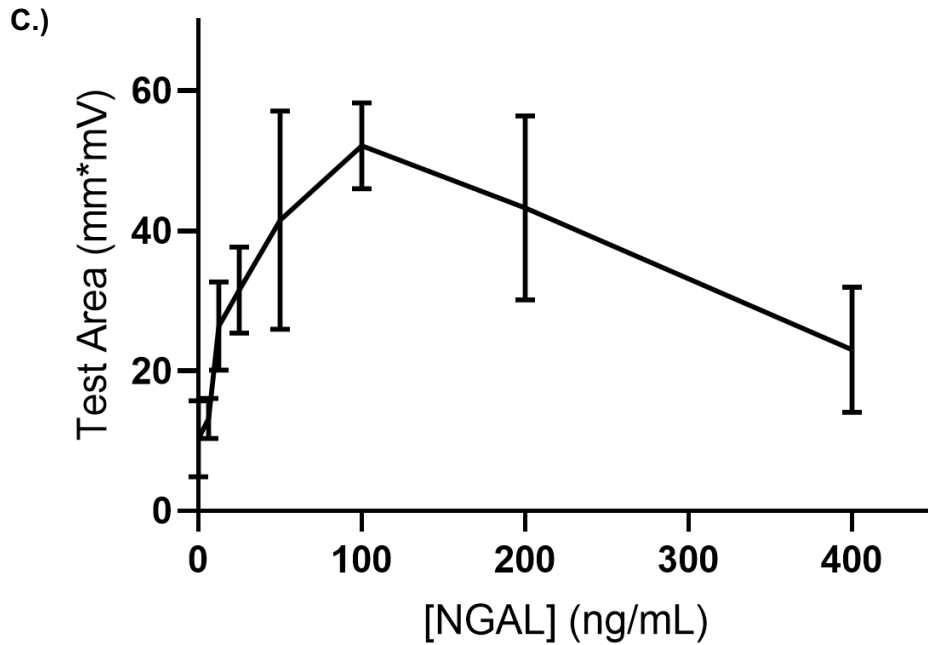
Figure 20. Dipstick assay standard curves and dipstick format for **A)** CRP; **B)** PCT; and **C)** NGAL.

Standard curves for each dipstick assay were generated (Figure 20) by testing each optimized assay with a range of appropriate biomarker concentrations based on the clinical range. These standard curves were produced by measuring the signal intensity of the test line area in mm*mV for each dipstick using an LFR in reflective mode on the E1/D2 channel. LODs were calculated as described previously for CRP, PCT, and NGAL, respectively: 4.01 µg/mL, 0.17 ng/mL, and 26.3 ng/mL. As expected, the dipstick assays have higher LODs (by about 1 order of magnitude) than the corresponding ELISAs for each biomarker. Although the LODs for the CRP, PCT, and NGAL dipstick assays are still sufficient given the clinical range for each, the NGAL assay had a noticeably decreased signal compared to CRP and PCT. The NGAL assay also appears to be experiencing the hook effect due to the downward signal trend with increasing concentration. The hook effect is generally characterized as a loss in test line signal

caused by saturation of the available binding sites on the test line.[96] This prevents the expected sandwich complex formation on the test line, therefore resulting in decreased signal.

An essential component for a working assay is the running buffer. This is added with the sample to initiate the assay in an LFA format, or in a well with the spiked biomarker when testing the dipstick assays. Since a multiplexed assay would require a single buffer, three different buffers were tested with each dipstick assay to observe the effect of buffer on overall signal and signal-to-noise (Figure 21). The most used buffers were chosen for this analysis—50 mM borate buffer, PBS, and 4-(2-hydroxyethyl)-1-piperazineethanesulfonic acid (HEPES).

CRP
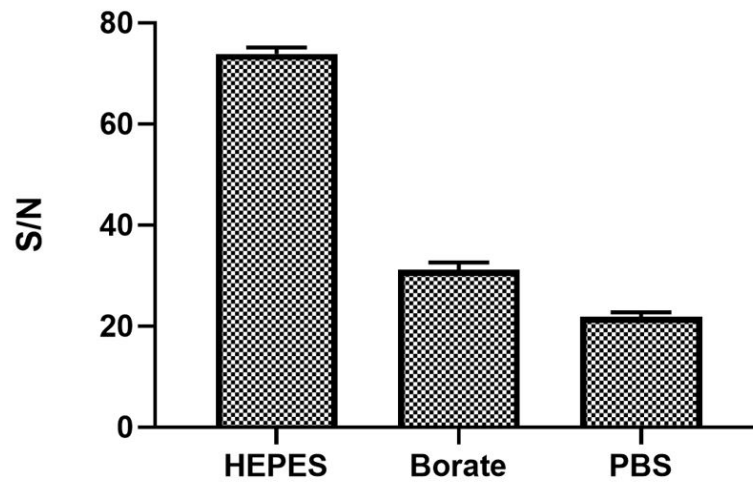
PCT
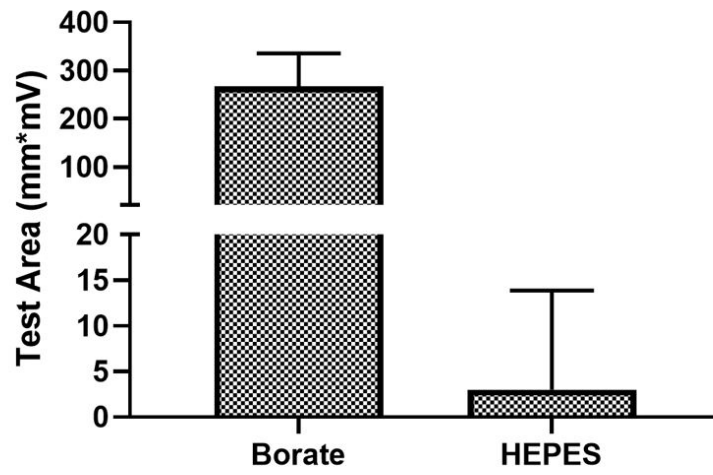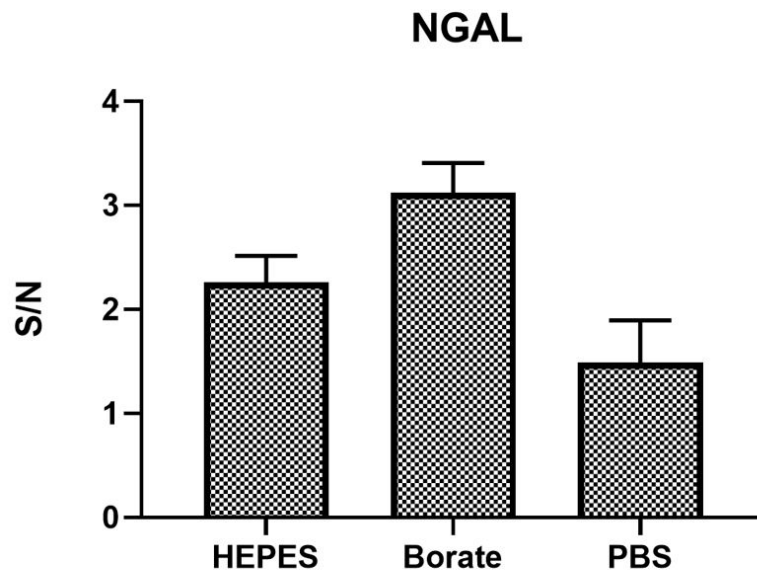
Figure 21. Performance results for individual CRP, PCT, and NGAL dipstick assays in varying buffers.

It should be noted that CRP and NGAL buffer comparison is displayed using signal-to-noise while PCT is displayed using the dipstick assay test line area. This is due to the LFR not detecting background noise from the test line of negative samples for the PCT dipstick assays. This made it impossible to calculate signal-to-noise. Therefore, buffers were compared using the intensity of the test line for the PCT assays instead. PCT and NGAL assays performed best in borate buffer while the CRP assay performed best in HEPES buffer. However, since borate buffer had the best results for two out of the three biomarkers, and the CRP assay still had very high signal-to-noise when performed with borate buffer, this buffer was chosen moving forward in multiplexed assay development.

After individual dipstick assays were developed and tested, each assay was analyzed for cross-reactivity by testing each individual assay against a different biomarker. These studies revealed that the α-PCT detection antibody (HM563) bound to the α-CRP capture antibody (HM121), causing a strong false positive result on the CRP dipstick assays (Figure 22). This was confirmed by ELISA (data not shown) which revealed that in the presence of only buffer, the PCT detection antibody bound to the CRP capture antibody.
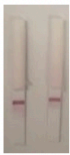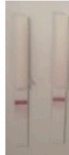
Figure 22. CRP dipstick assays analyzed with buffer, rcCRP, and rcPCT.

Furthermore, when a three-line dipstick assay was developed for simultaneous CRP, PCT, and NGAL detection additional cross-reactivity was discovered. This assay was developed similarly to the individual dipstick assays, except the capture antibody for each biomarker (CRP, PCT, NGAL) was dispensed onto a nitrocellulose card 2 mm apart to

accommodate the three lines. The assays were also run similarly to individual assays, except 5 µL of each conjugate was added with the sample. False positives were observed for both CRP and PCT when the three-line dipstick assay was run in borate buffer with all three AuNP-Ab conjugates (Figure 23).
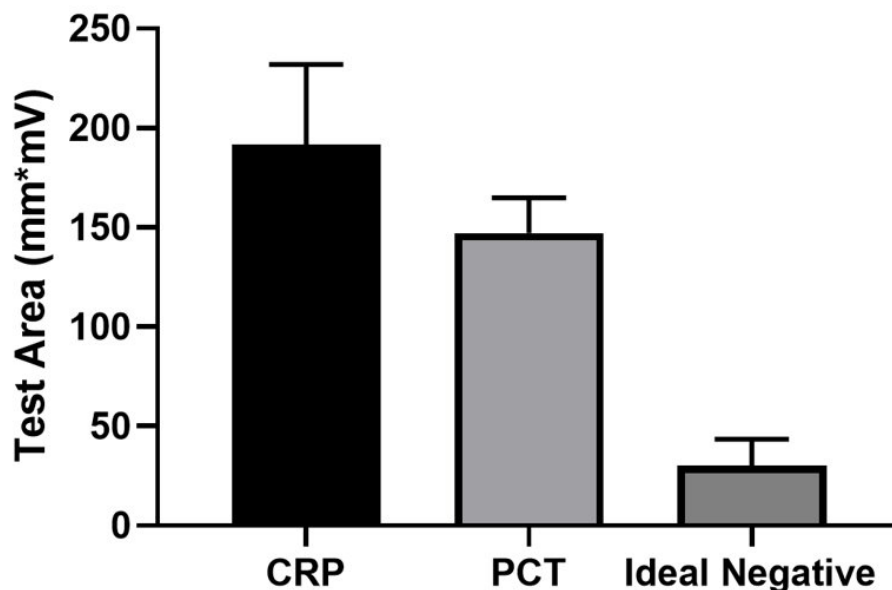
Figure 23. Test line area for CRP and PCT test lines on a three-line dipstick assay tested with true negative samples (borate buffer with AuNP-Ab conjugates).

The cross-reactivity observed in buffer with all AuNP-Ab conjugates together suggests that there is an interaction occurring between the conjugates that is causing the false positive PCT test line. This was not previously observed when analyzing the individual PCT assay or when testing PCT antibodies against other antibodies with an ELISA.

Conclusion

As was discussed in Chapter I, the prevalence of cross-reactivity and unwanted interactions in multiplexed assays is well known. However, the development process of multiplexed assays is rarely described in the few publications describing novel multiplexed assays, especially when going beyond a two-plexed assay. Additionally, the degree or the specifics to which cross-reactivity occurs is not elucidated even when cross-reactivity is mentioned in published articles. It is imperative to understand the potential interactions that are occurring in order to prevent these interactions going forward. For the cross-reactivity observed here, there are a few possibilities as to what is happening. Since the false positive results are witnessed in the absence of any antigen, it is possible that either the antibodies are adsorbing to one another or that any sections left exposed on the AuNP surface of the Ab conjugate is facilitating electrostatic interactions with the capture antibody on the test line of the dipstick assay, resulting in AuNP-Ab aggregation and therefore, a positive test line. However, the latter option is unlikely due to the false positive results observed in both the dipstick assay and ELISA format, the latter of which does not contain AuNP-Ab conjugates. Alternatively, it is possible there are unknown contaminants or protein additives in the commercial antibody solutions that are forming complexes with the AuNP-Ab conjugates, therefore contributing to the false positive results.

To this end, this chapter described the iterative development of individual ELISAs and individual dipstick assays for the detection of CRP, PCT, and NGAL. The cross-reactivity between a few components observed when attempting to design a multiplexed assay is

discussed. By continuing to be transparent about the exact interactions contributing to cross-reactivity, increased solutions may be explored to combat this issue that hinders widespread development of multiplexed diagnostics and in turn, the innumerable applications with which multiplexed diagnostics could be utilized.

Acknowledgements

CHAPTER IV

MODIFICATIONS TO A MULTIPLEXED DIPSTICK ASSAY FORMAT TO MINIMIZE

CROSS-REACTIVITY

Introduction

While cross-reactivity is common when combining reagents for differential biomarker

detection, there has been some research progress in using various strategies to reduce

the frequency of these unwanted interactions, either by spatial separation or other

techniques to reduce the frequency of these interactions. When attempting to overcome

cross-reactivity challenges involving paper-based diagnostic assays specifically, there

are some limitations given the nature of the assay's material. However, a few methods

have been employed by various research groups to eliminate or reduce cross-reactivity

associated with multiplexing. One example of this is from Zhao *et al*. who designed a 10-

channel LFA for the detection of ten different foodborne pathogens.[97] The individual

channels consisted of individual LFAs for the detection of single pathogens. These LFAs

were arranged in a circle around a common inlet for the sample to be distributed to all ten

LFAs. This enabled complete separation of detection reagents and capture elements,

eliminated the possibility of cross-reactivity. Similarly, Pomili *et al.* designed a multiplexed

paper-based device for the simultaneous detection of three salivary biomarkers by

creating distinct channels using CO_2 laser cutting.[98] This method allowed for the

construction of hydrophobic barriers within chromatography paper. These barriers that

made up the individual channels surrounded a common sample zone for sample deposition. This device also served to separate individual reagents required for the detection of each biomarker, removing the potential for cross-reactivity. Lastly, Lin *et al.* developed a microfluidic paper-based analytical device using polyurethane acrylate to pattern hydrophobic barriers within a nitrocellulose membrane.[99] This device again allowed for simultaneous detection of two cancer biomarkers while keeping reagents for each biomarker isolated within their respective "immunozones". Spatial separation of reagents like what has been discussed in these methods is the most straight forward and common way to reduce the likelihood of cross-reactivity, but there are other potential solutions such as changing the assay format to remove certain interactions, or altering methods associated with reagent preparation. This chapter will focus on attempts to curb cross-reactivity by using traditional spatial separation methods as well as others based on the components that appear to be cross-reacting.

One of the methods that was utilized to eliminate the observed interactions between our chosen CRP capture antibody and PCT detection antibody is wax printing. This was used to form hydrophobic barriers within the nitrocellulose membrane that is the basis for the individual dipstick assays developed thus far. Wax based inks are one material that have been used for the fabrication of paper-based microfluidics. These inks have been used to wax print hydrophobic barriers within paper, another technique to spatially separate reagents using these hydrophobic "walls" that can create reservoirs or channels within the paper membrane.[46,100–102] After wax ink is deposited onto a paper-based material, the

membrane is then heated to enable the wax to spread through the thickness of the paper, generating hydrophobic channels or reservoirs.

Furthermore, due to the low sensitivity associated with the NGAL dipstick assay discussed in the previous chapter, this assay was replaced with an assay for detection of HRP2, the primary malarial biomarker.[103] This biomarker is associated specifically with malarial infection caused by *Plasmodium falciparum* and is a protein excreted in human blood by the malaria-causing parasite.[104] The decision to include HRP2 detection in the assay was due to the laboratory's extensive experience with malaria POC diagnostics and the global need for a fever differentiation POC device, especially in malarial endemic regions.[103,105–108] While sensitive and specific malaria RDTs have long been sought after, the demand for a quick malaria diagnosis became even more heightened during the 2014-2016 West Africa Ebola crisis. This region is one where malaria is endemic and during this time, anyone who had a fever, a symptom common to both malaria and Ebola, was placed into quarantine. This meant that a patient with malaria or another fever-causing illness would be placed into quarantine with those sick with Ebola, instead of being given anti-malarial drugs or other illness appropriate medicine. Due to the level of contagion of Ebola, those who did not initially have Ebola could very well contract it and potentially die given Ebola's roughly 50% fatality rate (WHO, 2021).[109] This can very well be prevented in the future with the advent and distribution of POC tools able to differentially diagnose malaria from other fever-causing illnesses such as bacterial infection. A diagnostic device such as this would not only properly diagnose malaria patients, but also decrease the amount of unnecessary antibiotics used. Since PCT and CRP are both markers of

bacterial infection, a diagnostic tool that could simultaneously detect all three markers would be highly advantageous in the differential diagnosis of malaria versus a bacterial infection.

Methods

Reagents and Materials

Colored wax ink was purchased from Professor Color (Camarillo, CA). Food dye was purchased from McCormick (Baltimore, MD). Whatman FF120HP nitrocellulose membranes, Whatman CF7 wicking pads, Whatman 3MM chromatography paper, Whatman Fusion 5 matrix membrane, and Whatman glass fiber conjugate pads were purchased from Cytiva Life Sciences (Marlborough, MA). Glass fiber conjugate pads were also purchased from Millipore Sigma (St. Louis, MO). α-PCT antibodies (HM078, HM081, HM220) were purchased from EastCoast Bio (Maryland Heights, MO). α-HRP2 antibodies (ABMAL-0404 and ABMAL-0405) were purchased from Arista Biologicals (Allentown, PA). Goat α-mouse antibodies were purchased from Fitzgerald (Acton, MA). Recombinant *Pf*HRP2 was purchased from Immunology Consultants Laboratory Inc. (Portland, OR). An InnovaCoat GOLD Conjugation kit was purchased from Abcam (Cambridge, UK).

Wax Printing Protocol

The patterns used to wax print on the paper-based membrane were first designed using Inkscape. These patterns were then printed onto the nitrocellulose membrane using a Xerox Phaser 8560DN Thermal Color Workgroup Printer with high quality settings. Since

the membrane is thinner in width compared to the smallest setting on the paper tray, the membrane was taped to a wider piece of paper to ensure the membrane stayed in place as it went through the printer. For the experiments using a conjugate pad, the conjugate pad was adhered to the nitrocellulose membrane before using it to wax print hydrophobic barriers. The membranes were then placed into an oven at 125 °C for 5 minutes to allow for the wax to melt through the thickness of the membrane.

3D Printing Protocol

Custom cassettes to house the dipstick assays and future LFAs were designed using Autodesk Fusion 360. The cassettes were then printed using PrusaSlicer and a Prusa i3 MK3 3D Printer (Prague, Czech Republic) with polyethylene terephthalate with added glycol (PETG) filament.

Multiplexed Dipstick Assay Protocol

Dipstick assays containing dots for test and control regions instead of lines were manufactured similarly to the dipstick assays described previously with a few notable changes. A BioDot AD 1520 Aspirate/Dispense Platform (Irvine, CA) was used to dispense three 40 nL drops of 1 mg/mL goat α-mouse antibody onto a pre-backed nitrocellulose membrane card to form three control dots at the top of each dipstick assay. Below each control dot, 40 nL drops consisting of 2 mg/mL of each capture antibody (CRP, PCT, HRP2) was dispensed. This is to mimic the format of a traditional dipstick assay of LFA so that each test dot may have a corresponding control dot above it. The nitrocellulose card was then dried in an oven at 37 °C for 2 hours and subsequently

blocked using PPF blocking solution. The card was dried again in an oven at 37 °C overnight, a wicking pad was added to the top of the card with approximately a 3 mm overlap with the nitrocellulose membrane, and the card was cut into 12 mm wide test strips using a BioDot CM4000 Guillotine Cutter (Irvine, CA).

Competitive Assay Protocol

To develop competitive assays in contrast to the sandwich assays that have been described thus far, the protocol is the same as what is described above, except 2 mg/mL of recombinant antigen was dispensed to make up the test region instead of capture antibody.

AuNP Conjugate Methods

For passive adsorption, detection antibodies were incubated with AuNPs for 30 minutes on a plate shaker at 0.01 mg/mL. After this, 10% (w/v) BSA in 50 mM borate buffer solution was added (10% based on total volume) and incubated for 1 hr on a plate shaker. The solution was then centrifuged for 30 min at 4 °C and 2500 g before the supernatant was removed and the remaining pellet was resuspended in 50 mM borate diluent buffer with 1% (w/v) BSA. The solution was centrifuged again for 30 min at 4 °C and 2500 g. The supernatant was removed, and the pellet was resuspended in the diluent buffer and adjusted to an optical density (OD) of 10. This was measured by analyzing the absorbance at 535 nm with an Agilent 6453 G1103A spectrophotometer (Santa Clara, CA). The final AuNP-Ab conjugates were stored in 0.1% (w/v) Tween-20 at 4 °C.

For covalent linking, a commercial conjugation kit was used to prepare AuNP-Ab conjugates and manufacturer protocols were followed.

ImageJ Analysis

Immediately after the dipstick assays were completed, they were placed in a custom cassette to ensure images were consistent. Images of the three-plex dipstick assays for detection of CRP, PCT, and HRP2 were taken with an iPhone 11 Pro in a well-lit room. These images were then opened ImageJ and the image was cropped to only include the assay and not the cassette. Images were then inverted, and the line tool was used to draw a line the width of the test (known distance of 12 millimeters) to change the scale from pixels to millimeters. The line tool was then used to draw a line vertically from the control dot to the test dot and a profile was plotted showing the intensity of each dot in gray scale values. A higher gray value corresponds to a higher signal intensity. The data points from each profile were exported for processing in Python.

Results and Discussion

To examine whether the conjugation method for the formation of the AuNP-Ab conjugates had an impact on the performance of the dipstick assays, a covalent conjugation method was compared to passive adsorption, specifically with the chosen PCT detection antibody (HM563) since this is the antibody that appears to be aggregating on the CRP test line. Passive adsorption, or passive nanoparticle conjugation, is frequently used in the development of LFAs due it's ease and relative effectiveness. In contrast, covalent conjugation is a more involved process but offers reproducible results and increased

72

stability in harsh buffering conditions.[110] Furthermore, the antibody coating procedure involved with covalent conjugation methods are not dependent on the isoelectric point of the antibody, whereas this can affect the results of passive adsorption. A commercially available conjugation kit was used for covalently linking AuNPs to primary lysine residues
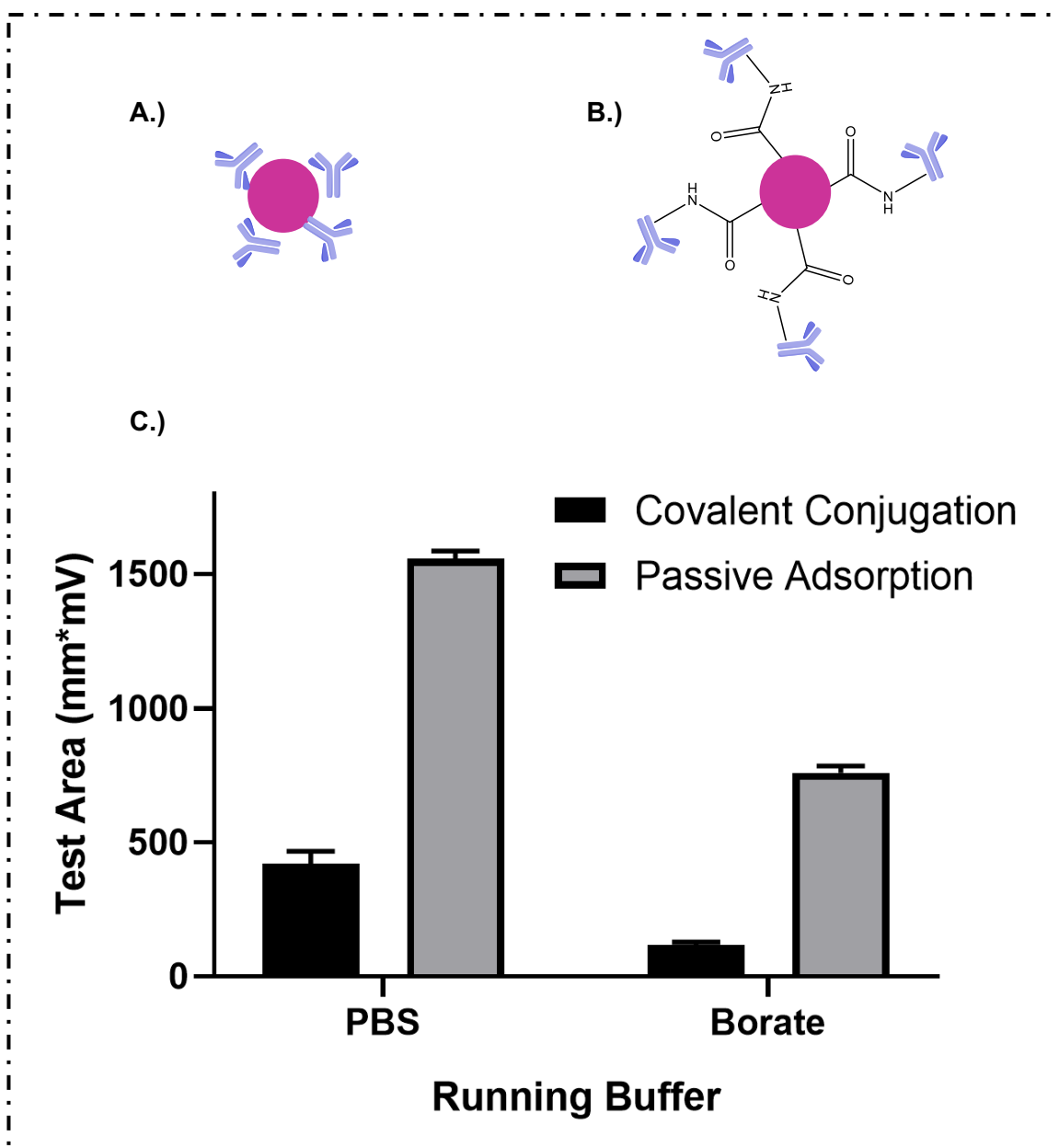
Figure 24. Depiction of **A)** passive AuNP conjugation, **B)** covalent AuNP conjugation and **C)** performance of both conjugation methods in two different running buffers.

on the antibody. Although the nature of the reaction is kept propriety, this kit likely uses EDC/NHS coupling to link carboxyl-functionalized AuNPs to the primary lysine residues on the antibodies. CRP dipstick assays were run as previously described with the covalent PCT AuNP-Ab conjugates in triplicate in both PBS and borate buffer (Figure 24).

The results of AuNP conjugation comparison showed approximately an 84% decrease in test line signal when forming AuNP-Ab conjugates via covalent conjugation compared to passive adsorption in borate buffer, drastically decreasing the false positive signal. Running buffer composition also appears to influence test line signal with an approximately 71% decrease in test line signal when using covalently linked AuNP-Ab conjugates in borate buffer compared to PBS and a 51% decrease when using passively adsorbed AuNP-Ab conjugates. It should also be noted that the control line signal intensity decreased proportionately (data not shown) as well. This could be explained by passive adsorption methods tending to have increased antibody loading on the AuNP surface, increasing assay sensitivity. The overall decrease in test line signal when using covalently linked AuNP-Ab conjugates might be explained by the more controlled orientation of antibodies on the AuNP surface, reducing the likelihood that any regions of the Ab that were binding before are now hidden due to the fixed orientation of the Abs on the AuNP.

Three new PCT detection antibodies were screened (HM078, HM081, HM220) to determine whether a different detection antibody was better suited for this multiplexed assay and could eliminate false positive signals all together. These antibodies were tested

by using passively adsorbed AuNP-Ab conjugated on a multiplexed dipstick assay containing test lines for CRP, PCT, and NGAL. HM078 and HM081 showed minimal binding in true negative samples containing borate buffer but resulted in very low sensitivity when rcPCT was spiked into samples (data not shown). Alternatively, HM220 showed promising results when tested with true negative samples and had comparative results to HM563 when testing the HM220 AuNP-Ab conjugate in samples containing rcPCT (Figure 25). Given the improved performance of using HM220 as a PCT detection antibody compared to HM564, HM220 was used in the development of any dipstick assays going forward.
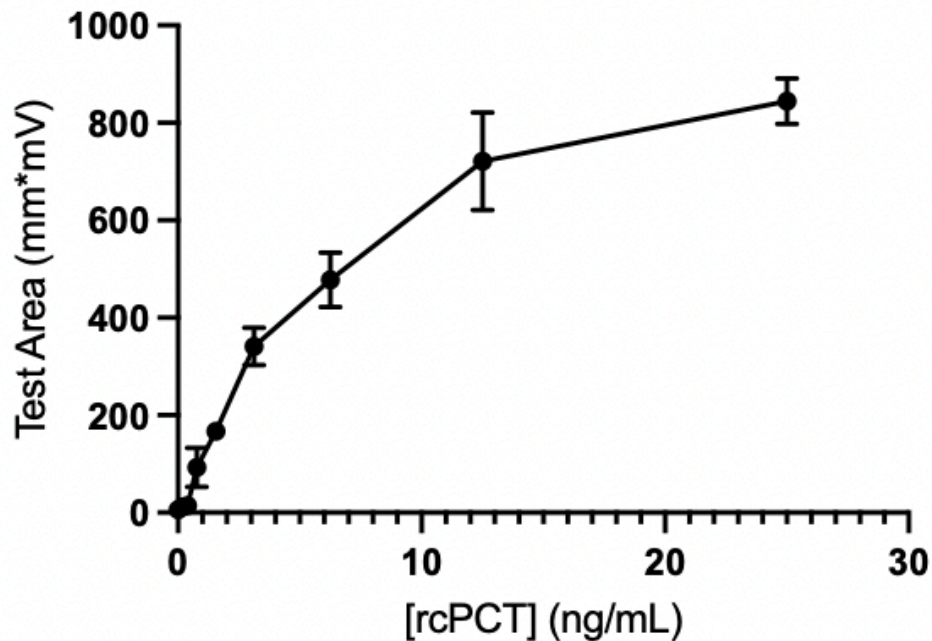
Figure 75. Performance of PCT dipstick assay using AuNP-Ab conjugates containing HM220 antibody.

Since HM220 did not bind as strongly to the CRP test line, causing false positive results, multiplexed dot dipstick assays were designed for simultaneous detection of CRP, PCT, and HRP2. The method is described above. Dots were used in lieu of a traditional line format so that it closely mimicked the format of the proposed final device which would contain dots forming a bioactive barcode for mobile diagnostic test processing. The multiplexed assays were run with spiked samples containing a single analyte at a time and AuNP-Ab conjugates against all analytes so that individual standard curves could be obtained from the multiplex format (Figure 26). Test dot signal is scaled from 0 to 1 and plotted for each of the assays.

A.)
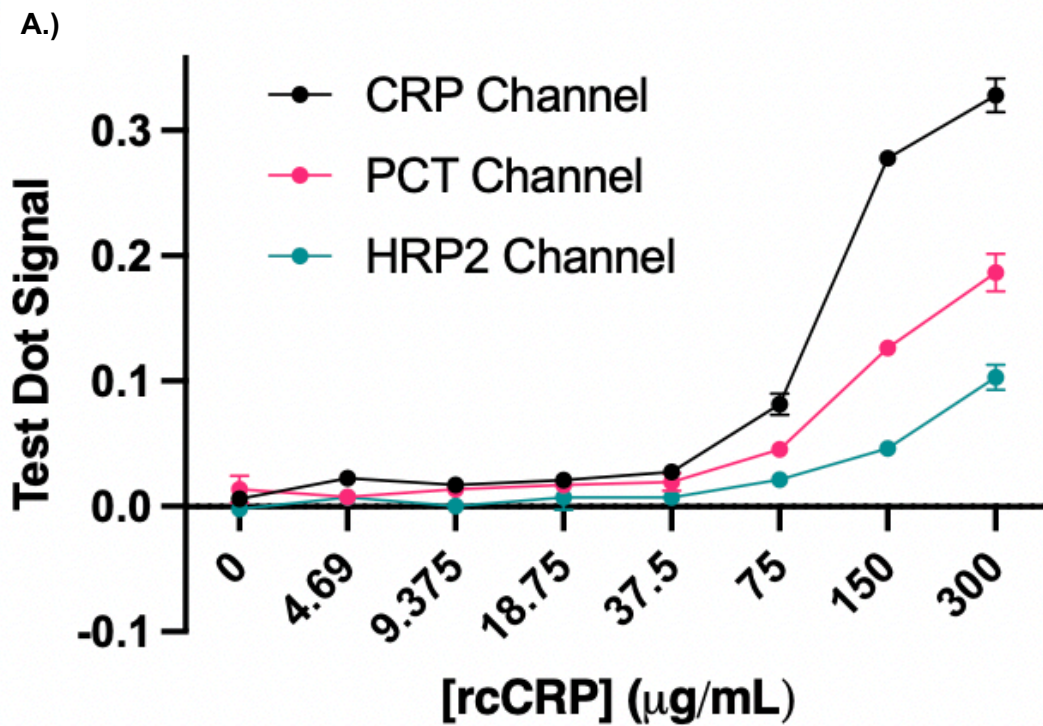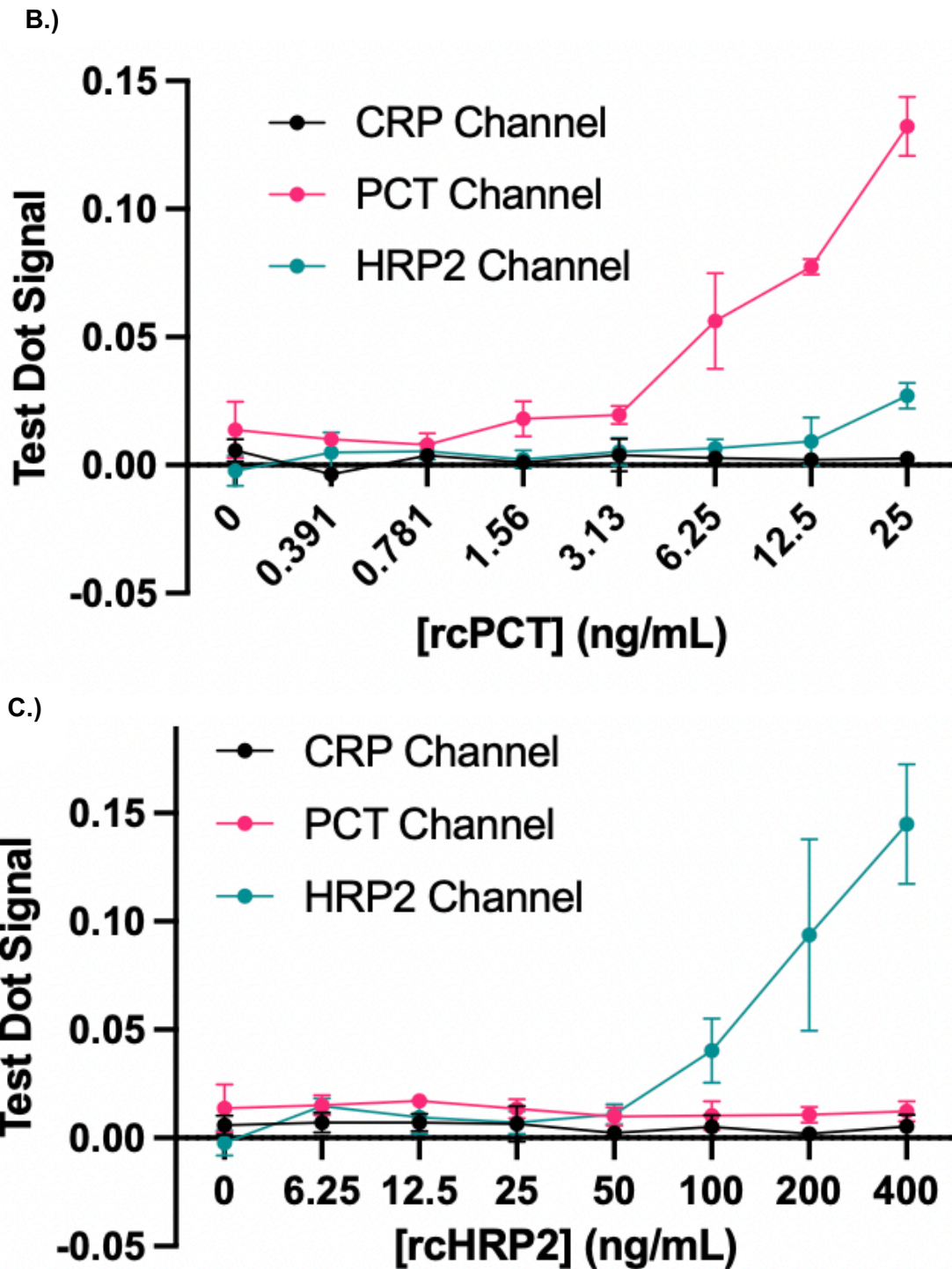
Figure 26. Standard curves for multiplex dot assays with individual analytes spiked into solution **A.)** CRP; **B.)** PCT; and **C.)** HRP2.

The multiplexed assays run in the presence of PCT and HRP2 showed good discrimination, with little to no false positives occurring for the detection of the other analytes. However, when CRP was spiked into solution, there was some binding of AuNP-Ab conjugate to all three test dots, even though CRP was the only analyte in solution. This signaled that there were interactions causing conjugate to bind where it should not be. To remove the false positives occurring for the HRP2 test dots, the sandwich assay that had been used until now was converted to a competitive assay. In contrast to a sandwich assay, competitive immunoassays work by immobilizing the target analyte instead of a capture antibody onto the membrane to form the test dot. In the presence of that analyte in a sample, it binds to the corresponding AuNP-Ab conjugate, leaving none left to bind on the test dot region. This results in the opposite visible outcome of a sandwich assay where a positive test result is indicated by no signal at the test dot.
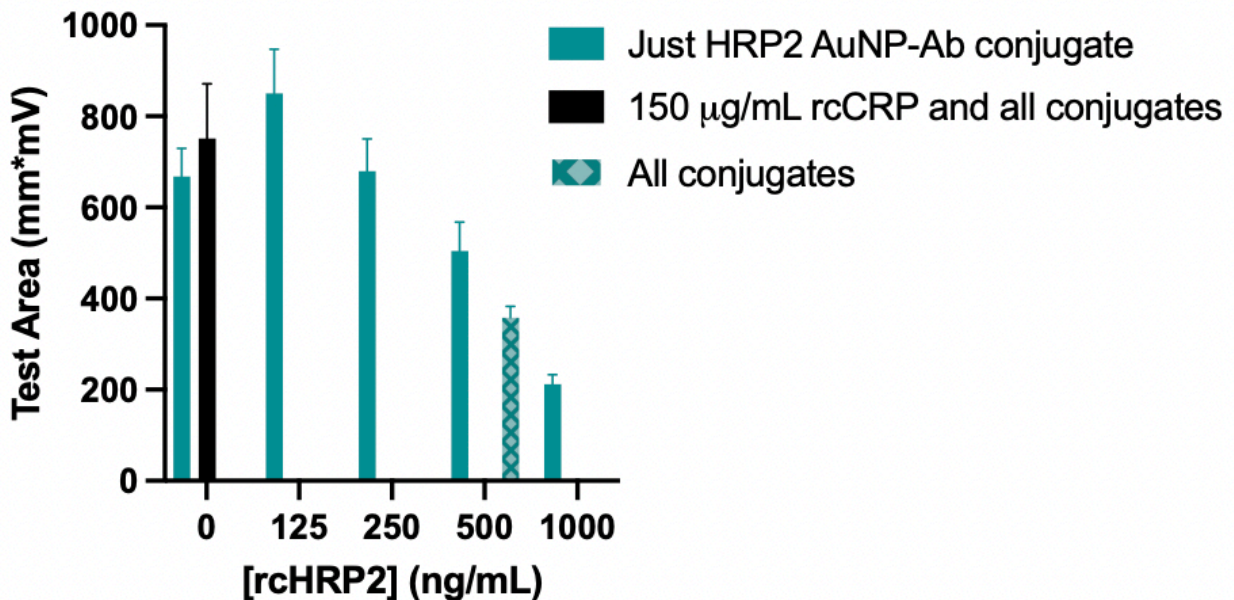
Figure 27. HRP2 competitive dipstick assay run with only αHRP2 AuNP-Ab conjugate, with all AuNP-Ab conjugates, and with rcCRP spiked into solution.

A competitive format was tested for detection of HRP2. This format was initially executed on a traditional dipstick assay format with a test and control line (Figure 27). The test was originally run with a range of HRP2 concentrations and only αHRP2 AuNP-Ab conjugate to determine the success of the assay. As expected, test area signal decreased with an increase in HRP2 concentration. Since the multiplexed dot assays indicated presence of CRP caused a false positive HRP2 result, an HRP2 competitive dipstick assay was also run with a 150 μg/mL rcCRP solution in 50 mM borate buffer and the addition of all AuNP-Ab conjugates. These test conditions mimic those from Figure 26A. The test area was not affected by the presence of CRP, suggesting the new format reduced the interactions causing the false positive initially. Next, to ensure the addition of all conjugates did not impact the outcome of the competitive assay, all conjugates were added to a solution of 500 ng/mL rcHRP2 in 50 mM borate buffer. The test area was slightly decreased when all conjugates were present in solution compared to when only the αHRP2 AuNP-Ab conjugate is present in solution. To further see how the HRP2 competitive assay would perform when combined with the sandwich assays for CRP and PCT, a multiplexed dot assay was developed and run with varying concentrations of rcCRP in 50 mM borate buffer and all AuNP-Ab conjugates (Figure 28).
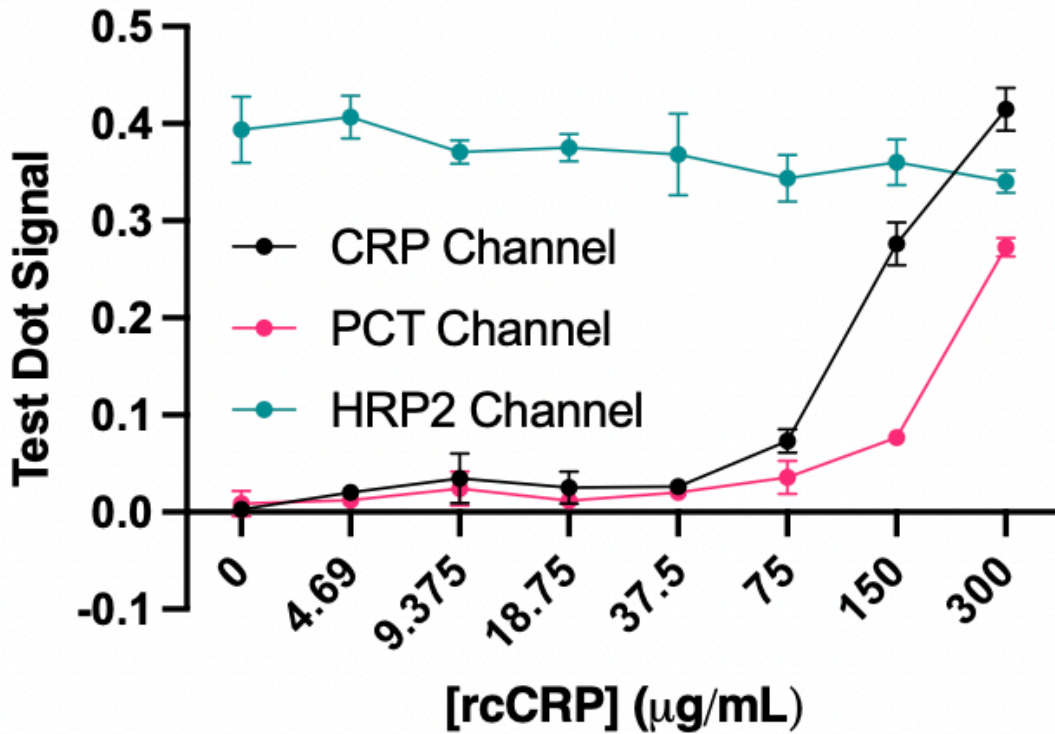
Figure 28. Multiplex dot assay incorporating HRP2 competitive assay with CRP and PCT sandwich assays.

The test signal for HRP2 remained consistent and high across all CRP concentrations that were evaluated, properly indicating the absence of HRP2 in the sample. However, the PCT channel continued to give false positive results in the absence of PCT, with the signal increasing proportionally to the CRP concentration. This indicated that the false positive result was likely in part due to the CRP antigen and PCT-specific reagents. An ELISA confirmed that the false positive is the result of the PCT capture antibody forming a sandwich complex with the CRP antigen and CRP detection antibody.

As new cross-reactive and nonspecific binding scenarios continue to present themselves, the only way to prevent these interactions is to separate the reagents used for detection of each analyte. This also gives flexibility in choosing reagents appropriate for detection of a single analyte, instead of having to screen reagents that work for all other components in the immunoassay. For this separation, a wax printing method was explored to alter a traditional dipstick assay format. Wax printing was used to form hydrophobic channels on a nitrocellulose membrane to probe whether this method could be incorporated into a traditional dipstick or LFA format to spatially separate reagents, and therefore, remove the possibility of any future cross-reactivity issues (Figure 29). Initial experiments were completed with food dye to visualize fluid flow on the membrane. After equidistant lines were wax printed onto the nitrocellulose membrane card to form channels and the cards were heated to melt the wax, a wicking pad and conjugate pad were attached, and the nitrocellulose was cut so that there were two channels for each assay. 5 µL of pink food dye color was then added to the conjugate pad in one channel and 5 µLof blue food dye was added to the conjugate pad in the other channel. The assay was placed in a reservoir with borate buffer, the optimized running buffer, which initiated the movement of the dye up the assay. Some initial experiments showed separation of the colors in their respective channels (Figure 30B). However, while there was separation in the two channels containing the food dye, cross over into a channel (as seen on the leftmost side in Figure 30B) that did not have any food dye deposited is visible, indicating that reagents are not fully contained within the channel they were deposited.

A.)

B.)
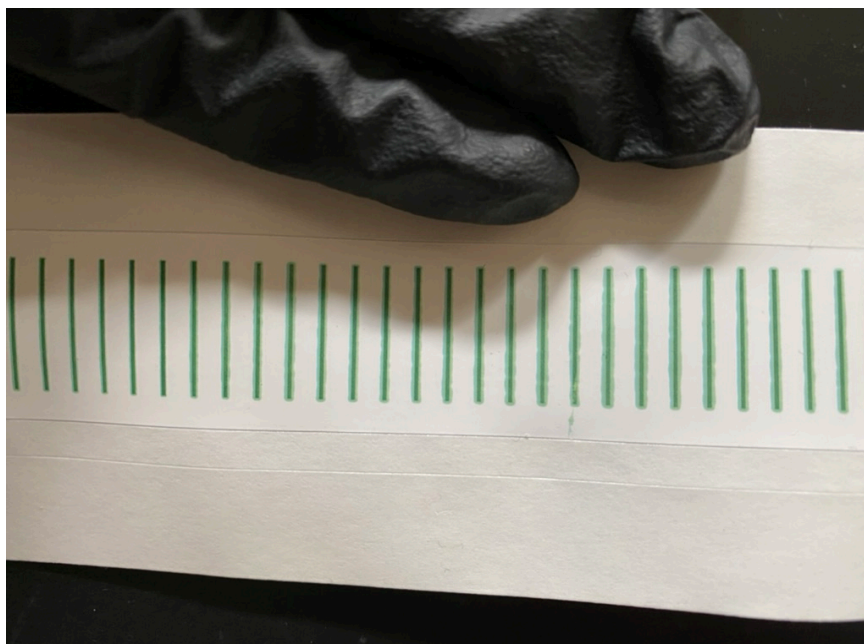
Figure 29. Images of initial wax printed channels on a nitrocellulose membrane **A.)** before baking and **B.)** after baking.

It was hypothesized that this dye crossover was due to inefficient contact between the conjugate pad and the membrane, therefore leading to wax not fully penetrating the conjugate pad-membrane junction and, therefore, allowing the food dye to flow into an

A.)
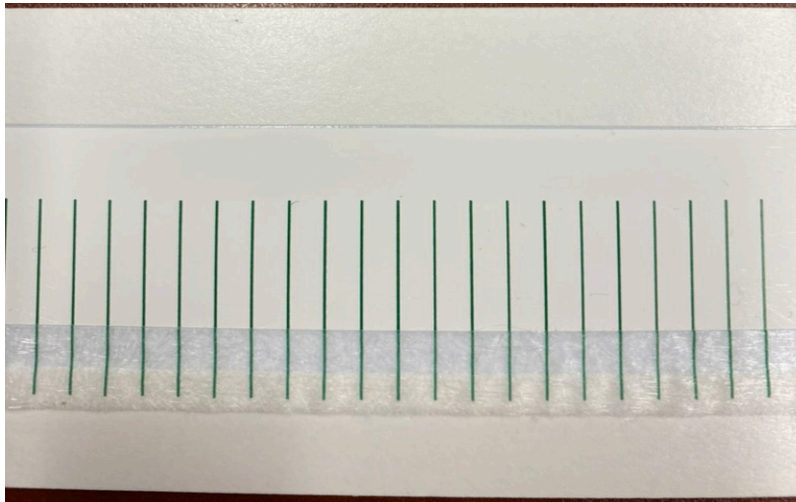
B.)
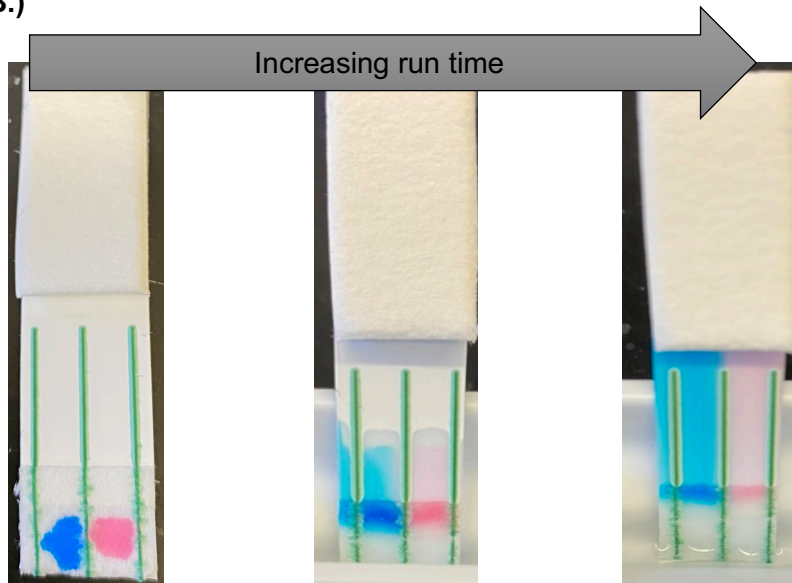
Figure 30. Images of the **A.)** optimized placement and spacing of wax printed channels and **B.)** preliminary results of dipstick assays containing hydrophobic channels with different colored food dye as a sample for a proof-of-concept study.

adjacent channel. On a pre-backed membrane card like the one used in these studies,

there is a narrow strip of adhesive for addition of a conjugate pad and the card is

structured so that there are a few millimeters of overlap between the conjugate pad and

nitrocellulose membrane where antibodies are immobilized. When the nitrocellulose

card (after baking) is bent at an angle so that the area under the conjugate pad can be

viewed, no wax can be seen penetrating to the nitrocellulose layer. A few methods were

used to try to improve penetration of the wax through both the conjugate pad and

membrane including modified designs, varying conjugate pad materials, conjugate pad

pretreatment, and the use of adhesive at the junction. The best results in separation of

the food dyes in each channel were observed when Whatman 3MM chromatography

paper was used as the conjugate pad and when tape was placed around the conjugate

pad-nitrocellulose membrane junction (Figure 31). Other adhesives such as super glue

entirely prevented fluid flow up the membrane as the glue spread faster than it dried,

A.)   **B.)**
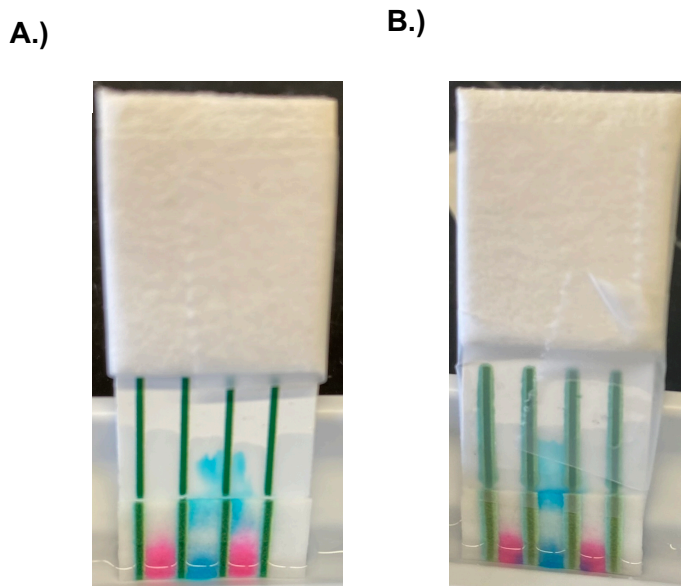
Figure 31. Dipstick assays using Whatman 3MM chromatography paper as the conjugate pad **A.)** without tape and **B.)** with tape around the assay.

causing a barrier of glue across the width of the test. This was true with other adhesives sampled as well.

With an optimal conjugate pad material chosen, experiments were conducted to analyze the effectiveness of using wax printed channels with reagents used in the dipstick assay discussed in Chapter III that showed cross-reactivity. To accomplish this, capture antibodies previously chosen for CRP, PCT, and HRP2 were immobilized as dots within each channel. A control dot was also present in each channel above each test dot. The conjugate pads were pretreated with 20% sucrose (v/v), 0.25% Tween-20 (v/v), and 2% BSA (w/v) in 50 mM borate buffer before being dried in an oven at 40 °C for 2 hours and placed in a dry box overnight. The conjugate pad was then adhered to the nitrocellulose membrane and 4 µL of AuNP-Ab conjugates were pipetted into their respective channels prior to being dried in an oven at 40 °C for 1.5 hours. Each assay was then placed in a reservoir with 300 µL of 50 mM borate buffer which initiated the movement of the conjugates up the test.

These assays continued to display false positives, like the previous format, evidenced by a visible test dot in the CRP channel in the absence of any analyte (Figure 32). This showed that the reagents were not sufficiently separated by the wax barriers constructing each channel although preliminary tests with food dyes appeared to show separation.

Figure 32. Dipstick assays run in triplicate with each channel corresponding (left to right) to detection of CRP, PCT, and HRP2.

While it may be possible to use wax printed channels as a reagent separation technique with further optimization and modification, the one certain way to provide that separation is to completely separate all components of the assay, as previous studies described at the beginning of this chapter have done. As a proof-of-concept, a custom cassette was designed and 3D printed for the housing of three individual LFAs in parallel so that they may be run simultaneously while ensuring no crossover of reagents (Figure 33).

Figure 33. Custom 3D printed cassette that fits three single LFAs.

A custom top to fit this cassette with a single inlet that sits above and spans the length of all three sample pads would allow for a streamlined device. With the proposed design, a user would follow the same steps for a single LFA while having the benefits of multiplexed detection.

Conclusion

Possible modifications to paper-based multiplexed immunoassays are limited due to the inherent nature and size of the assay. A few strategies were discussed in this chapter that improved the outcome of a multiplexed dipstick assay for detection of CRP, PCT, and HRP2 by minimizing nonspecific binding and cross-reactivity. Namely, it was found that when the gold nanoparticle conjugation method was altered for the AuNP-Ab conjugate containing the PCT detection antibody that was causing a false positive CRP result, the test line signal (and false positive) reduced in intensity. Additionally, by switching one of the assays in the multiplexed test to a competitive assay removed a component (the HRP2 capture antibody) that could be contributing to the observed false positives found for both PCT and HRP2 when in the presence of CRP analyte. Lastly, a wax printing strategy was employed in an attempt to spatially separate reagents within

individual channels. While this method still displayed cross-over of reagents, it is a promising strategy for the modification of nitrocellulose membranes. A custom cassette was also designed and printed as a proof-of-concept for the housing of three individual assays in parallel.

Future Directions

Future research surrounding diminishing or eliminating cross-reactivity in multiplexed assays would focus on spatial separation of reagents as it is the only guaranteed way to remove the possibility of unintended interactions for any biomarker or use-case. For the wax printing method, a dipstick assay could be constructed from the base materials instead of using a pre-backed nitrocellulose card, for example. This would allow for flexibility and control when adding the wax barriers. The main obstacle that was encountered in this work was the lack of wax penetration at the conjugate pad-nitrocellulose membrane junction. By assembling those pieces manually, this has the potential to be overcome. Additional conjugate pad materials could also be screened to assess which allows for the most thorough melting of the wax. Another method that could be used for the generation of hydrophobic barriers is photolithography. Previous studies have shown success with using photolithographic patterning on cellulose.[111,112] If an entire paper-based assay could be constructed on cellulose, individual channels could be created for the complete separation of reagents while keeping the final immunoassay suitable for use in resource-limited settings or at the POC. While photolithographic methods are more costly, they produce higher resolution patterns and

could offer a method for more widespread development of multiplexed paper-based assays.

Additionally, the advent and increasing use of smartphones as digital readers for POC immunoassays offers an array of advantages and possibly even some solutions with false positive results. If there is a scenario where the false positive results or nonspecific binding on a test region is significantly below the value of a true positive and is consistent across all test conditions, image processing can be built into the reading mechanism of the smartphone to subtract background signal. Depending on the specific test, image processing may eliminate the need for further optimization or screening of additional reagents.

CHAPTER V

CONCLUSION

In this work, the background, importance, and development of POC diagnostics, specifically LFAs and multiplexed paper-based immunoassays, was discussed. Chapter I focused on the introduction and widespread use of POC diagnostic tools in clinical settings and how their utility has only been bolstered in the wake of recent epidemics and pandemics. Chapter II described the first known study to analyze and track colloidal gold redistribution from AuNP-Ab conjugates upon test completion on commercially available malaria LFAs using ICP-OES. This study showcased how the major elements in an LFA that provide visual signal, AuNP-Ab conjugates, may not be optimized to provide the most sensitive LFAs, with a large portion of AuNP-Ab conjugates nonspecifically adhering to sections of the test that do not provide any signal. This preliminary study is one of the few to examine the impacts of the longstanding and conventional approaches using in LFA development, which are largely based in empirical design rather than methodically thought-out steps. In Chapter III, the development process for individual and multiplexed paper-based dipstick immunoassays is outlined including antibody screening and the development of in-house ELISAs. The results of these individual and multiplexed assays are also discussed. These results, some of which included false positive results when integrating into a multiplexed format, segued into a discussion in Chapter IV of methods that were implemented to minimize this cross-reactivity. Additionally, the development of a

dipstick assay for malaria fever differentiation was described along with optimization measures. Lastly, a proof-of-concept 3D printed cassette to house three separate LFAs was showcased as a solution for complete reagent separation and therefore, reduced cross-reactivity.

Cross-reactivity and nonspecific binding continues to plague multiplexed immunoassay development and commercialization, especially paper-based assays that are designed to be used in low-resource settings or at the POC. Lack of transparency and studies surrounding these issues slows down the paper-based diagnostics pipeline, and most importantly, the multiplexed diagnostics pipeline. Multiplexed diagnostics, particularly those that can be used quickly and at the POC, have been recognized as crucial tools for specific and timely diagnosis of a variety of illnesses. It is forecasted that the global multiplexed diagnostics market value will be worth around $31 billion by the year 2027.[113,114] Further propelling the future diagnostic market is the increase in use of digital health platforms and the added criterion of real-time connectivity to the previously discussed REASSURED diagnostic criteria. The use of a virtual physician's office has called for the integration of technology as tools to aid in the communication between the physician and patient along with as a tool for mobile diagnosis. This has come in the form of smartphones as optical sensors for POC tests as well as the use of machine learning in conjunction with image processing to produce a diagnostic readout.[115–119]

Similar to the now widespread use of smartwatches to track steps, heart rate, and sleep, smart multiplexed diagnostics not only have the power to remove any subjective reading

of POC tests and to sense readouts, but also to pave the way for next-generation personalized diagnostics for self-health tracking.[119] Furthermore, the implementation of these smart diagnostics with machine learning methods can make existing multiplexed diagnostics more effective and specific, potentially reducing background noise that may impact test results as well. Overall, the use of emerging technology in conjunction with multiplexed POC diagnostics has the potential to further the multiplexed diagnostics pipeline and make digital health a more attractive option for healthcare moving forward.

APPENDIX A

SUPPORTING INFORMATION: CHAPTER II

Table A1: ICP-OES operating conditions.

OPTIMA 7000 DV OPERATING CONDITIONS	
Spray chamber	Cyclonic
Nebulizer	GemCone
Injector	2.0 mm Alumina
Plasma gas	15 L
Auxillary gas	0.2 L
Nebulizer gas	0.60 L
RF Power	1300 W
Plasma view	Axial
Read delay	30 s
Peristaltic pump flow rate	1.50 mL/min
Replicates	3
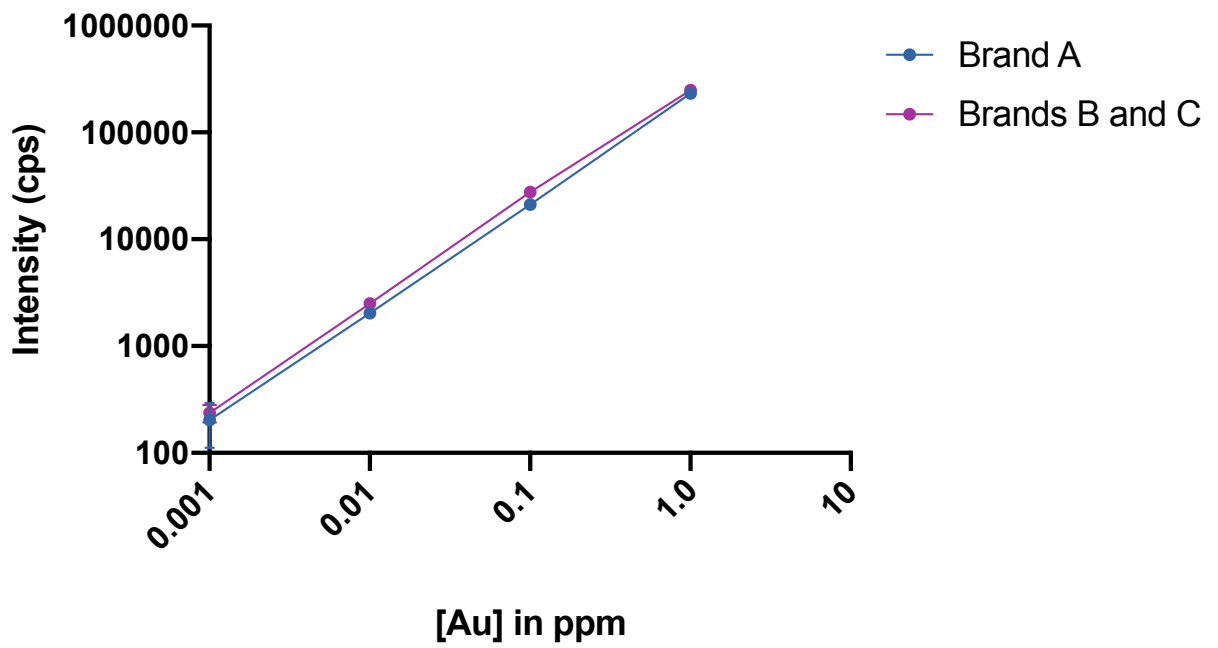
Figure A1. Standard curves (log-log) obtained from ICP-OES utilizing five concentrations: 1.0, 0.1, 0.01, 0.001 and 0.0001 [Au] in ppm for A) Brand A, and B) Brands B-C. Some error bars are smaller than width of data point.

A.

B.
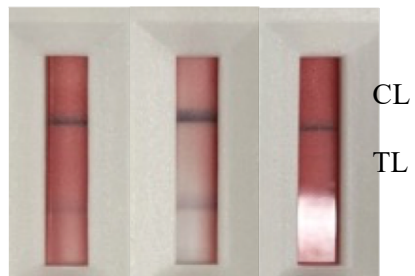
C.
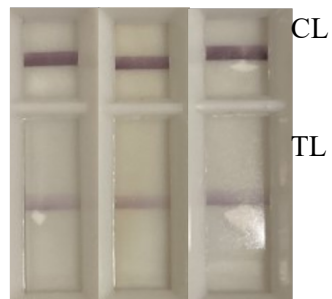
Figure A2. Representative pictures of LFAs at 100 p/µL. A) Brand A; B) Brand B; and C) Brand C
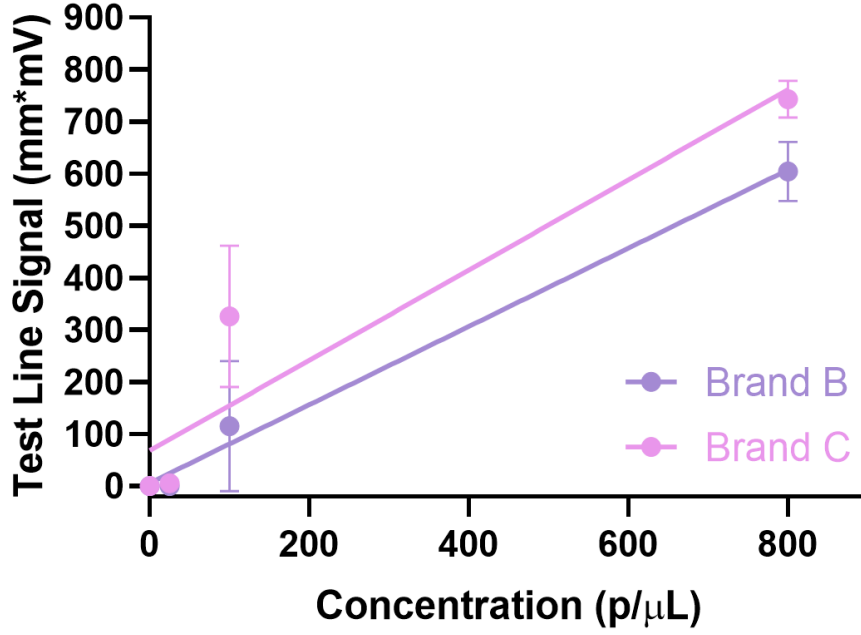
Figure A3. Lateral Flow Reader test line signal at three parasite concentrations for Brands B and C.
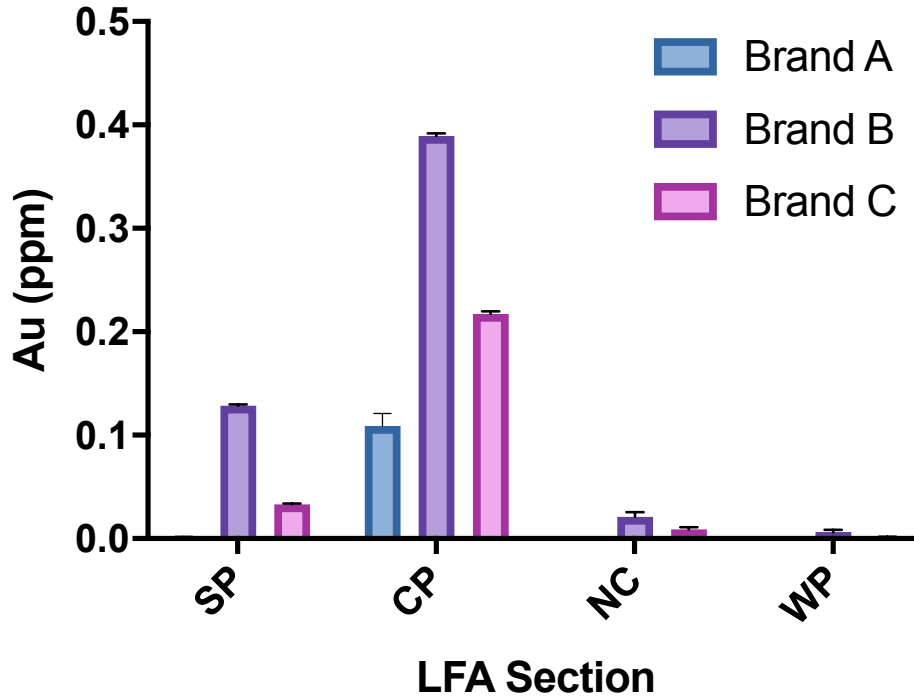
Figure A4. Comparison of gold content for sample pad (SP), conjugate pad (CP), nitrocellulose (NC), and wicking pad (WP) on each section of an unused LFA from three different brands.

REFERENCES

(1)   Caliendo, A. M.; Gilbert, D. N.; Ginocchio, C. C.; Hanson, K. E.; May, L.; Quinn, T. C.; Tenover, F. C.; Alland, D.; Blaschke, A. J.; Bonomo, R. A.; Carroll, K. C.; Ferraro, M. J.; Hirschhorn, L. R.; Joseph, W. P.; Karchmer, T.; MacIntyre, A. T.; Reller, L. B.; Jackson, A. F. Better Tests, Better Care: Improved Diagnostics for Infectious Diseases. *Clin. Infect. Dis. Off. Publ. Infect. Dis. Soc. Am.* **2013**, *57* (Suppl 3), S139–S170. https://doi.org/10.1093/cid/cit578.

(2)   Drain, P. K.; Hyle, E. P.; Noubary, F.; Freedberg, K. A.; Wilson, D.; Bishai, W. R.; Rodriguez, W.; Bassett, I. V. Diagnostic Point-of-Care Tests in Resource-Limited Settings. *Lancet Infect. Dis.* **2014**, *14* (3), 239–249. https://doi.org/10.1016/S1473-3099(13)70250-0.

(3)   Heidt, B.; Siqueira, W. F.; Eersels, K.; Diliën, H.; van Grinsven, B.; Fujiwara, R. T.; Cleij, T. J. Point of Care Diagnostics in Resource-Limited Settings: A Review of the Present and Future of PoC in Its Most Needed Environment. *Biosensors* **2020**, *10* (10), 133. https://doi.org/10.3390/bios10100133.

(4)   Cunningham, J.; Jones, S.; Gatton, M. L.; Barnwell, J. W.; Cheng, Q.; Chiodini, P. L.; Glenn, J.; Incardona, S.; Kosack, C.; Luchavez, J.; Menard, D.; Nhem, S.; Oyibo, W.; Rees-Channer, R. R.; Gonzalez, I.; Bell, D. A Review of the WHO Malaria Rapid Diagnostic Test Product Testing Programme (2008–2018): Performance, Procurement and Policy. *Malar. J.* **2019**, *18* (1), 387. https://doi.org/10.1186/s12936-019-3028-z.

(5)   *The role of RDTs in malaria control*. https://www.who.int/teams/global-malaria-programme/case-management/diagnosis/rapid-diagnostic-tests/role-in-malaria-control (accessed 2022-08-24).

(6)   Otoo, J. A.; Schlappi, T. S. REASSURED Multiplex Diagnostics: A Critical Review and Forecast. *Biosensors* **2022**, *12* (2), 124. https://doi.org/10.3390/bios12020124.

(7)   Smith, S.; Korvink, J. G.; Mager, D.; Land, K. The Potential of Paper-Based Diagnostics to Meet the ASSURED Criteria. *RSC Adv.* **2018**, *8* (59), 34012–34034. https://doi.org/10.1039/C8RA06132G.

(8)   Land, K. J.; Boeras, D. I.; Chen, X.-S.; Ramsay, A. R.; Peeling, R. W. REASSURED Diagnostics to Inform Disease Control Strategies, Strengthen Health Systems and Improve Patient Outcomes. *Nat. Microbiol.* **2019**, *4* (1), 46–54. https://doi.org/10.1038/s41564-018-0295-3.

(9)   Dincer, C.; Bruch, R.; Kling, A.; Dittrich, P. S.; Urban, G. A. Multiplexed Point-of-Care Testing – XPOCT. *Trends Biotechnol.* **2017**, *35* (8), 728–742. https://doi.org/10.1016/j.tibtech.2017.03.013.

(10)   Oeschger, T.; McCloskey, D.; Kopparthy, V.; Singh, A.; Erickson, D. Point of Care Technologies for Sepsis Diagnosis and Treatment. *Lab. Chip* **2019**, *19* (5), 728–737. https://doi.org/10.1039/C8LC01102H.

(11)   Joung, H.-A.; Ballard, Z. S.; Wu, J.; Tseng, D. K.; Teshome, H.; Zhang, L.; Horn, E. J.; Arnaboldi, P. M.; Dattwyler, R. J.; Garner, O. B.; Di Carlo, D.; Ozcan, A. Point-of-Care Serodiagnostic Test for Early-Stage Lyme Disease Using a Multiplexed Paper-Based Immunoassay and Machine Learning. *ACS Nano* **2020**, *14* (1), 229–240. https://doi.org/10.1021/acsnano.9b08151.

(12)   Xiong, X.; Zhang, J.; Wang, Z.; Liu, C.; Xiao, W.; Han, J.; Shi, Q. Simultaneous Multiplexed Detection of Protein and Metal Ions by a Colorimetric Microfluidic Paper-Based Analytical Device. *Biochip J.* **2020**, *14* (4), 429–437. https://doi.org/10.1007/s13206-020-4407-9.

(13)   Hristov, D.; Rijal, H.; Gomez-Marquez, J.; Hamad-Schifferli, K. Developing a Paper-Based Antigen Assay to Differentiate between Coronaviruses and SARS-CoV-2 Spike Variants. *Anal. Chem.* **2021**, *93* (22), 7825–7832. https://doi.org/10.1021/acs.analchem.0c05438.

(14)   Yang, M.; Zhang, W.; Yang, J.; Hu, B.; Cao, F.; Zheng, W.; Chen, Y.; Jiang, X. Skiving Stacked Sheets of Paper into Test Paper for Rapid and Multiplexed Assay. *Sci. Adv.* **2017**, *3* (12), eaao4862. https://doi.org/10.1126/sciadv.aao4862.

(15)   Climent, E.; Biyikal, M.; Gröninger, D.; Weller, M. G.; Martínez-Máñez, R.; Rurack, K. Multiplexed Detection of Analytes on Single Test Strips with Antibody-Gated Indicator-Releasing Mesoporous Nanoparticles. *Angew. Chem. Int. Ed.* **2020**, *59* (52), 23862–23869. https://doi.org/10.1002/anie.202009000.

(16) Wang, J.; Li, W.; Ban, L.; Du, W.; Feng, X.; Liu, B.-F. A Paper-Based Device with an Adjustable Time Controller for the Rapid Determination of Tumor Biomarkers. *Sens. Actuators B Chem.* **2018**, *254*, 855–862. https://doi.org/10.1016/j.snb.2017.07.192.

(17) Wu, Y.; Ren, Y.; Han, L.; Yan, Y.; Jiang, H. Three-Dimensional Paper Based Platform for Automatically Running Multiple Assays in a Single Step. *Talanta* **2019**, *200*, 177–185. https://doi.org/10.1016/j.talanta.2019.03.033.

(18) Zhang, Y.; Yu, Y.; Ying, J. Y. Multi-Color Au/Ag Nanoparticles for Multiplexed Lateral Flow Assay Based on Spatial Separation and Color Co-Localization. *Adv. Funct. Mater.* **2022**, *32* (7), 2109553. https://doi.org/10.1002/adfm.202109553.

(19) Reboud, J.; Xu, G.; Garrett, A.; Adriko, M.; Yang, Z.; Tukahebwa, E. M.; Rowell, C.; Cooper, J. M. Paper-Based Microfluidics for DNA Diagnostics of Malaria in Low Resource Underserved Rural Communities. *Proc. Natl. Acad. Sci.* **2019**, *116* (11), 4834–4842. https://doi.org/10.1073/pnas.1812296116.

(20) Lim, W. Y.; Thevarajah, T. M.; Goh, B. T.; Khor, S. M. Paper Microfluidic Device for Early Diagnosis and Prognosis of Acute Myocardial Infarction via Quantitative Multiplex Cardiac Biomarker Detection. *Biosens. Bioelectron.* **2019**, *128*, 176–185. https://doi.org/10.1016/j.bios.2018.12.049.

(21) Garibyan, L.; Avashia, N. Research Techniques Made Simple: Polymerase Chain Reaction (PCR). *J. Invest. Dermatol.* **2013**, *133* (3), e6. https://doi.org/10.1038/jid.2013.1.

(22) Yang, S.; Rothman, R. E. PCR-Based Diagnostics for Infectious Diseases: Uses, Limitations, and Future Applications in Acute-Care Settings. *Lancet Infect. Dis.* **2004**, *4* (6), 337–348. https://doi.org/10.1016/S1473-3099(04)01044-8.

(23) Islam, K. U.; Iqbal, J. An Update on Molecular Diagnostics for COVID-19. *Front. Cell. Infect. Microbiol.* **2020**, *10*, 560616. https://doi.org/10.3389/fcimb.2020.560616.

(24) Elnifro, E. M.; Ashshi, A. M.; Cooper, R. J.; Klapper, P. E. Multiplex PCR: Optimization and Application in Diagnostic Virology. *Clin. Microbiol. Rev.* **2000**, *13* (4), 559–570.

(25) Huang, H.-S.; Tsai, C.-L.; Chang, J.; Hsu, T.-C.; Lin, S.; Lee, C.-C. Multiplex PCR System for the Rapid Diagnosis of Respiratory Virus Infection: Systematic Review and Meta-Analysis. *Clin. Microbiol. Infect.* **2018**, *24* (10), 1055–1063. https://doi.org/10.1016/j.cmi.2017.11.018.

(26) Research, C. for B. E. and. NGI UltraQual Multiplex PCR Assay for HCV, HIV-1, HIV-2 and HBV. *FDA* **2022**.

(27) *BinaxNOW^{TM} Influenza A & B Card 2*. https://www.globalpointofcare.abbott/en/product-details/binaxnow-influenza-a-and-b-2.html (accessed 2022-08-16).

(28) *Sofia 2 Flu + SARS Antigen FIA | Quidel*. https://www.quidel.com/immunoassays/sofia-2-flu-sars-antigen-fia (accessed 2022-08-16).

(29) *WHO | Malaria rapid diagnostic test performance. Results of WHO product testing of malaria RDTs: round 8 (2016-2018)*. WHO. http://www.who.int/malaria/publications/atoz/9789241514965/en/ (accessed 2019-11-22).

(30) Liu, Y.; Zhan, L.; Qin, Z.; Sackrison, J.; Bischof, J. C. Ultrasensitive and Highly Specific Lateral Flow Assays for Point-of-Care Diagnosis. *ACS Nano* **2021**, *15* (3), 3593–3611. https://doi.org/10.1021/acsnano.0c10035.

(31) Singhroy, D. N.; MacLean, E.; Kohli, M.; Lessem, E.; Branigan, D.; England, K.; Suleiman, K.; Drain, P. K.; Ruhwald, M.; Schumacher, S.; Denkinger, C. M.; Waning, B.; Van Gemert, W.; Pai, M. Adoption and Uptake of the Lateral Flow Urine LAM Test in Countries with High Tuberculosis and HIV/AIDS Burden: Current Landscape and Barriers. *Gates Open Res.* **2020**, *4*, 24. https://doi.org/10.12688/gatesopenres.13112.2.

(32) Jeong, H. W.; Heo, J. Y.; Park, J. S.; Kim, W. J. Effect of the Influenza Virus Rapid Antigen Test on a Physician's Decision to Prescribe Antibiotics and on Patient Length of Stay in the Emergency Department. *PLoS ONE* **2014**, *9* (11), e110978. https://doi.org/10.1371/journal.pone.0110978.

(33) Peci, A.; Winter, A.-L.; King, E.-C.; Blair, J.; Gubbay, J. B. Performance of Rapid Influenza Diagnostic Testing in Outbreak Settings. *J. Clin. Microbiol.* **2014**, *52* (12), 4309–4317. https://doi.org/10.1128/JCM.02024-14.

(34) Parolo, C.; Sena-Torralba, A.; Bergua, J. F.; Calucho, E.; Fuentes-Chust, C.; Hu, L.; Rivas, L.; Álvarez-Diduk, R.; Nguyen, E. P.; Cinti, S.; Quesada-González, D.; Merkoçi, A. Tutorial: Design and Fabrication of Nanoparticle-Based Lateral-Flow Immunoassays. *Nat. Protoc.* **2020**, *15* (12), 3788–3816. https://doi.org/10.1038/s41596-020-0357-x.

(35) Posthuma-Trumpie, G. A.; Korf, J.; van Amerongen, A. Lateral Flow (Immuno)Assay: Its Strengths, Weaknesses, Opportunities and Threats. A Literature Survey. *Anal. Bioanal. Chem.* **2009**, *393* (2), 569–582. https://doi.org/10.1007/s00216-008-2287-2.

(36) Halperin, R. F.; Stafford, P.; Johnston, S. A. Exploring Antibody Recognition of Sequence Space through Random-Sequence Peptide Microarrays. *Mol. Cell. Proteomics MCP* **2011**, *10* (3), M110.000786. https://doi.org/10.1074/mcp.M110.000786.

(37) Schwenk, J. M.; Igel, U.; Neiman, M.; Langen, H.; Becker, C.; Bjartell, A.; Ponten, F.; Wiklund, F.; Grönberg, H.; Nilsson, P.; Uhlen, M. Toward Next Generation Plasma Profiling via Heat-Induced Epitope Retrieval and Array-Based Assays. *Mol. Cell. Proteomics MCP* **2010**, *9* (11), 2497–2507. https://doi.org/10.1074/mcp.M110.001560.

(38) Butterfield, L. H.; Potter, D. M.; Kirkwood, J. M. Multiplex Serum Biomarker Assessments: Technical and Biostatistical Issues. *J. Transl. Med.* **2011**, *9*, 173. https://doi.org/10.1186/1479-5876-9-173.

(39) Dias, J. T.; Lama, L.; Gantelius, J.; Andersson-Svahn, H. Minimizing Antibody Cross-Reactivity in Multiplex Detection of Biomarkers in Paper-Based Point-of-Care Assays. *Nanoscale* **2016**, *8* (15), 8195–8201. https://doi.org/10.1039/C5NR09207H.

(40) Juncker, D.; Bergeron, S.; Laforte, V.; Li, H. Cross-Reactivity in Antibody Microarrays and Multiplexed Sandwich Assays: Shedding Light on the Dark Side of Multiplexing. *Curr. Opin. Chem. Biol.* **2014**, *18*, 29–37. https://doi.org/10.1016/j.cbpa.2013.11.012.

(41) Pla-Roca, M.; Leulmi, R. F.; Tourekhanova, S.; Bergeron, S.; Laforte, V.; Moreau, E.; Gosline, S. J. C.; Bertos, N.; Hallett, M.; Park, M.; Juncker, D. Antibody Colocalization Microarray: A Scalable Technology for Multiplex Protein Analysis in Complex Samples. *Mol. Cell. Proteomics MCP* **2012**, *11* (4), M111.011460. https://doi.org/10.1074/mcp.M111.011460.

(42) Ellington, A. A.; Kullo, I. J.; Bailey, K. R.; Klee, G. G. Antibody-Based Protein Multiplex Platforms: Technical and Operational Challenges. *Clin. Chem.* **2010**, *56* (2), 186–193. https://doi.org/10.1373/clinchem.2009.127514.

(43) de Koning, L.; Liptak, C.; Shkreta, A.; Bradwin, G.; Hu, F. B.; Pradhan, A. D.; Rifai, N.; Kellogg, M. D. A Multiplex Immunoassay Gives Different Results than Singleplex Immunoassays Which May Bias Epidemiologic Associations. *Clin. Biochem.* **2012**, *45* (10), 848–851. https://doi.org/10.1016/j.clinbiochem.2012.04.006.

(44) Mohd Hanafiah, K.; Arifin, N.; Bustami, Y.; Noordin, R.; Garcia, M.; Anderson, D. Development of Multiplexed Infectious Disease Lateral Flow Assays: Challenges and Opportunities. *Diagnostics* **2017**, *7* (3), 51. https://doi.org/10.3390/diagnostics7030051.

(45) Schenk, F.; Weber, P.; Vogler, J.; Hecht, L.; Dietzel, A.; Gauglitz, G. nter. Development of a Paper-Based Lateral Flow Immunoassay for Simultaneous Detection of Lipopolysaccharides of Salmonella Serovars. *Anal. Bioanal. Chem.* **2018**, *410* (3), 863–869. https://doi.org/10.1007/s00216-017-0643-9.

(46) Carrilho, E.; Martinez, A. W.; Whitesides, G. M. Understanding Wax Printing: A Simple Micropatterning Process for Paper-Based Microfluidics. *Anal. Chem.* **2009**, *81* (16), 7091–7095. https://doi.org/10.1021/ac901071p.

(47) Kosack, C. S.; Page, A.-L.; Klatser, P. R. A Guide to Aid the Selection of Diagnostic Tests. *Bull. World Health Organ.* **2017**, *95* (9), 639–645. https://doi.org/10.2471/BLT.16.187468.

(48) Koczula, K. M.; Gallotta, A. Lateral Flow Assays. *Essays Biochem.* **2016**, *60* (1), 111–120. https://doi.org/10.1042/EBC20150012.

(49) Tsai, T.-T.; Huang, T.-S.; Chen, C.-A.; Ho, N. Y.-J.; Chou, Y.-J.; Chen, C.-F. Development a Stacking Pad Design for Enhancing the Sensitivity of Lateral Flow Immunoassay. *Sci. Rep.* **2018**, *8* (1). https://doi.org/10.1038/s41598-018-35694-9.

(50) Yetisen, A. K.; Akram, M. S.; Lowe, C. R. Paper-Based Microfluidic Point-of-Care Diagnostic Devices. *Lab. Chip* **2013**, *13* (12), 2210–2251. https://doi.org/10.1039/C3LC50169H.

(51) Hu, J.; Wang, S.; Wang, L.; Li, F.; Pingguan-Murphy, B.; Lu, T. J.; Xu, F. Advances in Paper-Based Point-of-Care Diagnostics. *Biosens. Bioelectron.* **2014**, *54*, 585–597. https://doi.org/10.1016/j.bios.2013.10.075.

(52) Yang, J.; Wang, K.; Xu, H.; Yan, W.; Jin, Q.; Cui, D. Detection Platforms for Point-of-Care Testing Based on Colorimetric, Luminescent and Magnetic Assays: A Review. *Talanta* **2019**, *202*, 96–110. https://doi.org/10.1016/j.talanta.2019.04.054.

(53) Hristov, D.; Rodriguez-Quijada, C.; Gomez-Marquez, J.; Hamad-Schifferli, K. Designing Paper-Based Immunoassays for Biomedical Applications. *Sensors* **2019**, *19* (3), 554. https://doi.org/10.3390/s19030554.

(54) Bahadır, E. B.; Sezgintürk, M. K. Lateral Flow Assays: Principles, Designs and Labels. *TrAC Trends Anal. Chem.* **2016**, *82*, 286–306. https://doi.org/10.1016/j.trac.2016.06.006.

(55) Davies, R. J.; Eapen, S. S.; Carlisle, S. J. Lateral-Flow Immunochromatographic Assays. In *Handbook of Biosensors and Biochips*; Marks, R. S., Cullen, D. C., Karube, I., Lowe, C. R., Weetall, H. H., Eds.; John Wiley & Sons, Ltd: Chichester, UK, 2008. https://doi.org/10.1002/9780470061565.hbb110.

(56) O'Farrell, B. Lateral Flow Technology for Field-Based Applications—Basics and Advanced Developments. *Top. Companion Anim. Med.* **2015**, *30* (4), 139–147. https://doi.org/10.1053/j.tcam.2015.12.003.

(57) Bishop, J. D.; Hsieh, H. V.; Gasperino, D. J.; Weigl, B. H. Sensitivity Enhancement in Lateral Flow Assays: A Systems Perspective. *Lab. Chip* **2019**, *19* (15), 2486–2499. https://doi.org/10.1039/C9LC00104B.

(58) Li, C.; Vandenberg, K.; Prabhulkar, S.; Zhu, X.; Schneper, L.; Methee, K.; Rosser, C. J.; Almeide, E. Paper Based Point-of-Care Testing Disc for Multiplex Whole Cell Bacteria Analysis. *Biosens. Bioelectron.* **2011**, *26* (11), 4342–4348. https://doi.org/10.1016/j.bios.2011.04.035.

(59) Berli, C. L. A.; Kler, P. A. A Quantitative Model for Lateral Flow Assays. *Microfluid. Nanofluidics* **2016**, *20* (7), 104. https://doi.org/10.1007/s10404-016-1771-9.

(60) Qian, S.; Bau, H. H. A Mathematical Model of Lateral Flow Bioreactions Applied to Sandwich Assays. *Anal. Biochem.* **2003**, *322* (1), 89–98. https://doi.org/10.1016/j.ab.2003.07.011.

(61) Qian, S.; Bau, H. H. Analysis of Lateral Flow Biodetectors: Competitive Format. *Anal. Biochem.* **2004**, *326* (2), 211–224. https://doi.org/10.1016/j.ab.2003.12.019.

(62) Khlebtsov, B. N.; Tumskiy, R. S.; Burov, A. M.; Pylaev, T. E.; Khlebtsov, N. G. Quantifying the Numbers of Gold Nanoparticles in the Test Zone of Lateral Flow Immunoassay Strips. *ACS Appl. Nano Mater.* **2019**, *2* (8), 5020–5028. https://doi.org/10.1021/acsanm.9b00956.

(63) Hou, X.; Amais, R. S.; Jones, B. T.; Donati, G. L. Inductively Coupled Plasma Optical Emission Spectrometry. In *Encyclopedia of Analytical Chemistry*; John Wiley & Sons, Ltd, 2016; pp 1–25. https://doi.org/10.1002/9780470027318.a5110.pub3.

(64) Markwalter, C. F.; Ricks, K. M.; Bitting, A. L.; Mudenda, L.; Wright, D. W. Simultaneous Capture and Sequential Detection of Two Malarial Biomarkers on Magnetic Microparticles. *Talanta* **2016**, *161*, 443–449. https://doi.org/10.1016/j.talanta.2016.08.078.

(65) Bauer, W. S.; Richardson, K. A.; Adams, N. M.; Ricks, K. M.; Gasperino, D. J.; Ghionea, S. J.; Rosen, M.; Nichols, K. P.; Weigl, B. H.; Haselton, F. R.; Wright, D. W. Rapid Concentration and Elution of Malarial Antigen Histidine-Rich Protein II Using Solid Phase Zn(II) Resin in a Simple Flow-through Pipette Tip Format. *Biomicrofluidics* **2017**, *11* (3). https://doi.org/10.1063/1.4984788.

(66) Schneider, C. A.; Rasband, W. S.; Eliceiri, K. W. NIH Image to ImageJ: 25 Years of Image Analysis. *Nat. Methods* **2012**, *9* (7), 671–675. https://doi.org/10.1038/nmeth.2089.

(67)   Bretherick, L.; Urben, P. G.; Pitt, M. J. *Bretherick's Handbook of Reactive Chemical Hazards*; Elsevier: Amsterdam, The Netherlands; Boston, Mass., 2007.

(68)   Bauer, W. S.; Gulka, C. P.; Silva-Baucage, L.; Adams, N. M.; Haselton, F. R.; Wright, D. W. Metal Affinity-Enabled Capture and Release Antibody Reagents Generate a Multiplex Biomarker Enrichment System That Improves Detection Limits of Rapid Diagnostic Tests. *Anal. Chem.* **2017**, *89* (19), 10216–10223. https://doi.org/10.1021/acs.analchem.7b01513.

(69)   Davis, K. M.; Gibson, L. E.; Haselton, F. R.; Wright, D. W. Simple Sample Processing Enhances Malaria Rapid Diagnostic Test Performance. *The Analyst* **2014**, *139* (12), 3026–3031. https://doi.org/10.1039/c4an00338a.

(70)   Scherr, T. F.; Gupta, S.; Wright, D. W.; Haselton, F. R. Mobile Phone Imaging and Cloud-Based Analysis for Standardized Malaria Detection and Reporting. *Sci. Rep.* **2016**, *6* (1), 1–9. https://doi.org/10.1038/srep28645.

(71)   CDC. *What Exactly is Antibiotic Resistance?*. Centers for Disease Control and Prevention. https://www.cdc.gov/drugresistance/about.html (accessed 2021-01-06).

(72)   *Outpatient Antibiotic Prescriptions — United States, 2019 |Antibiotic Use | CDC*. https://www.cdc.gov/antibiotic-use/data/report-2019.html (accessed 2022-09-07).

(73)   *All Antibiotic Classes | A.R. & Patient Safety Portal*. https://arpsp.cdc.gov/profile/antibiotic-use/217 (accessed 2021-01-07).

(74)   Sproston, N. R.; Ashworth, J. J. Role of C-Reactive Protein at Sites of Inflammation and Infection. *Front. Immunol.* **2018**, *9*. https://doi.org/10.3389/fimmu.2018.00754.

(75)   Black, S.; Kushner, I.; Samols, D. C-Reactive Protein. *J. Biol. Chem.* **2004**, *279* (47), 48487–48490. https://doi.org/10.1074/jbc.R400025200.

(76)   Haran, J. P.; Beaudoin, F. L.; Suner, S.; Lu, S. C-Reactive Protein as Predictor of Bacterial Infection among Patients with an Influenza-like Illness. *Am. J. Emerg. Med.* **2013**, *31* (1), 137–144. https://doi.org/10.1016/j.ajem.2012.06.026.

(77)   Memar, M. Y.; Varshochi, M.; Shokouhi, B.; Asgharzadeh, M.; Kafil, H. S. Procalcitonin: The Marker of Pediatric Bacterial Infection. *Biomed. Pharmacother. Biomedecine Pharmacother.* **2017**, *96*, 936–943. https://doi.org/10.1016/j.biopha.2017.11.149.

(78)   Gilbert, D. N. Procalcitonin as a Biomarker in Respiratory Tract Infection. *Clin. Infect. Dis.* **2011**, *52* (suppl_4), S346–S350. https://doi.org/10.1093/cid/cir050.

(79)   Lee, H. Procalcitonin as a Biomarker of Infectious Diseases. *Korean J. Intern. Med.* **2013**, *28* (3), 285–291. https://doi.org/10.3904/kjim.2013.28.3.285.

(80)   Hu, L.; Shi, Q.; Shi, M.; Liu, R.; Wang, C. Diagnostic Value of PCT and CRP for Detecting Serious Bacterial Infections in Patients With Fever of Unknown Origin: A Systematic Review and Meta-Analysis. *Appl. Immunohistochem. Mol. Morphol.* **2017**, *25* (8), e61. https://doi.org/10.1097/PAI.0000000000000552.

(81)   Simon, L.; Gauvin, F.; Amre, D. K.; Saint-Louis, P.; Lacroix, J. Serum Procalcitonin and C-Reactive Protein Levels as Markers of Bacterial Infection: A Systematic Review and Meta-Analysis. *Clin. Infect. Dis. Off. Publ. Infect. Dis. Soc. Am.* **2004**, *39* (2), 206–217. https://doi.org/10.1086/421997.

(82)   Herberg, J.; Huang, H.; Thezenas, M. L.; Janes, V.; Carter, M.; Gormley, S.; Hamilton, M. S.; Kessler, B.; Levin, M.; Casals-Pascual, C. Lipocalin-2 Is a Sensitive and Specific Marker of Bacterial Infection in Children. *bioRxiv* **2019**, 623819. https://doi.org/10.1101/623819.

(83)   Venge, P. Human Neutrophil Lipocalin (HNL) as a Biomarker of Acute Infections. *Ups. J. Med. Sci.* **2018**, *123* (1), 1–8. https://doi.org/10.1080/03009734.2017.1420112.

(84)   Xu, S. Y.; Pauksen, K.; Venge, P. Serum Measurements of Human Neutrophil Lipocalin (HNL) Discriminate between Acute Bacterial and Viral Infections. *Scand. J. Clin. Lab. Invest.* **1995**, *55* (2), 125–131. https://doi.org/10.3109/00365519509089604.

(85)   Cai, Q.; Zhang, X.; Shen, L.; Wang, T. Clinical Application Value of Serum Neutrophil Gelatinase-Associated Lipocalin in Neonatal Sepsis. *Transl. Pediatr.* **2022**, *11* (1), 12026–12126. https://doi.org/10.21037/tp-21-587.

(86) Fang, C.; Wang, Z.; Dai, Y.; Chang, W.; Sun, L.; Ma, X. Serum Human Neutrophil Lipocalin: An Effective Biomarker for Diagnosing Bacterial Infections. *Clin. Biochem.* **2019**. https://doi.org/10.1016/j.clinbiochem.2019.10.003.

(87) Ashkenazi-Hoffnung, L.; Oved, K.; Navon, R.; Friedman, T.; Boico, O.; Paz, M.; Kronenfeld, G.; Etshtein, L.; Cohen, A.; Gottlieb, T. M.; Eden, E.; Chistyakov, I.; Srugo, I.; Klein, A.; Ashkenazi, S.; Scheuerman, O. A Host-Protein Signature Is Superior to Other Biomarkers for Differentiating between Bacterial and Viral Disease in Patients with Respiratory Infection and Fever without Source: A Prospective Observational Study. *Eur. J. Clin. Microbiol. Infect. Dis.* **2018**, *37* (7), 1361–1371. https://doi.org/10.1007/s10096-018-3261-3.

(88) Channon-Wells, S.; O'Connor, D. Host Gene Signature Shows Promise to Distinguish Bacterial and Viral Infections. *Lancet Digit. Health* **2021**, *3* (8), e465–e466. https://doi.org/10.1016/S2589-7500(21)00136-9.

(89) Oved, K.; Cohen, A.; Boico, O.; Navon, R.; Friedman, T.; Etshtein, L.; Kriger, O.; Bamberger, E.; Fonar, Y.; Yacobov, R.; Wolchinsky, R.; Denkberg, G.; Dotan, Y.; Hochberg, A.; Reiter, Y.; Grupper, M.; Srugo, I.; Feigin, P.; Gorfine, M.; Chistyakov, I.; Dagan, R.; Klein, A.; Potasman, I.; Eden, E. A Novel Host-Proteome Signature for Distinguishing between Acute Bacterial and Viral Infections. *PloS One* **2015**, *10* (3), e0120012. https://doi.org/10.1371/journal.pone.0120012.

(90) Strehlitz, A.; Goldmann, O.; Pils, M. C.; Pessler, F.; Medina, E. An Interferon Signature Discriminates Pneumococcal From Staphylococcal Pneumonia. *Front. Immunol.* **2018**, *9*. https://doi.org/10.3389/fimmu.2018.01424.

(91) Aydin, S. A Short History, Principles, and Types of ELISA, and Our Laboratory Experience with Peptide/Protein Analyses Using ELISA. *Peptides* **2015**, *72*, 4–15. https://doi.org/10.1016/j.peptides.2015.04.012.

(92) Engvall, E.; Perlmann, P. Enzyme-Linked Immunosorbent Assay (ELISA) Quantitative Assay of Immunoglobulin G. *Immunochemistry* **1971**, *8* (9), 871–874. https://doi.org/10.1016/0019-2791(71)90454-X.

(93) Lequin, R. M. Enzyme Immunoassay (EIA)/Enzyme-Linked Immunosorbent Assay (ELISA). *Clin. Chem.* **2005**, *51* (12), 2415–2418. https://doi.org/10.1373/clinchem.2005.051532.

(94) *Basic principles and types of ELISA | Abcam*. https://www.abcam.com/kits/elisa-principle#What%20is%20an%20ELISA (accessed 2022-08-22).

(95) Eden, E.; Srugo, I.; Gottlieb, T.; Navon, R.; Boico, O.; Cohen, A.; Bamberger, E.; Klein, A.; Oved, K. Diagnostic Accuracy of a TRAIL, IP-10 and CRP Combination for Discriminating Bacterial and Viral Etiologies at the Emergency Department. *J. Infect.* **2016**, *73* (2), 177–180. https://doi.org/10.1016/j.jinf.2016.05.002.

(96) Ross, G. M. S.; Filippini, D.; Nielen, M. W. F.; Salentijn, G. IJ. Unraveling the Hook Effect: A Comprehensive Study of High Antigen Concentration Effects in Sandwich Lateral Flow Immunoassays. *Anal. Chem.* **2020**, *92* (23), 15587–15595. https://doi.org/10.1021/acs.analchem.0c03740.

(97) Zhao, Y.; Wang, H.; Zhang, P.; Sun, C.; Wang, X.; Wang, X.; Yang, R.; Wang, C.; Zhou, L. Rapid Multiplex Detection of 10 Foodborne Pathogens with an Up-Converting Phosphor Technology-Based 10-Channel Lateral Flow Assay. *Sci. Rep.* **2016**, *6*, 21342. https://doi.org/10.1038/srep21342.

(98) Pomili, T.; Donati, P.; Pompa, P. P. Paper-Based Multiplexed Colorimetric Device for the Simultaneous Detection of Salivary Biomarkers. *Biosensors* **2021**, *11* (11), 443. https://doi.org/10.3390/bios11110443.

(99) Lin, D.; Li, B.; Fu, L.; Qi, J.; Xia, C.; Zhang, Y.; Chen, J.; Choo, J.; Chen, L. A Novel Polymer-Based Nitrocellulose Platform for Implementing a Multiplexed Microfluidic Paper-Based Enzyme-Linked Immunosorbent Assay. *Microsyst. Nanoeng.* **2022**, *8* (1), 1–10. https://doi.org/10.1038/s41378-022-00385-z.

(100) Lu, Y.; Shi, W.; Jiang, L.; Qin, J.; Lin, B. Rapid Prototyping of Paper-Based Microfluidics with Wax for Low-Cost, Portable Bioassay. *ELECTROPHORESIS* **2009**, *30* (9), 1497–1500. https://doi.org/10.1002/elps.200800563.

(101) Qamar, A. Z.; Amar, K.; Kohli, P.; Chowdhury, F.; Shamsi, M. H. Wax Patterned Microwells for Stem Cell Fate Study. *RSC Adv.* **2016**, *6* (106), 104919–104924. https://doi.org/10.1039/C6RA22422A.

(102) Altundemir, S.; Uguz, A. K.; Ulgen, K. A Review on Wax Printed Microfluidic Paper-Based Devices for International Health. *Biomicrofluidics* **2017**, *11* (4), 041501. https://doi.org/10.1063/1.4991504.

(103) Markwalter, C. F.; Gibson, L. E.; Mudenda, L.; Kimmel, D. W.; Mbambara, S.; Thuma, P. E.; Wright, D. W. Characterization of Plasmodium Lactate Dehydrogenase and Histidine-Rich Protein 2 Clearance Patterns via Rapid On-Bead Detection from a Single Dried Blood Spot. *Am. J. Trop. Med. Hyg.* **2018**, *98* (5), 1389–1396. https://doi.org/10.4269/ajtmh.17-0996.

(104) Yerlikaya, S.; Owusu, E. D. A.; Frimpong, A.; DeLisle, R. K.; Ding, X. C. A Dual, Systematic Approach to Malaria Diagnostic Biomarker Discovery. *Clin. Infect. Dis.* **2022**, *74* (1), 40–51. https://doi.org/10.1093/cid/ciab251.

(105) Markwalter, C. F.; Mudenda, L.; Leelawong, M.; Kimmel, D. W.; Nourani, A.; Mbambara, S.; Thuma, P. E.; Wright, D. W. Evidence for Histidine-Rich Protein 2 Immune Complex Formation in Symptomatic Patients in Southern Zambia. *Malar. J.* **2018**, *17*, 256. https://doi.org/10.1186/s12936-018-2400-8.

(106) Gibson, L. E.; Markwalter, C. F.; Kimmel, D. W.; Mudenda, L.; Mbambara, S.; Thuma, P. E.; Wright, D. W. Plasmodium Falciparum HRP2 ELISA for Analysis of Dried Blood Spot Samples in Rural Zambia. *Malar. J.* **2017**, *16*, 350. https://doi.org/10.1186/s12936-017-1996-4.

(107) Kantor, A. G.; Markwalter, C. F.; Nourani, A.; Wright, D. W. An Antibody-Free Dual-Biomarker Rapid Enrichment Workflow (AnDREW) Improves the Sensitivity of Malaria Rapid Diagnostic Tests. *Anal. Biochem.* **2021**, *612*, 114020. https://doi.org/10.1016/j.ab.2020.114020.

(108) DeSousa, J. M.; Jorge, M. Z.; Lindsay, H. B.; Haselton, F. R.; Wright, D. W.; Scherr, T. F. Inductively Coupled Plasma Optical Emission Spectroscopy as a Tool for Evaluating Lateral Flow Assays. *Anal. Methods* **2021**, *13* (18), 2137–2146. https://doi.org/10.1039/D1AY00236H.

(109) *Ebola virus disease*. https://www.who.int/news-room/fact-sheets/detail/ebola-virus-disease (accessed 2022-09-08).

(110) *Gold Nanoparticle Covalent Conjugation – Fortis Life Sciences*. https://www.fortislife.com/lateral-flow-covalent-conjugation (accessed 2022-09-08).

(111) Wolfberger, A.; Petritz, A.; Fian, A.; Herka, J.; Schmidt, V.; Stadlober, B.; Kargl, R.; Spirk, S.; Griesser, T. Photolithographic Patterning of Cellulose: A Versatile Dual-Tone Photoresist for Advanced Applications. *Cellulose* **2015**, *22* (1), 717–727. https://doi.org/10.1007/s10570-014-0471-4.

(112) Nishat, S.; Jafry, A. T.; Martinez, A. W.; Awan, F. R. Paper-Based Microfluidics: Simplified Fabrication and Assay Methods. *Sens. Actuators B Chem.* **2021**, *336*, 129681. https://doi.org/10.1016/j.snb.2021.129681.

(113) Inc, iHealthcareAnalyst. *Global Multiplexed Diagnostics Market $31.3 Billion by 2027*. iHealthcareAnalyst, Inc. - Healthcare Market Research. https://www.ihealthcareanalyst.com/global-multiplexed-diagnostics-market/ (accessed 2022-09-21).

(114) Research, T. M. *Multiplexed Diagnostics Market to Rise at CAGR of 17.9% during Forecast Period, Observes TMR Study*. GlobeNewswire News Room. https://www.globenewswire.com/news-release/2022/03/17/2405471/0/en/Multiplexed-Diagnostics-Market-to-Rise-at-CAGR-of-17-9-during-Forecast-Period-Observes-TMR-Study.html (accessed 2022-09-21).

(115) Martinez-Hurtado, J. L.; Yetisen, A. K.; Yun, S.-H. Multiplex Smartphone Diagnostics. In *Multiplex Biomarker Techniques: Methods and Applications*; Guest, P. C., Ed.; Methods in

Molecular Biology; Springer: New York, NY, 2017; pp 295–302. https://doi.org/10.1007/978-1-4939-6730-8_26.

(116) Sun, F.; Ganguli, A.; Nguyen, J.; Brisbin, R.; Shanmugam, K.; Hirschberg, D. L.; Wheeler, M. B.; Bashir, R.; Nash, D. M.; Cunningham, B. T. Smartphone-Based Multiplex 30-Minute Nucleic Acid Test of Live Virus from Nasal Swab Extract. *Lab. Chip* **2020**, *20* (9), 1621–1627. https://doi.org/10.1039/D0LC00304B.

(117) *Smartphone-based clinical diagnostics: towards democratization of evidence-based health care - Hernández-Neuta - 2019 - Journal of Internal Medicine - Wiley Online Library*. https://onlinelibrary-wiley-com.proxy.library.vanderbilt.edu/doi/full/10.1111/joim.12820 (accessed 2022-08-23).

(118) Ballard, Z. S.; Joung, H.-A.; Goncharov, A.; Liang, J.; Nugroho, K.; Di Carlo, D.; Garner, O. B.; Ozcan, A. Deep Learning-Enabled Point-of-Care Sensing Using Multiplexed Paper-Based Sensors. *Npj Digit. Med.* **2020**, *3* (1), 1–8. https://doi.org/10.1038/s41746-020-0274-y.

(119) Beduk, T.; Beduk, D.; Hasan, M. R.; Guler Celik, E.; Kosel, J.; Narang, J.; Salama, K. N.; Timur, S. Smartphone-Based Multiplexed Biosensing Tools for Health Monitoring. *Biosensors* **2022**, *12* (8), 583. https://doi.org/10.3390/bios12080583.